NTNU

Norwegian University of
Science and Technology

Distribution of Phosphorus between FeSi/Si and $CaO\text{-}SiO_2$ Slags at 1600^{o} C

Nina Kvitastein

Chemical Engineering and Biotechnology
Submission date: June 2017
Supervisor: Gabriella Tranell, IMA

Norwegian University of Science and Technology
Department of Materials Science and Engineering

Preface

This report describes the phosphorus distribution between ferrosilicon or silicon and slag.

The master's thesis is written for the course TMT4900 as a part of the study program Chemical Engineering and Biotechnology at Norwegian University of Science and Technology, NTNU. The work was carried out during the spring semester of 2017 at the Department of Materials Science and Engineering.

I would like to thank my supervisor Gabriella Tranell for her help and support with the master's thesis. Thank you to Torild Krogstad for preparing my samples for ICP-analysis. I would also like to show my appreciation to Torill Sørløkk for conducting XRF-analysis and Syverin Lierhagen for conducting ICP-MS analysis. Thank you also to Jonas Gjøvik and Dmitry Slizovskiy for help with various task. I greatly appreciate the help I have received from Ivar Andre Ødegaard and Egil Krystad. I am also thankful the training I received from Erlend Bjørnstad and Hamideh Kaffash with the TF2-furnace and for Erlend sharing his knowledge on statistical analysis. The help from Elmira Moosavi-Khoonsari with calculations in FactSage and as a discussion partner is greatly appreciated.

Trondheim, June 2017

Nina Augestad Kvitastein

Abstract

The aim of this thesis was to determine data for the phosphorus(P) distribution coefficients between ferrosilicon(FeSi) or silicon(Si) and calcia-silica($CaO-SiO_2$) slags. The work was carried out due to inconsistencies in literature on the phosphorus distribution between Si and slag and because phosphorus distribution between FeSi and $CaO-SiO_2$ slag has not been previously been determined for silicon rich FeSi alloys.

Calcia-silica slags of compositions 43:57,50:50 and 65:35 in weight%(wt%) doped with approximately 300 parts per million(ppm) of P and Fe:Si alloys of compositions
20:80,50:50, and 80:20 (wt%) have been prepared in induction furnaces. Equilibrium experiments were performed by holding metal and slag in a graphite crucible inside a furnace with resistance heating for 3 hours at 1600 °C in argon atmosphere. The samples were then quenched. After sample preparation, slag and metal were analyzed by Inductive Coupled Plasma Mass Spectroscopy. One experiment was also conducted with 20:80 wt% Fe:Si and $CaO-SiO_2$ containing 5.4 wt% P_2O_5. After a holding time of 3 hours at 1600 °C, the sample was cooled at a rate of 1 °C per minute down to the solidification temperature of the metal (1360°C). This sample was analyzed by Electron Probe Micro Analyzer.

Equilibrium experiments with quenching showed that the phosphorus distribution coefficients between Fe50:Si50 (wt%) and SiO_2-CaO slags were 0.08 ± 0.06, 0.14 ± 0.15 and 0.53 ± 0.42 for CaO contents of slag of 35, 50 and 57 wt% respectively. Experiments with Fe20:Si80 and SiO_2-CaO slags gave values for the phosphorus distribution coefficient of 0.14 ± 0.15, 0.13 ± 0.3 and 0.52 ± 0.41 for CaO concentration in slag of 35,50 and 57 wt% respectively. Between Si and $CaO-SiO_2$ slags the phosphorus distribution coefficients were 0.12 ± 0.09 and 0.4 for CaO concentration in slag of 50 and 57% respectively.

The main findings were that the phosphorus distribution coefficient did not change significantly with alloy composition. Slag composition on the other hand had a large impact on the phosphorus distribution coefficient. The phosphorus distribution coefficient increases with increasing basicity or CaO/SiO2 ratio of

the slag. Increasing the basicity also lead to increased calcium pick up in the metal which was consistent with published data. Thermodynamic modeling of the system should be conducted by including phosphorus in slag in the form of both phosphate and phosphide. The average loss of phosphorus after the experiment was 100 ppm. The use of graphite crucible most likely leads to the loss of phosphorus as P_4 in gas phase. The experiment with controlled cooling gave equal concentration of phosphorus in FeSi and Si. Phosphorus was not detected in the slag matrix. Some minor areas in the slag which also contained alumina and magnesia had a phosphorus concentration double of what was detected in the metals.

Sammendrag

Målet med denne masteroppgaven var å bestemme data for fordelingskoeffisienten av fosfor mellom ferrosilisum(FeSi) eller silisium(Si) og calcia-silica ($CaO-SiO_2$) slagg. Arbeidet ble gjennomført grunnet uoverensstemmelser i verdier av fosforfordeling mellom Si og slagg i litteraturen samt mangel på litteratur på fordelingen av fosfor mellom FeSi og slagg for legeringer med høyt Si innhold.

SiO_2-CaO slagger med sammensetninger av 43:57,50:50 og 65:35 i vekt% og Fe:Si legeringer med sammensetninger av 20:80, 50:50 og 80:20 i vekt% ble produsert i induksjonsovner. Likevektsforsøk ble deretter utført med slagg og metall i en ovn med mostandsoppvarming. Slagg og metall ble tilsatt en grafittdigel og holdt i ovnen i 3 timer i argon atmosfære ved 1600 °C. Deretter ble prøven raskt nedkjølt. Etter prøvepreparering ble slagg og metall analysert med induktivt koblet plasma massespektrometri. Ett eksperiment ble også utført med $CaO-SiO_2$ slagg med 5.4 vekt% P_2O_5 og Fe:Si 20:80 i vekt%. Eksperimentet ble utført på samme måte som i eksperimentene beskrevet tidligere. Den eneste forskjellen var at når holdetiden på tre timer var over, ble prøven kjølt ned sakte med en rate på 1 grad per minutt ned til 1360 °C, som er størkningstemperaturen til legeringen.

Forsøk med Fe50:Si50 og SiO_2-CaO slagger gav en fordelingskoeffisient av fosfor på $0,08 \pm 0,06$, $0,14 \pm 0,15$ og $0,53 \pm 0,42$ ved CaO innhold av slagg på henholdsvis 35, 50 og 57 vekt%. Forsøk med Fe20:Si80 og $CaO-SiO_2$ slagger gav en fordelingskoeffisient av fosfor på $0,14 \pm 0,5$, $0,13 \pm 0,3$ og $0,52 \pm 0,41$ ved CaO innhold av slagg på henholdsvis 35, 50 og 57 vekt%. Forsøk med Si og $CaO-SiO_2$ slagger gav fordelingskoeffisienter på $0,12 \pm 0,09$ og 0.4 ved CaO innhold av slagg på henholdsvis 50 og 57 vekt%.

Hovedkonklusjonene fra arbeidet gjort i denne masteroppgaven er at legeringssammensetning ikke påvirker fosforfordelingen i noen betydelig grad. Slaggsammensetning ser derimot ut til å påvirke fosforfordeling i nokså stor grad. Fosforfordelingen øker med økende basisitet, eller CaO/SiO_2 forhold. Ved å øke mengden CaO i slagg øker også mengden Ca som løser seg i metallet. Termodynamisk modellering av systemet har vist seg å være best dersom fosfor inkluderes som både fosfat og fosfid i slagg. I gjennomsnitt var den totale fosforkonsentrasjonen etter likevektsforsøkene

100 ppm lavere enn initalverdien. Bruk av grafittdigler fører mest sannsynlig til tap av fosfor i gassfase som P_4. Eksperimentet med kontrollert nedkjøling viste at konsentrasjonen av fosfor i FeSi og Si var lik samt at ingen fosfor ble detektert i hoved slaggfasen. Det var noen små områder i slagget som inneholdt MgO og Al_2O_3 i tillegg til CaO og SiO_2 der forsforinnholdet var det dobbelte av det som var observert i FeSi og Si.

Contents

Chapter 1

Introduction

There is an increasing demand for clean energy because of the negative effect fossil based energy sources have on the environment. Solar energy is an example of an important clean energy source. In 2014, solar energy accounted for 4% of the electricity generation from renewable sources [1]. Silicon is the material with the largest market share of the photovoltaic (PV) materials. In 2015 Si wafer based PV-technology had a market share of 93% [2].

Silicon requires a very pure material when used for solar cells. In order to produce solar grade silicon(SoG-Si), one of the impurities that it is crucial to remove is phosphorus. The impurity concentration of phosphorus in solar grade silicon has to be below 10^{-5} mass percent [3]. Silicon is produced in an electric arc furnace, and according to Myrhaug and Tveit(2000), 45% of phosphorus in the furnace originates from quartz, 45% from reducing agents and 10% from the electrode [4].

Phosphorus is a doping element in silicon wafers. Removal of phosphorus from silicon would make it easier to control the doping concentration when doping at a later stage. This is particularly important if the target is p-type doped silicon wafer which is doped with trivalent impurities like for instance boron. Phosphorus also affects the electrical properties of silicon and thereby the electrical properties of the final solar cell. According to Jiang et al.(2014) [5] phosphorus reduces electrical resistivity and minority carrier lifetime. Resistivity is a measure of how strongly the material resists the flow of electric current and minority carrier lifetime is a measure of the time it takes in average for an excess carrier to recombine. Niewelt et al. (2015) [6] presented how phosphorus leads to a high variation in the resistivity profile along the silicon ingot height when grown by Czochralski method or by directional solidification. The variation in resistivity is a result of the segregation coefficient of P being relatively high. One method to avoid the resistivity change is by compensation. Compensation is the presence of both B and

P in silicon. However the addition of B leads to light induced degradation because of complex formation with oxygen [6]. In addition the presence of both elements would lead to a lower yield because of a larger area where P and Si segregates towards the end of the ingot. This area would need to be removed.

The segregation coefficient of phosphorus in silicon is 0.35 [7]. Segregation coefficient is the ratio of the concentration of impurities in solid phase and concentration of impurities in liquid phase. This is shown in equation 1.1.

$$k = \frac{C_s}{C_l} \tag{1.1}$$

A segregation coefficient of 0.35 implies that 35% of phosphorus originally present in the liquid phase will solidify in silicon. Because of the high segregation coefficient, phosphorus is difficult to remove by directional solidification which is the traditional method of impurity removal.

It is expected that P introduced in raw materials to some extent is leached in hydro-metallurgical treatment in parts of the industry today. This assumption is based on the work of Meteleva-Fischer et al. [8] where they found that alloying metallurgical grade silicon with approximately 5% Ca lead to phosphorus migrating to inter-metallic phases and it was successfully removed during acid leaching. For production of ultra pure silicon, chemical processes are applied today. Examples of chemical processes are the Siemens process and Fluidized Bed Reactor. It is believed that phosphorus is distributed to other phases in the distillation of trichlorosilane. The downsides of these processes are that they have a high energy consumption and are not environmentally friendly.

Ferrosilicon is an alloying element of steel in addition to being a de-oxidizer of steel. Silicon steels have important electrical properties as it for instance increase the electrical resistivity of steel [9]. World Steel Association released in 2017 a short range outlook for 2017-2018. According to their forecast, the global steel demand will increase with 1.3 % in 2017. The total global steel demand will then be 1535.2 Mt [10]. In 2018 it is believed that the demand will reach 1548.5 Mt.

Basu (2007) studied the dephosphorization during steel making in his PhD thesis and made an overview of how phosphorus affects the various properties of steel [11]. An image is collected from his thesis and given in figure 1.1.

Table 1 : Effect of phosphorus in steel [2]

Property		Effect of phosphorus
Strength		++ (ferrite strengthener)
Bake hardenability		+
Ductility		– –
Fe-Zn galvanneal		may improve resistance to powdering
Phosphatability		+
Enamelling steels	Fish-scaling	–
	Pickling	+
Weldability		Not harmful for < 0.1 mass%
Core loss in motor laminations		– –
Fracture toughness		– –

+ increase ++ strong increase – decrease – – strong decrease

Figure 1.1: Image from Basu(2007) [11] presenting how phosphorus affects steel properties

The effect of phosphorus in steel can be both beneficial and detrimental. For instance phosphorus increases the tensile strength of low carbon sheet steel. Phosphorus has also shown to make steel brittle. Because phosphorus segregates to the grain boundaries in austenite and ferrite steels, it reduces hot ductility and promotes integranular failure [12].

Li et al. studied the effect of phosphorus on the micro structure and mechanical properties of strip cast iron steel [13]. They found that increasing the content of phosphorus made the grains finer. Phosphorus in steel reduced the plastic property of steels. Lowering the phosphors content in austenitic stainless steels, improves the resistance to stress corrosion [14].

1.1 Objectives

The aim of the master's thesis is two folded and deals with equilibrium distribution of phosphorus between FeSi/Si and CaO-SiO_2 slags in addition to the phosphorus distribution between slag, ferrosilicon and silicon. This is done to gain insight in the way phosphorus act in silicon and ferrosilicon as phosphorus is a problem in both silicon and ferrosilicon production. By the use of experimental data, it is possible to get a good thermodynamic understanding of phosphorus behaviour in a range of slag and alloy compositions. Investigating the distribution of phosphorus between slag and FeSi/Si is important to optimize phosphorus removal from both FeSi and Si. Literature on the distribution of phosphorus between slag and molten iron and between silicon and slag exist today. However, there is a lack of data in the literature for the distribution of P between Fe-Si and slag.

Experimental data will also be compared with equilibrium calculations in FactSage 7.1 [15].

1.1.1 Distribution of P between FeSi/Si and slag

Phosphorus equilibrium concentration of slag and metal will be determined after equilibrium experiments with $CaO-SiO_2$ slags doped with phosphorus together with Fe-Si or Si. Equal amounts of slag and metal in a graphite crucible will be inserted to a heated resistance heating furnace and held for three hours at 1600 °C. The compositions of FeSi that will be used are 20:80, 50:50 and 80:20 in wt%. Slag compositions used for the experiments will be 50:50, 43:57 and 65:35 wt% of SiO_2:CaO. All slags will be doped with 300 ppm of P by adding P_2O_5. After the experiments are conducted, slag and metal will be separated and analyzed by inductively coupled mass spectrometry(ICP-MS).

1.1.2 Distribution of P between FeSi, Si and slag

Slag made in the specialization project by the author will be used to perform distribution experiments which will be analyzed with electron probe micro analyzer (EPMA). The normalized slag composition is 45.8wt%CaO, 47.6wt% SiO_2 and 5.4 wt% P_2O_5. The experiments will be performed by holding the slag and FeSi (20:80 wt%) together at a temperature of 1600 °C for three hours, and then cooling it down with a rate of 1 °C per minute down to the solidification temperature of the metal which is 1360 °C. Then the furnace will be turned off. The controlled cooling is done to precipitate out silicon in addition to ferrosilicon when solidifying as according to solidification theory. The three phases will subsequently be analyzed using EPMA to evaluate the P distribution between them.

Chapter 2

Theoretical Background and Literature review

Since the master's thesis deals with phosphors in FeSi, Si and $CaO-SiO_2$ slag, the following chapter aims at getting an understanding of the micro structure and thermodynamics of phosphorus in FeSi, Si and slag. Phosphorus has shown to exist as different species in slag. Therefore various articles where the dominant phosphorus specie has been evaluated will be presented here.

A short evaluation of the thermodynamic and kinetic properties of phosphorus removal by slag has been conducted.

The experimental work deals with the distribution of phosphorus between FeSi or Si and CaO-SiO_2 slags. Therefore literature regarding the distribution equilibria of P between Si and slag and FeSi and slag has been reviewed. Literature on the distribution of P between Fe or steel and slag was also investigated in order to relate it to the experimental data found with refining of FeSi. The effect of slag basicity and oxygen potential on the phosphorus distribution has been especially studied.

2.1 P in Si

2.1.1 Microstructure

Jung et al.(2011) studied the micro-structure of Si after slag refining with $CaO-SiO_2-CaF$ slag. Electron probe micro analyzer was the analysis method used and the results are given in figure 2.1. Image a) presents the SEM image where the Ca_3P_2 compound is formed at the grain boundary. Images b)-d) are mapping images of P, Ca and Si respectively. From these images it is evident that phosphorus is more stable in the Ca phase than the Si phase. This is interesting

due to the fact that acid solutions will corrode silicon, but not the compound of calcium and phosphorus so that acid leaching can be used as an additional refining step to remove phosphorus from silicon.

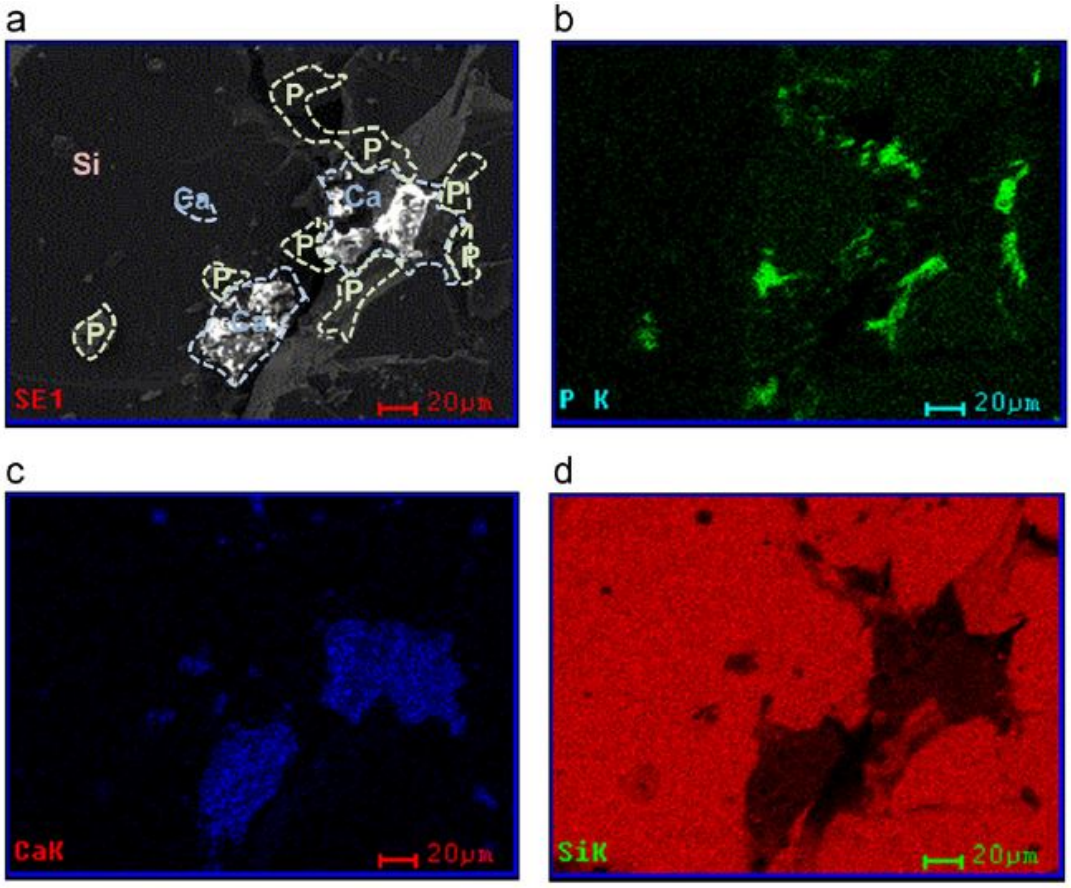

Figure 2.1: Image of Si after slag refining a: SEM image, b:mapping of P, c: mapping of Ca, d: mapping of Si.

Møll(2014) [16] found that phosphorus existed in a Al_2CaSi_2 inter-metallic phase when solidifying metallurgical grade silicon(MG-Si). Meteleva-Fischer et al.(2012) alloyed MG-Si with calcium and saw that the $FeSi_2Ti$ phase was enriched with phosphorus. Shimpo et al.(2004) [17] found that phosphorus existed in a $CaSi_2$ phase, however this was not observed by Meteleva-Fisher et al. The authors claim that the deviation might be because of Meteleva-Fisher et al. using materials with various impurities while Shimpo et al. used pure Si with 3 wt% P alloyed with Ca.

2.1.2 Thermodynamics of P in molten Si

Miki et al.(1996) studied the thermodynamics of phosphorus in molten Si [3]. The authors determined the Gibbs energy change, ΔG^o, of phosphorus dissolution in

molten Si at temperatures from 1450 to 1575 °C. The experiments were conducted by equilibrating a Si-P alloy with a controlled partial pressure of phosphorus in a gas mix of argon and phosphorus. 10 grams of alloy was used for graphite crucibles and 3 grams of alloy was used for alumina crucibles. The equilibrium time was found to be 151 ks (42 hrs). Samples were taken by sampling using a quartz tube and analyzed with spectrophotometry.

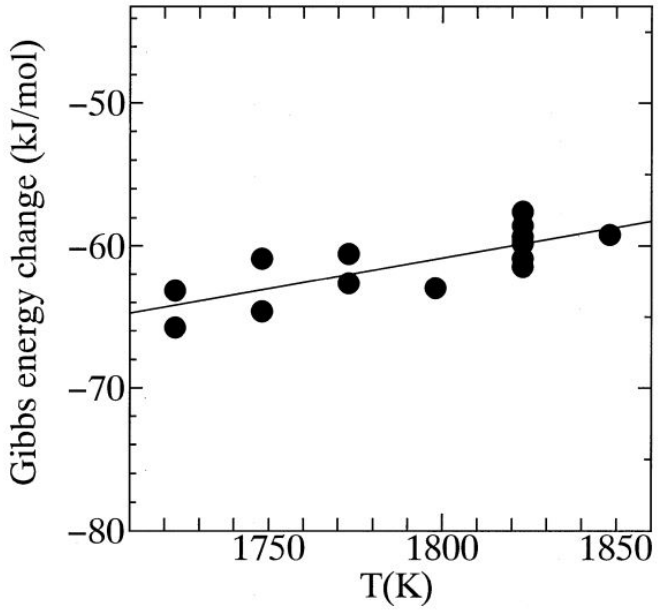

Figure 2.2: Image collected from Miki et al.(1996) presenting the Gibbs energy of dissolution of P in Si as a function of temperature.

The dissolution reaction of phosphorus into silicon is expressed by equation 2.1 and the Gibbs energy change of the P dissolution is shown in equation 2.2 and 2.3. From these equations, the Gibbs energy can be calculated from the measured phosphorus content in silicon at constant temperature and partial pressure of phosphorus. Here P_2 is the phosphorus partial pressure, R the gas constant, T absolute temperature and fp the activity coefficient of P in Si.

$$\frac{1}{2}P_2(g) = \underline{P}(\text{mass pct in Si}) \tag{2.1}$$

$$\Delta G^o = -\text{RTln}\frac{f_p \cdot [\text{mass pct P}]}{p_{p_2}^{1/2}} \tag{2.2}$$

$$\Delta G^o = -139,000(\pm 2000) + 43.4(\pm 10.1T)(J/mol) \tag{2.3}$$

The Gibbs energy change as a function of temperature is given in figure 2.2 for the dissolution of P in Si.

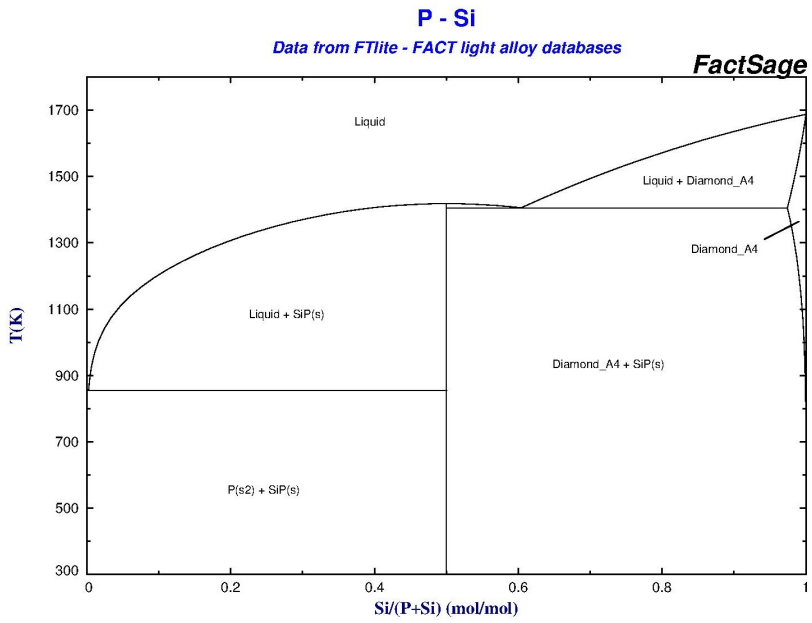

Figure 2.3: P-Si phase diagram from FactSage [15]

Miki et al.(1996) also calculated the Gibbs energy change of mono-atomic gas into silicon as presented in equations 2.4 and 2.5.

$$P(g) = \underline{P}(\text{mass pct in Si}) \tag{2.4}$$

$$\Delta G^0 = -387,000(\pm 2000) + 142(\pm 10T)(J/mol) \tag{2.5}$$

According to the authors, mono-atomic phosphorus vapour is dominant at a phosphorus concentration in silicon below 0.005 mass % P.

Shimpo et al.(2004) [17] studied the effect of Ca on P in Si. The authors equilibrated liquids of silicon and lead which were immiscible. They found that the interaction parameter between calcium and phosphorus in silicon is $\varepsilon^P_{CainSi} = -14.6(\pm 1.7)$. Since the interaction parameter is negative, this means that phosphorus is more stable in silicon due to calcium.

The Si-P phase diagram is found from FactSage FTlite database and given in figure 2.3. From the phase diagram we see that phosphorus solubility limit is 2.5 mole percent at 1132 °C.

2.2 P in Fe-Si

2.2.1 Microstructure

Horn et al.(1998) studied the micro-structure of FeSi75 alloys with respect to phosphorus [18]. The background for the study was that ferrosilicon alloys produced the toxic gas phosphine when wet. Previous research from Michigan Tech has shown that phosphides of Al and Ca exist in FeSi45 and FeSi65 with 10 wt% Mn and 0.13 to 1.2 wt% P. These alloys were made in the laboratory. The phosphides were present as inclusions at the interface between silicon and $FeSi_2$. Horn et al.(1998) studied commercial FeSi alloys in addition to synthetic alloys to determine the presence of phosphorus in FeSi75. According to the FeSi-phase diagram, the phases present in FeSi75 should be $FeSi_2$ and Si. The micro-structure they found with scanning electron microscope (SEM) consisted of silicon dendrites surrounded by $FeSi_2$ matrix. In addition they found micro cracks in the $FeSi_2$ matrix. The authors believed that the reason why the cracks existed was because of a higher thermal expansion coefficient of $FeSi_2$ than Si. Both the commercial and synthetic alloys showed a phosphorus rich inclusion phase at the interface between Si and $FeSi_2$. It appears that the inclusions formed at the end of in the micro cracks. Figure 2.4 depicts the phosphide inclusions in FeSi75. The difference between the commercial alloys and the synthetic alloys was that the synthetic alloys contained larger inclusions in number and size. The main phosphides were of calcium (Ca_3P_2), aluminum (AlP) and magnesium (Mg_3P_2). Phosphorus present as phosphides could react with moisture through the micro cracks and produce PH_3. Phosphorus might also be present as stable phosphorus which is believed to exist as solid solution in the $FeSi_2$ phase. Figure 2.5 gives an overview of the amount of stable phosphorus and the amount of phosphorus as phosphide inclusions in four commercial alloys.

Table II. Phosphorus Distribution in Commercial Ferrosilicon Alloys

Commercial Ferrosilicon	Stable P (Wt Pct)*	Reactive P (Wt Pct)**	Total P (Wt Pct)†	Pct of P as PH_3‡
Commercial 1	0.017	0.006	0.023	26.1
Commercial 2	0.016	0.004	0.020	20.0
Commercial 3	0.015	0.007	0.022	31.2
Commercial 4	0.016	0.005	0.021	23.8

Figure 2.5: Table from Horn et al.(1998) [18] presenting where phosphorus is present in commercial ferrosilicon alloys.

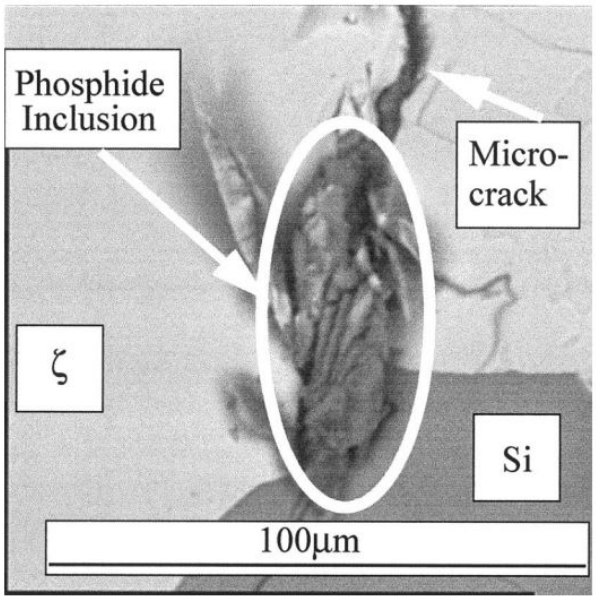

Figure 2.4: Figure of the position of phosphide inclusions in a commercial FeSi75 alloy. The image is taken from Horn et al.(1998) [18].

2.2.2 Thermodynamics of P in molten FeSi

Ueda et al. (1997) [19] studied the thermodynamics of phosphorus in molten Si-Fe at 1723 K(1450°C) for an alloy containing one mole fraction of P and between 0 and 65 mole % Fe. The basis for the study was to evaluate the process for removal of phosphorus from ferrosilicon. This was done by equilibrating the Si-Fe-P alloy in argon which was de-oxidized. The partial pressure of phosphorus was controlled.

The dissolution of phosphorus in the alloy is described in equation 2.6.

$$\frac{1}{2}P_2(g) = \underline{P}(X)_{\text{in Si}} \tag{2.6}$$

The equilibrium constant,K, is described in equation 2.7. X_P is the mole fraction of phosphorus, γ_P is the activity coefficient of phosphorus in the alloy and P_{P_2} is the phosphorus partial pressure.

$$K = \frac{\gamma_P \cdot X_P}{P_{P_2}^{\frac{1}{2}}} \tag{2.7}$$

Taking the logarithm of both sides of equation 2.7, gives equation 2.8.

$$lnK = ln\gamma_P + lnX_P - \frac{1}{2}lnP_{P_2} \tag{2.8}$$

A graphite crucible was used, so the activity coefficient of phosphorus can be described as equation 2.9.

$$ln\gamma_P = ln\gamma_P^{Fe} + ln\gamma_P^P + ln\gamma_P^C \tag{2.9}$$

The authors neglect the effect of carbon content because of the low solubility of carbon in silicon due to SiC formation. In addition they assume that Henry's law is applicable for SiP when the amount of phosphorus is below 0.1 mass pct. The self-interaction activity coefficient of phosphorus,γ_P^P, is also neglected. The interaction coefficients, ε_P^{Fe} and ρ_P^{Fe} are first and second order respectively. These are introduced in equation 2.10. Equation 2.11 can be used to find the values of the interaction coefficients by plotting the left hand side of the equation as a function of X_{Fe}. This is done in figure 2.6b. The interaction coefficients ε_P^{Fe} and ρ_P^{Fe} are found by regression as 7.43 and -16.4 respectively.

$$lnK = \varepsilon_P^{Fe} X_{Fe} + \rho_P^{Fe} X_{Fe}^2 + lnX_P - \frac{1}{2} lnP_{P_2} \tag{2.10}$$

$$\frac{lnK - lnX_P + \frac{1}{2} lnP_{P_2}}{X_{Fe}} = \varepsilon_P^{Fe} + \rho_P^{Fe} X_{Fe} \tag{2.11}$$

The regular solution model is introduced, and the activity coefficient of phosphorus is shown in equation 2.12

$$ln\gamma_P = 7.43 X_{Fe} - 16.4 X_{Fe}^2, (0 \leqslant X_{Fe} \leqslant 0.65) \tag{2.12}$$

Figure 2.6a shows how the phosphorus content decreases below X_{Fe} =0.23 when iron is added to silicon at a temperature of 1723K (1450 °C) and a partial pressure of phosphorus of $1.84 \cdot 10^{-1}$ Pa. At values of X_{Fe} larger than 0.23, the phosphorus content increases.

Alloying of silicon with iron up to X_{Fe}=0.23 increases the phosphorus activity coefficient. The ternary regular solution is used as shown in equation 2.13 where the excess Gibbs energy of mixing silicon with iron is are given on mole fraction basis. Ueda et al. claim that strong interactions between Fe and Si could explain the shift shift in phosphorus content in the alloy with increasing iron content.

$$\Delta\overline{G}_{P(Si-Fe)} = X_{Si}\Delta\overline{G}_{P(Si)} + X_M\Delta\overline{G}_{P(Fe)} - \Delta G_{(Si-M)}^{Fe,excess} \tag{2.13}$$

Figure 2.6c show the calculated $\Delta\overline{G}_{P(Si-Fe)}$ and γ_P where the black dots are from the article of Ueda et al. and the other values are from other articles. The authors state that the deviations of the measurements from the estimations are due to assumptions made which might not be accurately enough. The regular solution model includes the interactions of the three binaries. However, the interactions of the atoms of the ternary Si-P-Fe might be different.

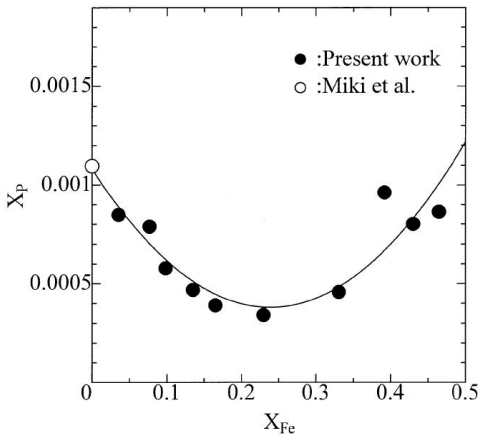

(a) X_P as a function of X_{Fe} at T=1723K, $P_{P_2} = 1.84 \cdot 10^{-}1Pa$.

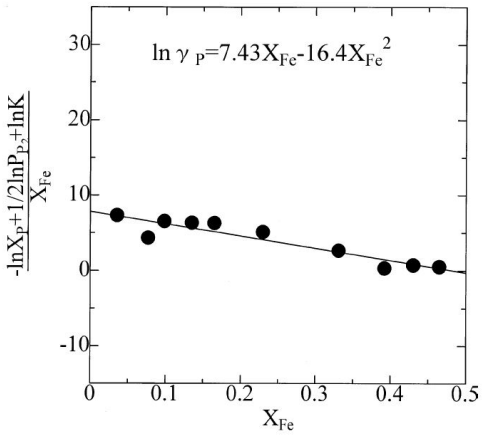

(b) Graph for determination of interaction coefficients.

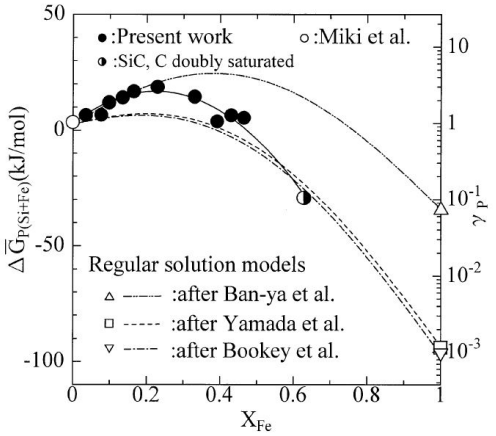

(c) Graph showing $\Delta \overline{G}_{P(Si+Fe)}$.

Figure 2.6: Figures from Ueda et al. presenting thermodynamics of P in molten Si-Fe.

Calcium addition is also discussed as a method to increase the removal of phosphorus. It is believed that Ca_3P_2 is formed as presented in equation 2.14

$$3Ca(l) + P_2(g) = Ca_3P_2 \tag{2.14}$$

Standard Gibbs energy of formation of reaction 2.14 is shown in equation 2.15

$$\Delta G^0 = -653460 + 144.01T(J/mol) \tag{2.15}$$

When Henry's law applies because of a low enough phosphorus content in the Fe-Si alloy, and the formation of Ca_3P_2 occurs, the phosphorus content can be expressed as in equation 2.16. It is then possible to find the phosphorus content at a specified calcium activity as a function of iron content.

$$X_P^2 \cdot a_{Ca}^3 = exp\Big(\frac{-2 \cdot \Delta\overline{G}_{P(Fe-Si)} - \Delta G^0}{RT}\Big) \tag{2.16}$$

Lynch(2009) used the data from Ueda et al.(1997) and presented the activity coefficient of P in Si-Fe molten alloy at 1723K(1450 °C) as a function of iron content. This is presented in figure 2.7. Here negative logarithmic values of the activity coefficient means that at this composition phosphorus in Fe-Si is less volatile and more stable than in silicon. Therefore an iron content higher than 65% gives a lower volatility in ferrosilicon than in silicon.

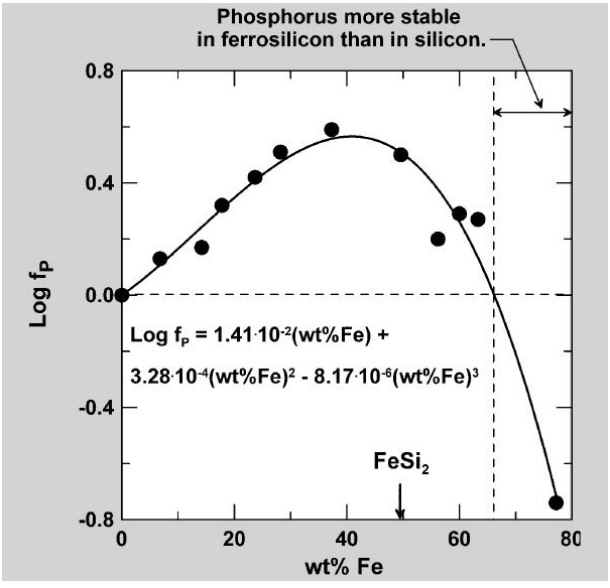

Figure 2.7: Figure from Lynch presenting the activity coefficient of P in Fe-Si [20].

2.3 P in slag

Dephosphorization in steel is mainly done by an oxidizing reaction so that phosphorus is transferred to slag as phosphate, $PO_4{}^{3-}$, by the reaction in equation 2.17. Dephosphorization of silicon and ferrosilicon on the other hand, should be done under reducing conditions in order to avoid oxidizing silicon rather than phosphorus. If phosphorus dissolve in the slag melt as a phosphide ion, the reaction is as shown in equation 2.18.

$$[P] + \frac{5}{4}O_2 + \frac{3}{2}O^{2-} = PO_4{}^{3-} \tag{2.17}$$

$$[P] + \frac{3}{2}O^{2-} = P^{3-} + \frac{3}{4}O_2 \tag{2.18}$$

The species in the slag are believed to be Ca_3P_2 for phosphide and Ca_3PO_4 for phosphate.

Several researchers have studied the phosphide and phosphate concentration as a function of oxygen potential using a variety of slag types. Table 2.1 gives and overview of articles where the dominant specie of phosphorus in slag as phosphate, $PO_4{}^{3-}$ or phosphide, P^{3-} is determined.

Table 2.1: Comparison of dominant phosphorus species at different experimental conditions.

Authors	Reference	P_{O_2}	atm.	temp.	slag	metal	eq.time	dominant specie	max Lp
Momokawa and Sano	[21]	$2.09 \cdot 10^{-20} - 9.12 \cdot 10^{-17}$	Ar-CO	1400-1550°C	$CaO\text{-}Al_2O_3$	Ag-P	9hrs	at 1550 °C P^{3-} at $P_{O_2} < 10^{-18}$	-
Tabuchi and Sano	[22]	$7.24 \cdot 10^{-18} - 1.82 \cdot 10^{-16}$	Ar-CO	1400-1550 °C	$CaO - CaF_2$	Fe-P-Al	1 hr	at 1550 °C P^{3-} at $P_{O_2} < 1.1 \cdot 10^{-16}$	-
Johnston and Barati	[23]	$10^{-19} - 4 - \cdot 10^{-18}$	Ar	1500°C	$Al_2O_3 - CaO - MgO - SiO_2$	Si	2hrs	$PO4^{3-}$	≈ 8.8
Kawamura et al.	[24]	-	Ar		$CaO\text{-}CaF_2$	Si	3hrs	P^{3-} and some $PO_4{}^{3-}$	0.6
Fujiwara	[25]	-	Ar	1600 °C	$CaO - Al_2O_3 - SiO_2$	Si-Al-Ca	5hs	P^{3-}	3
Li et al.	[26]	PO2 crit= $1.7 \cdot 10^{-19}$	Ar	1500°C	$CaO - Na_2O - Al_2O_3 - SiO_2$	Si-Cu	10 min	$PO4^{3-}$	1.1
Jung et al.	[27]	$1.5 \cdot 10^{-21} - 1.5 \cdot 10^{-18}$	Ar-H_2	1500 °C	$CaO - SiO_2 - CaF_2$	Si	12 hrs	P^{3-}	2.5

Momokawa and Sano(1982) [21] studied the effect of oxygen potential on phosphorus in the $CaO - Al_2O_3$ system. They equilibriated $CaO - Al_2O_3$ which was saturated with respect to $CaO{\cdot}Al_2O_3$ with Fe-P-Al alloys at 1500 °C for one hour in argon atmosphere. According to the authors, the amount of phosphide and phosphate in the system varies with varying oxygen partial pressure which in turn is dependent on the slag composition, temperature and partial pressure of phosphorus. The authors calculated the oxygen potential from the aluminium content in the alloy according to equation 2.19.

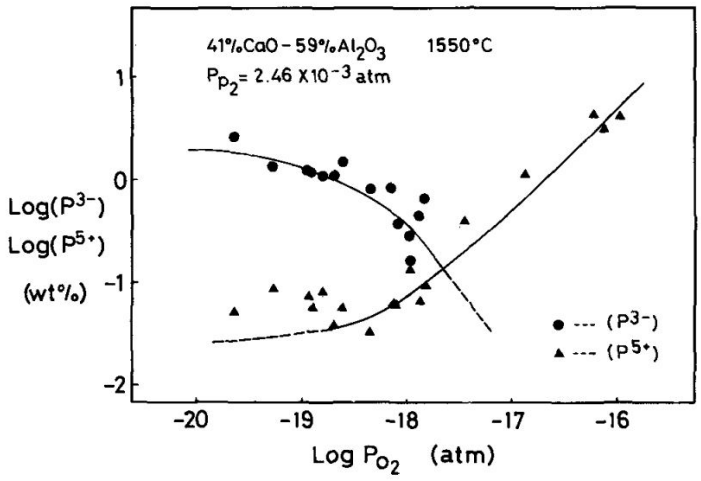

Figure 2.8: Figure from Momokawa and Sano presenting the effect of oxygen potential on the dominating specie of phosphorus in the slag.

$$logP_{O_2}(atm) = -21.3 - 1.33log(\gamma_{Al} \cdot N_{Al}) \tag{2.19}$$

Figure 2.8 from Momokawa and Sano gives the phosphate and phosphide concentrations as a function of oxygen potential. Phosphate ($PO_4{}^{3-}$) is the predominant specie in the oxide melt when the oxygen potential, P_{O_2}, is larger than 10^{-18} atm. At lower oxygen potentials, phosphide (P^{3-}) is the predominant specie. Oxygen ions comes from basic oxides like CaO dissociating as shown in equation 2.20. Oxygen potential arises from the equilibrium in equation 2.21.

$$CaO = Ca^{2+} + O^{2-} \tag{2.20}$$

$$SiO_2 = Si + O_2 \tag{2.21}$$

Tabuchi and Sano (1984) studied the thermodynamics of phosphorus in CaO-CaF melts [22]. The authors equilibriated Ag-P alloy with $CaO-CaF_2$ slag using a graphite boat and CO-Ar gas mixtures for 1 hour at temperatures from 1400 to 1550 °C. The effect of oxygen potential was similar to what was found by Momokawa and Sano(1982) with $PO_4{}^{3-}$ dominating at higher oxygen potentials and P^{3-} dominating at lower oxygen potentials. This is illustrated in figure 2.9a. Temperature dependence is also given in the same figure, and increasing temperature gives an increased oxygen potential where the predominating specie changes from phosphide to phosphate. According to the figure, the oxygen potential decreases by approximately one order of magnitude with an increase in temperature of 50 °C. Therefore one can assume that at 1600 °C, the oxygen potential where

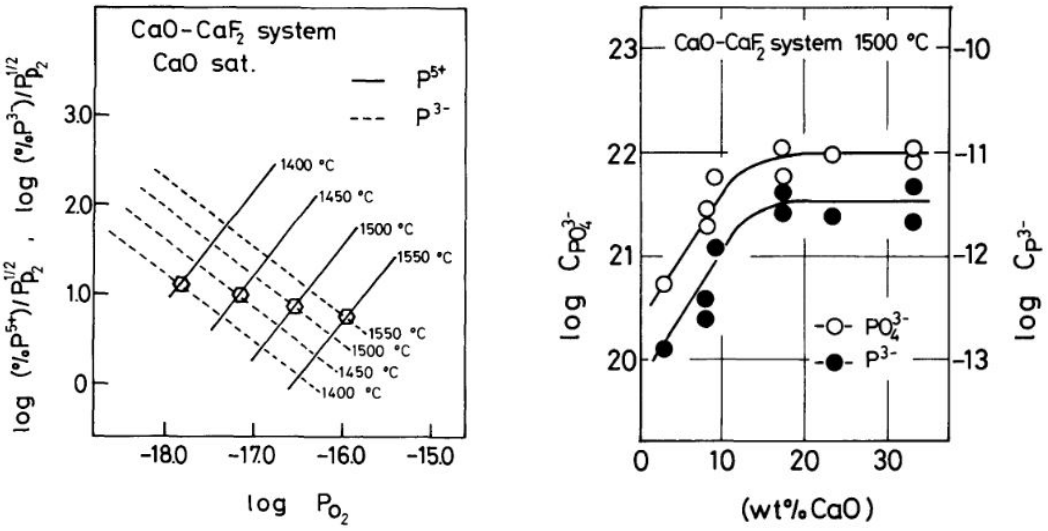

(a) Figure from Tabuchi et al. [22] presenting predominant specie of phosphorus in $CaO-CaF_2$ system saturated with CaO with varying oxygen potential.

(b) Figure from Tabuchi et al. [22] presenting the effect of wt% CaO on the concentration of phosphide and phosphate.

Figure 2.9: Figures from Tabuchi et al. [22]

the dominant specie changes would be approximately 10^{-15} atm. Figure 2.9b gives the phosphide and phosphate concentration in the $CaO-CaF_2$ melt as a function of wt% of CaO. The concentration of both ions increase up to 20 wt% of CaO which is the solubility of CaO in CaF_2. Then the concentration stabilizes.

Johnston and Barati(2010) [23] discussed the dominant phosphorus species in slag in their article. They found the oxygen potential in the system from calculations in FactSage to be in the order of 10^{-19} to $4 \cdot 10^{-18}$. The authors then referred to the article by Momokawa and Sano [21], described earlier in this thesis, and said that the both phosphate and phosphide should be present at these oxygen potentials. The authors then say that FactSage calculations give phosphate as the stable form of phosphorus. This is however expected because as known by the author of this thesis, phosphide is not included into the database in FactSage.

Kawamura et al.(2013) equilibriated MG-Si with $CaO-CaF_2$ slags at 1450 and 1500 °C [24]. They used a wet chemical method and determined that phosphorus was removed into the slag phase as mainly P^{3-}, but partly also by $PO4^{3-}$. After the crucible was cooled down, slag and metal were separated quickly in order to hinder phosphide hydration. Determination of the different P species were done by dissolving slag in HCl with flow of Ar gas. P^{3-} then evaporates as PH_3, and can be trapped by bromine water. $PO4^{3-}$ dissolves in the solution.

Fujiwara et al.(1996) equilibriated Si-Al-Ca alloy with $CaO-SiO_2-Al_2O_3$ slag

in Ar gas for 5 hours at 1600°C. They found that phosphorus was mainly present as phosphide in slag using the bromine water absorption method as described previosly. The authors claim that the removal of phosphorus will happen according to equation 2.18. If the basicity increases, the oxygen potential between flux and metal will decrease and according to Le Chatelier's principle the reaction in equation 2.18 will move towards the right producing more P^{3-}.

The phosphide capacity of a slag can be seen as a ability of a slag to take up phosphorus from the metal. It can be calculated from equation 2.18 and given in equation 2.22.

$$C_{P^{3-}} = \frac{(\%P^{3-})p_{O_2}^{3/4}}{p_{P_2}^{1/2}} \tag{2.22}$$

The oxygen potential given in the equation above, P_{O_2}, can be calculated according to equation 2.23 if Raoult's law is assumed applicable to the activity of silicon in the alloy.

$$logP_{O_2} = log(a_{\mathrm{SiO_2}}/X_{Si}) + \Delta G^0_{\mathrm{SiO_2}}/(2.303RT) \tag{2.23}$$

The phosphorus vapor pressure in equation 2.22 can be calculated according to equation 2.24 if Henry's law is assumed applicable for P in Si and if P is not affected by Ca or Al in the alloy. Here R is the gas constant,T the absolute temperature, a_{SiO_2} activity of SiO_2, X_{Si} mole fraction of silicon and $\Delta G^0_{SiO_2}$ the formation Gibbs energy of SiO_2.

$$logP_{P_2} = 2log[\%P] + 2\Delta G^0_P/(2.303RT) \tag{2.24}$$

Fujiwara et al.(1996) calculated the phosphide capacity of the $CaO-Al_2O_3-SiO_2$ slag and made a graph also containing the phosphide capacity from other literature sources. This graph is given in figure 2.10. It appears that slag of $CaO-Al_2O_3$ has the greatest phospide capacity.

Li et al. (2014) equilibriated Si-Cu alloy with $CaO-Na_2O-Al_2O_3-SiO_2$ in Ar atmosphere, 1500 °C for 10 minutes. The authors calculated the partial pressure of oxygen in FactSage from the equilibrium of SiO_2 and Si and determined a critical partial pressure where balance of oxygen potential and basicity gave the highest distribution. This critical partial pressure was equal to $1.7 \cdot 10^{-19}$. It is assumed in the article that phosphorus oxidizes to ${PO_4}^{3-}$ according to equation 2.17.

Jung et al.(2011) performed slag refining and acid leaching to remove phosphorus from Si. $CaO-SiO_2-CaF_2$ slag was heated with upgraded metallurgical silicon for 12 hrs at 1500 °C in an Ar-10% H_2 gas mixture. The authors assume that the distribution of phosphorus towards slag phase happens according to reaction 2.18

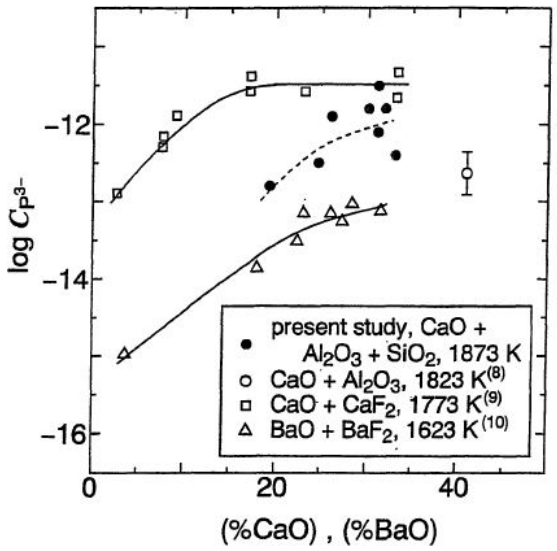

Figure 2.10: Image from Fujiwara et al.(1996) giving the phosphide capacity of different slags [25].

since increasing the oxygen potential lead to a decrease in the distribution of P towards slag phase. CaF_2 has according to Park et al.(2012) [28] shown to decrease the viscosity of $CaO-SiO_2-CaF_2$ slag from 0.3 to 0.1 Pa· s by increasing the CaF_2 concentration from 0 to 15 wt%. This is the case for a basicity of slag (CaO/SiO2) of 1. The structural reason for this decrease in viscosity is believed to be because of CaF_2 decreasing the degree of polymerization.

Sakamoto et al.(2012) [29] used magic angle spinning nuclear magnetic resonance (MAS-NMR) to find the local structure around phosphorus and silicon in the $CaO-SiO_2-PO_{2.5}$ system. They made slag by mixing SiO_2, $Ca_3(PO_4)_2$ and CaO and heating the mix to 1873K(1600 °C) in an electrical furnace and holding it for 1 hr in air. After the experiment was finished, the samples were quenched in water. Since the atmosphere is air, the experiments are conducted under oxidizing conditions. The authors found indications of that mono-phosphate complex ion, $PO_4{}^{3-}$ was the main component of phosphorus and the phosphate concentration did not change the dominant specie as suggested by Tagaya et al [30]. However there were small amounts of di-phosphate complexes ($P_2O_7{}^{4-}$) present. Since mono-phosphate complexes are the dominant species, the slag metal reaction in equation 2.17 is dominant.

Sakamoto et al.(2012) suggest that the chance of phosphorus consuming oxide ions and producing mono-phosphate are larger than silicon consuming oxide ions. The structure around the silicon atoms varied with the concentration of $PO_{2.5}$. By adding more $PO_{2.5}$, there is an increasing polymerization of the silicate network

where non-bridging oxygen atoms coordinated to silicon are exchanged with the bridging oxygen atoms coordinated to phosphorus. This means that there was a decrease in the number of non-bridging oxygen atoms around the silicon atom with increasing phosphate concentration.

2.4 Properties of slags for refining

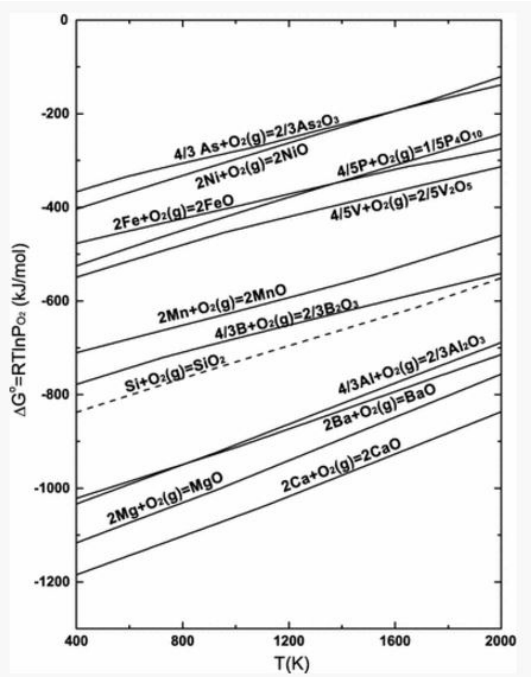

Figure 2.11: Ellingham diagram from Johnston et al.(2012) [31].

The slags used in the experimental work of this thesis are $CaO-SiO_2$ slags. The slag constituent SiO_2 is chosen to avoid high losses of silicon to the slag. CaO is chosen because it has a lower value of Gibbs free energy than SiO_2, which means that it is more stable and should not reduce into silicon as less stable oxides would do. The Ellingham diagram in figure 2.11, shows the relative stability of different oxides. Phosphorus is according to the diagram less stable as an oxide than silicon dioxide as its oxidation line lies at higher Gibbs energy than oxidation of silicon. However this is only the case if phosphorus works as an ideal solute in slag and silicon.

2.5 Kinetics of phosphorus removal

Krystad et al.(2012) studied the kinetics of boron transfer in slag refining of silicon. They found that the equilibrium time of boron transfer is approximately equal to 2 hours at 1600 °C with a slag composition of 50:50(wt%) CaO : SiO_2. Figure 2.13 is collected from Krystad et al.(2012) and gives the boron concentration in silicon as a function of time with equilibration with slags of various compositions. The equilibrium time is dependent on the diffusivity of the specie which can be represented by the Stokes-Einstein equation 2.25. Here k_B is the Boltzmann's constant, T is the absolute temperature, η represents the viscosity and r is the radius of a spherical particle in a fluid. However, as claimed by Jakobsson (2013), we do not have diffusion of spherical particles in the slag-silicon system [32], which makes the Stoke-Einstein equation not accurate. The equation can be used as an indication of what affects the diffusivity.

$$D = \frac{k_B T}{6\pi\eta r} \tag{2.25}$$

The diffusion coefficient of B and P in silicon is given in figure 2.12 as a function of temperature. As presented in the figure, the diffusion coefficients of B and P are almost equal in the given temperature range. Delannoy(2012) reported a molecular diffusivity,D, of P in liquid Si equal to $10^{-8} m^2/s$.

As mentioned previously, the viscosity influences the diffusivity as shown in equation 2.25. Figure 2.14 is collected from the Slag Atlas(1995) and shows that at a given temperature, the viscosity increases with increasing SiO_2 content of the $CaO-SiO_2$ slag. Therefore one would expect a slower mass transfer rate with increasing SiO_2 content or acidity of the slag. In this thesis the most acidic slag used is a slag with composition of SiO_2 : CaO 65:35(wt%).

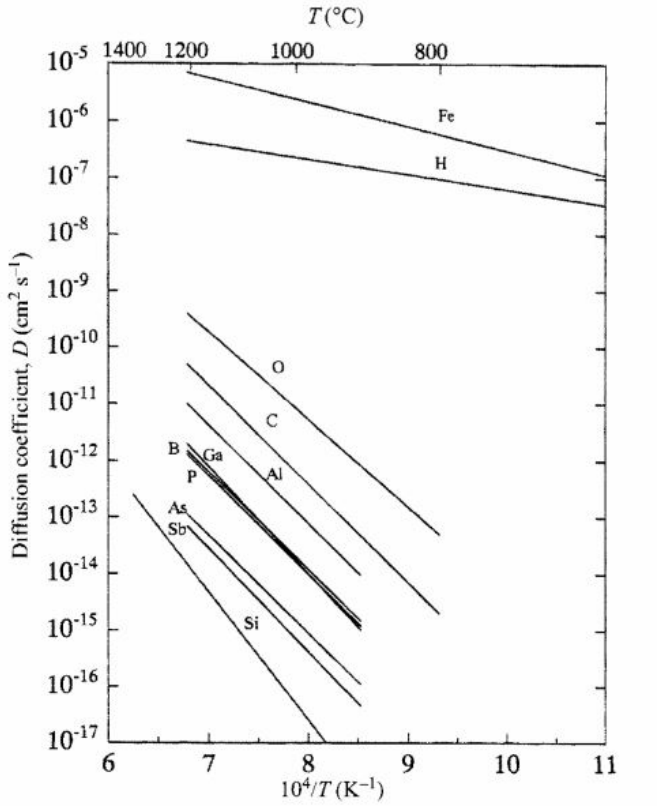

Figure 2.12: Figure from Encyclopedia of Materials- Science and Technology(2001) presenting the diffusion coefficient of dopants in silicon [33].

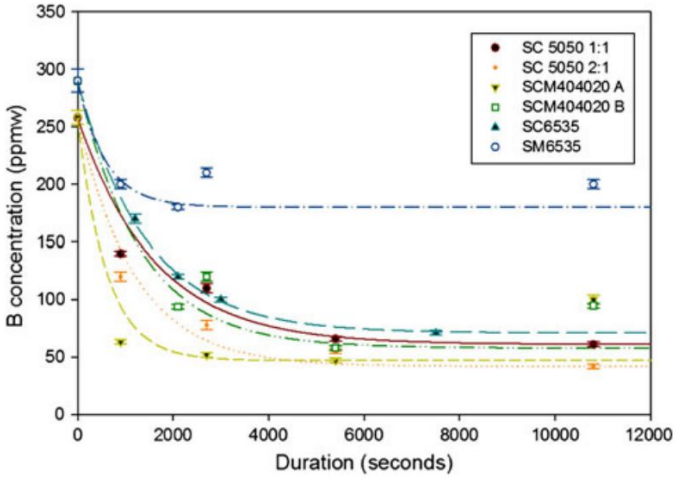

Figure 2.13: Equilibrium time for boron in silicon for equilibration with $CaO-SiO_2$(SC), $CaO-MgO-SiO_2$(SCM) and $MgO-SiO_2$(SM) slags from Krystad(2012) [34].

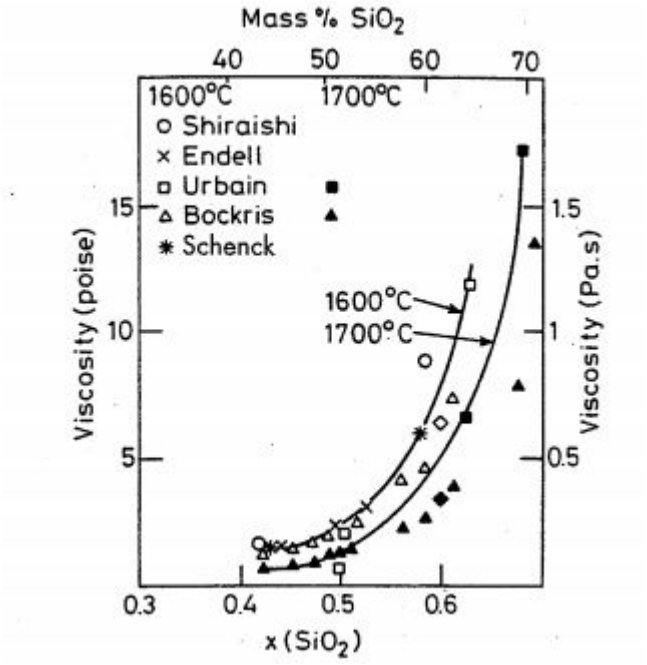

Figure 2.14: Viscosity as a function of SiO_2 content of SiO_2-CaO slag collected from Slag Atlas [35].

Bel'tyukov et al.(2014) made an overview of the kinematic viscosity of liquid FeSi alloy at 1600 °C as a function of silicon content found from different sources [36]. Figure 2.15 presents the figure collected from Bel'tyukov et al. As seen from the figure, the viscosity decreases with increasing Si content. The maximum Si content studied by the authors is 50 at%.

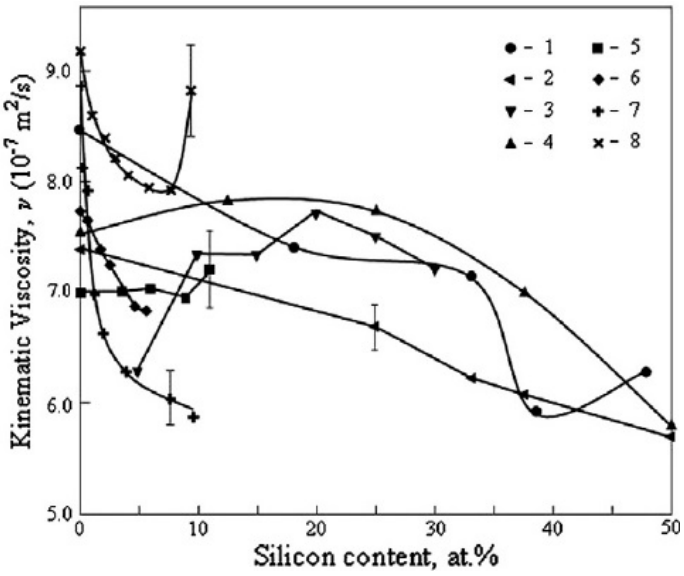

Figure 2.15: Figure from Bel'tyukov et al.(2014) [36] giving the kinematic viscosity of liquid FeSi at 1600 °C up to 50 at% of Si.

Nishimoto et al.(2012) found that the mass transfer of boron between Si and $CaO-SiO_2$ slag was controlled by mass transfer in slags [37]. If we assume that the mass transfer of phosphorus is similar to boron, the viscosity of the metal should not affect the mass transfer significantly.

2.6 Distribution equilibria of phosphorus between metal and slag phases

2.6.1 Distribution of P between Si and Fe-Si

Esfahani and Barati (2011) [38] alloyed metallurgical grade silicon with iron and formed an alloy with composition Si-28w% Fe. Phosphorus was also added to the mix in order to detect it in the analysis. The experiments were conducted in a muffle furnace with argon atmosphere at a temperature of 1550 °C. The holding time was four hours and the sample was cooled down slowly to 1007°C before it was quenched in water. The authors observed that there were silicon dendrites distributed within $FeSi_2$ particles. These are depicted in figure 2.16 which is collected from the article. The dark areas are the Si dendrites while the lighter areas are the $FeSi_2$ phases. The article presents several properties of iron which makes it a good candidate as a phosphorus getter. Iron has a low solubility in Si, only 0.018 ppmw at 1000°C and because of the low segregation coefficient of Fe in Si of $8 \cdot 10^{-6}$, it is possible to remove the remaining Fe through directional solidification. In addition iron has a high affinity of phosphorus. The economic and environmental reasons are high abundance and low cost in addition to the possibility of recycling the ferrosilicon.

Khajavi and Barati(2012) [39] did similar experiments as Esfahani and Barati, and studied the distribution of phosphorus between solid silicon and melt of iron-silicon 20-80 (wt%)(Fe-Si) using solvent refining. They alloyed silicon(99.998%) with iron and phosphorus. Experiments were performed by heating powders of each material to 1600 °C, keeping it for 4 hours, then cooling it down to 1300 °C and holding it at this temperature for 1 hour before quenching it in water. As Esfahani and Barati, they found that purified silicon crystals grew from Fe-Si melt while iron worked as a trapper of phosphorus impurities. The distribution coefficient is calculated according to equation 2.26.

$$K_p = \frac{C_{PinsolidSi}}{C_{PinFe-Simelt}} \tag{2.26}$$

They found that the distribution coefficient had a lower value than 0.35 at tem-

Figure 2.16: Image from Esfahani and Barati showing Si dendrites inside $FeSi_2$ matrix.

peratures above 1285 °C. A decrease in the distribution coefficient means that the concentration of phosphorus in the solid silicon decreases relative to the phosphorus content in the Fe-Si melt. Khajavi and Barati states that for silicon crystals to form at the equilibrium position at temperatures above the eutectic temperature, the alloy should contain more than 58.2% of Si. This is also evident from the phase diagram of Fe and Si in figure 2.17.

Interaction parameter between P and Fe

Khajavi and Barati(2012) [39] calculated the interaction parameter between iron and phosphorus in solid silicon, $\varepsilon^{P}_{\text{Fe in solid Si}}$, at temperatures 1210°C, 1260 °C and 1310 °C.

The interaction parameter of Fe on P, $\varepsilon^{P}_{\text{Fe in solid Si}}$ was calculated by the use of equations 2.27 through 2.29 and by plotting $\ln X_{\text{Fe in solid Si}}$ vs $X_{\text{P in solid Si}}$.

$$\frac{\Delta G^{\circ fus}_{M}}{RT} + ln a_{\text{Fe in Fe-Si melt}} = ln a_{\text{Fe in solid Si}} = ln\gamma_{\text{Fe in solid Si}} + ln X_{\text{Fe in solid Si}} = C(const) \tag{2.27}$$

$$ln\gamma_{\text{Fe in solid Si}} = ln\gamma^{\circ}_{\text{Fe in solid Si}} + \varepsilon^{Fe}_{\text{Fe in solid Si}} X_{\text{Fe in solid Si}} + \varepsilon^{P}_{\text{Fe in solid Si}} X_{\text{P in solid Si}} \tag{2.28}$$

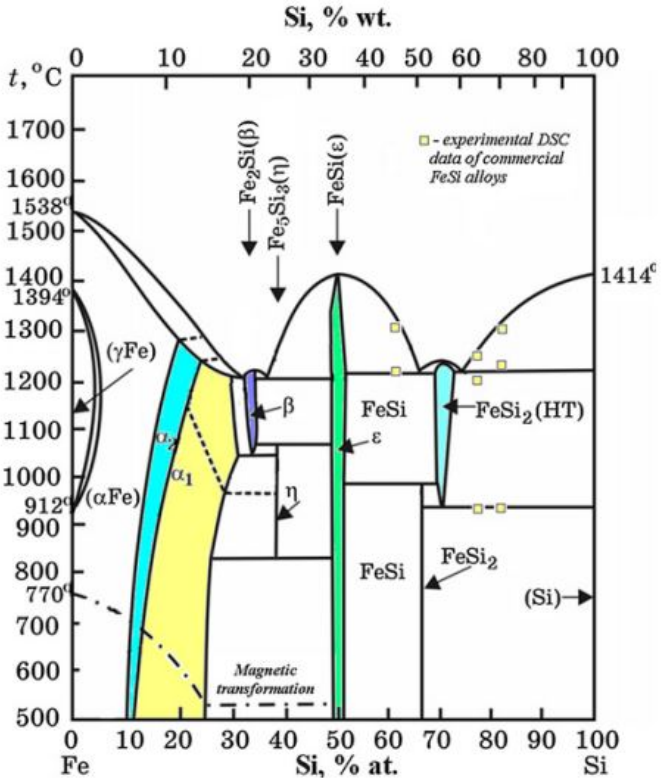

Figure 2.17: Phase diagram of Fe-Si from the Handbook of Ferroalloys [40].

$$ln X_{\text{Fe in solid Si}} = -\varepsilon^{P}_{\text{Fe in solid Si}} X_{\text{P in solid Si}} - ln\gamma^{\circ}_{\text{Fe in solid Si}} + C \tag{2.29}$$

Several assumptions were made. The activity of Fe in the alloy melt,a_{Fe}, is assumed constant because of a relatively constant amount of phosphorus in the Fe-Si melt. The self-interaction parameter of iron,ε^{Fe}_{Fe}, is considered equal to zero because of the low content of iron in solid silicon. The values of the interaction parameters were $\varepsilon^{P}_{\text{Fe in solid Si}}$ (1210 °C)=-1475, $\varepsilon^{P}_{\text{Fe in solid Si}}$ (1260 °C)=-4688 and $\varepsilon^{P}_{\text{Fe in solid Si}}$ (1310 °C)=-6115. Since the values are large and negative, this implies a great affinity of iron for phosphorus in silicon.

2.6.2 Distribution of P between slag and Si

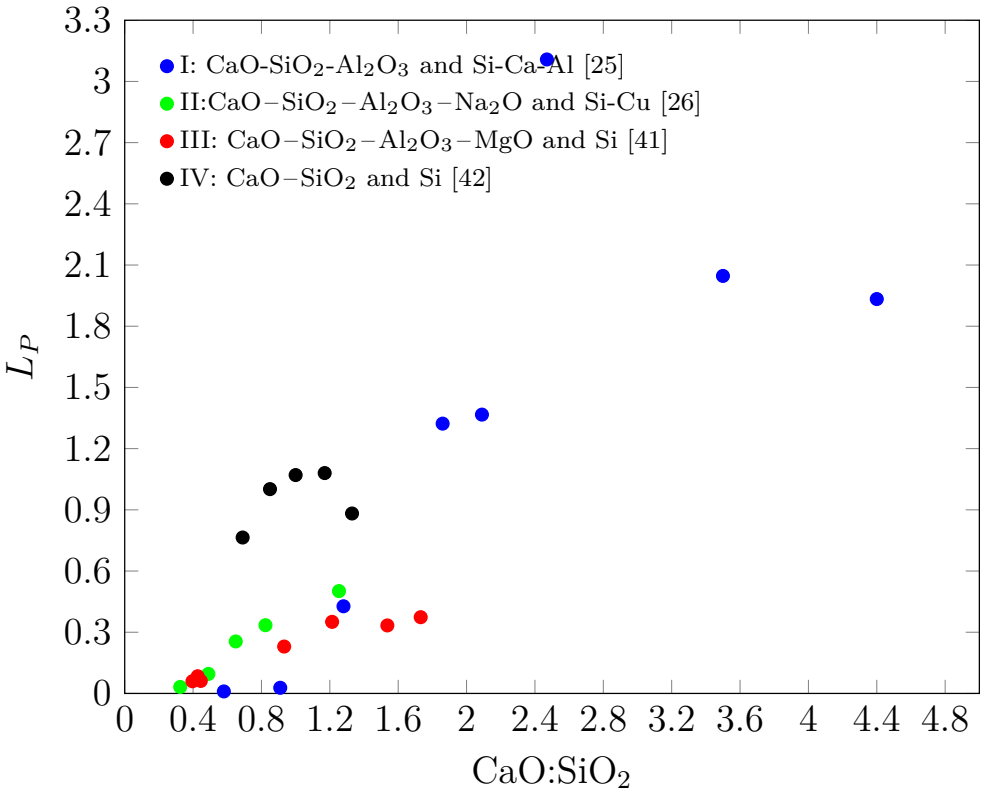

Figure 2.18: Distribution coefficient from various articles.

The distribution coefficient is given in equation 2.30 and can be used as a measure of how well slag removes phosphorus from metal. A distribution coefficient larger than 1, indicates a preference of phosphorus going into the slag phase. However if the value is lower than one, there is a preference of phosphorus going into the metal phase. Figure 2.18 presents the distribution coefficient as a function of the ratio of CaO and SiO_2 in the slag. Data utilized in the graph is collected from articles with various slag compositions as presented in the labels. Some of the articles use silicon alloyed with another metal like Cu or Al. The general trend is that the distribution coefficient increases with increasing CaO content of slag.

$$L_P = \frac{(wt\%P)_{slag}}{[wt\%P]_{metal}} \tag{2.30}$$

The following literature presents a review of the available articles for the distribution of P between Si and slag and between Si alloyed with another metal and slag.

Johnston and Barati(2010,2011,2012)

Johnston and Barati(2011) studied how slag basicity and oxygen potential affected the distribution of phosphorus between slag and silicon [41]. The type of slag used was $Al_2O_3-CaO-MgO-SiO_2$ and silicon was metallurgical silicon. 5.5 grams of P doped Si and 7.5 grams of flux were used in the experiments. The crucible material was magnesia or alumina and the furnace a vertical tube furnace. The crucible with slag and metal was flushed with Ar-gas in the cold zone, before lowering it into the hot zone where the temperature was increased to 1500 °C. Argon gas was also passed through the furnace during the experiments. The authors found that the concentration of phosphorus and boron became constant after 2 hrs.

Johnston and Barati(2011) suggested that silica works as an oxidizing agent, so that phosphorus is in oxide form in the slag. The basicity of the slag depends on the concentration of basic oxides. CaO is an example of a basic oxide while SiO_2 is an acidic oxide. The oxygen potential is the oxygen arising from the $Si-SiO_2$ equilibrium as expressed in equation 2.31. They also suggested that phosphorus associates with Ca in the system with varying $CaO:SiO_2$ ratios to form $Ca_3(PO_4)$ in slag. An excess amount of basic oxides could lower the oxygen potential and thereby lowering the distribution coefficient of phosphorus. The reason why is that an increase in basic oxides leads to a decrease in silica activity. However, as presented by Johnston and Barati(2010) [23], there is an increase in Lp with increasing P_{O_2} in addition to the effect of basicity on phosphorus being strong, since Lp does not decrease with highly basic slags which reduce P_{O_2}. Figure 2.19, gives the normalized distribution coefficient as a function of basicity. The distribution coefficient was normalized with estimated partial pressure of oxygen in order to study the effect of basicity only. As illustrated in the figure, the normalized phosphorus distribution coefficient increases with increasing basicity.

$$SiO_2 \rightleftharpoons Si + O_2 \tag{2.31}$$

The effect of the $SiO_2 : Al_2O_3$ ratio of the distribution of P between Si and slag was studied by Johnston and Barati (2010) [23] for a slag of $Al_2O_3-CaO-MgO-SiO_2$ with a fixed CaO and MgO content of 42 and 10 wt%. Figure 2.20 collected from the article shows that there is a slight increase in the distribution with increasing ratio of $SiO_2 : Al_2O_3$ up to a ratio of 2. At higher ratios there is a sharp increase. Since the optical basicity of Al_2O_3 is higher than for SiO_2 [35], the authors propose that oxygen partial pressure might influence the distribution coefficient more than slag basicity since the highest distribution is at the highest $CaO : SiO_2$ ratio. As presented in figure 2.20, the maximum Lp is 8.8 which is, according to this author's knowledge, the highest reported value of Lp. The slag composition at this value

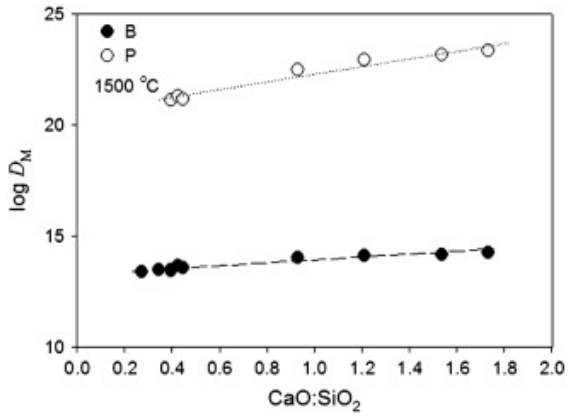

Figure 2.19: Figure from Johnston and Barati showing the normalized distribution coefficient of phosphorus with varying CaO:SiO_2 ratio.

of *Lp* was 9 % Al_2O_3 – 24 %CaO – 33 % MgO – 34 % SiO_2.

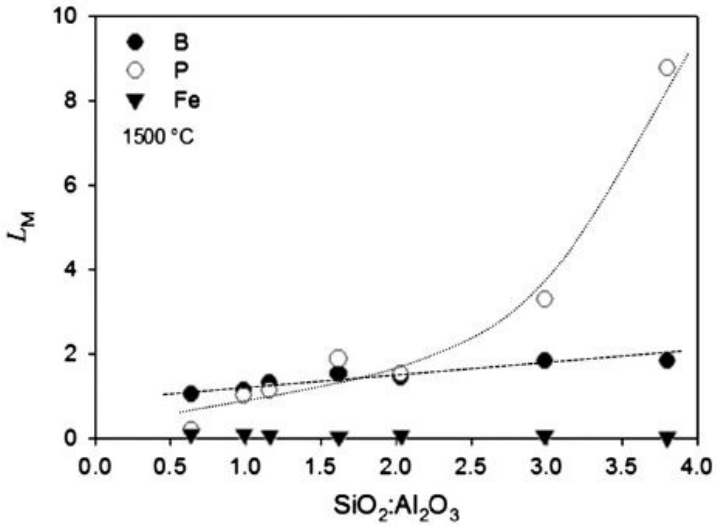

Figure 2.20: Image from Johnston and Barati(2010) presenting the effect of SiO_2 : Al_2O_3 ratio on the distribution of P between Si and Al_2O_3 – 42 %CaO – 10 %MgO – SiO_2 slag.

Johnston and Barati(2011) found that phosphorus also associates with Mg forming $Mg_3(PO_4)_2$ compound. FactSage calculations conducted by the authors showed that Ca compounds of phosphorus are more stable than Mg compounds of phosphorus. The formation of Mg-phosphate had a formation Gibbs energy of -1140 kJ while Ca-phosphate had a formation Gibbs energy of -1400 kJ at 1500 °C.

In the review of high temperature refining of metallurgical-grade silicon by Johnston et al.(2012) [31], they claim as previously shown by Johnston and Barati (2011) that refining of P from Si depends on the activity of SiO_2 and the amount

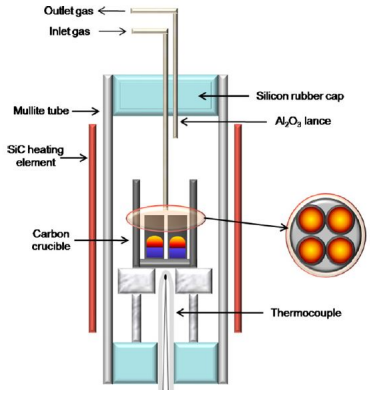

Figure 2.21: Experimental set up for slag refining from Jung et al. [27]

of oxygen anions in the slag. The authors then propose that the distribution of phosphorus as a function of basicity is expected to be a negative parabola function. The reason for the deviation from the linear increase with basicity shown by Johnston and Barati (2011) is claimed to be because of alumina also being present in the slag. Because of alumina being a network forming oxide by forming a complex, it is charge balanced with Ca^{2+}. CaO participating in the charge balancing reaction, cannot contribute to the oxygen anions in the slag. This gives an increased maximum value of the distribution, which is believed not reached in the range of CaO to SiO_2 ratio studied.

Jung et al. (2011)

Jung et al.(2011) performed slag refining and acid leaching to remove phosphorus [27]. Slag refining was conducted in an electric resistance furnace in clean argon and hydrogen gas atmosphere. The experimental set up is depicted in figure 2.21. The crucible material was carbon and the heating element was made of SiC. CaO-SiO_2-CaF_2 slag was heated together with upgraded metallurgical grade silicon with small amounts of reagent-grade phosphorus until equilibrium was reached. The holding time was 12h and the temperature 1773K (1500 °C).

Equation 2.32 shows the partial pressure of phosphorus and the reaction between slag and gas is presented in equation 2.33. From this equation they found the phopshide capacity as given in equation 2.34. Here the partial pressure of oxygen is determined by the equilibrium between SiO_2 and Si.

$$\frac{1}{2}P_2(g) = [P]_{Si,mass\%} \tag{2.32}$$

$$\frac{1}{2}P_2(g) + \frac{3}{2}O^{2-} = P^{3-} + \frac{3}{4}O_2 \tag{2.33}$$

$$C_{P^{3-}} = \frac{K_2 a_{O^{2-}}^{3/2}}{f_{P^{3-}}} = \frac{(\%P^{3-})p_{O_2}^{3/4}}{p_{P_2}^{1/2}} \tag{2.34}$$

After slag refining, Si was crushed to powder and sieved in the size range from 15 to 75 mm. Acid leaching was done with aqua regia, HCl and HF. These optimal leaching conditions were found after an extensive literature review.

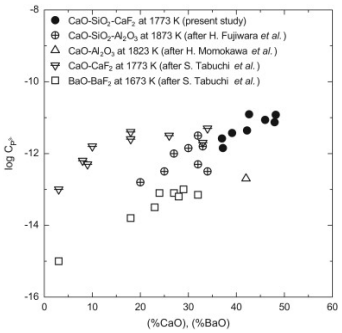

(a) Figure from Jung et al. showing how the basicity effects the phosphide capacity.

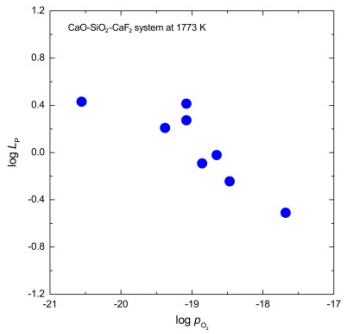

(b) Figure from Jung et al. showing how the oxygen potential affects the distribution coefficient of phosphorus.

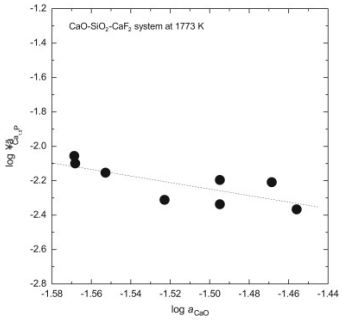

(c) Figure from Jung et al. showing how increasing the activity of CaO decreases the activity coefficient of phosphide ions.

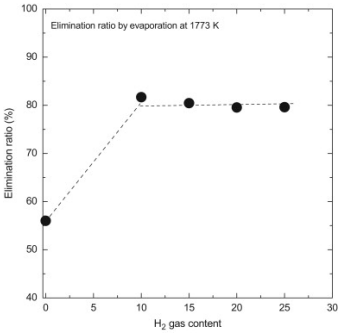

(d) Figure from Jung et al. showing how phosphorus is removed from silicon as a function of H_2 content.

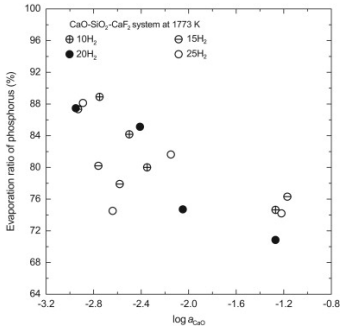

(e) Figure from Jung et al. showing how evaporation of phosphorus depends on the activity of CaO.

Figure 2.22: Figures from Jung et al. giving the different factors affecting the stability of P in slag.

Jung et al. presented some interesting results. As shown in figure 2.22a, increasing basicity lead to an increase in the capacity of phosphide as presented previously in equation 2.34. An increase in the oxygen potential decreased the distribution of phosphorus in slag phase relative to metal phase as presented in figure 2.22b. From the figure it appears that the maximum distribution coefficient is $10^{0.4} = 2.5$ Therefore they conclude that the the process is a reduction process

as previously shown in equation 2.33.

Phosphorus was either removed by slag refining or evaporation during the slag refining process. Increasing the basicity, which means increasing the amount of CaO, lead to a stabilized product of Ca and P in the slag, assumed to be Ca_3P_2. This reduced the evaporation of phosphorus. The result is presented in figure 2.22e. Figure 2.22c shows how increasing the activity of CaO decreases the activity coefficient of phosphide ions. Addition of H_2 up to 10% on the other hand, increased the evaporation as shown in figure 2.22d. Leaching was used in the end to remove P and Ca still present in Si after slag refining. As discussed in the section 2.1, phosphorus in Si is formed as Ca_3P_2 at the grain boundary in Si. The final removal efficiency of P after acid leaching was larger than 90%.

Lynch(2009)

Lynch(2009) claims in his review of refining methods of silicon that decreasing the oxygen potential and increasing the amount of CaO in the slag with molten silicon present, will lead to an increased concentration of calcium in silicon [20]. The increase in calcium would, according to the author, also lead to an increase in phosphorus concentration in silicon because of the formation of Ca_3P_2 compound.

Lynch made a graph of Henrian activity coefficients of solutes in molten silicon given in figure 2.23a. Calcium is shown to be the most stable solute in silicon. Using data from Fujiwara et al. [25], Lynch presented the distribution of P between slag and molten Si as a function of basicity as shown in figure 2.23b. The author also included the calcium concentration of silicon in parentheses to underline the fact that although increasing the basicity increases the distribution of P towards slag, it also increases the amount of Ca in silicon.

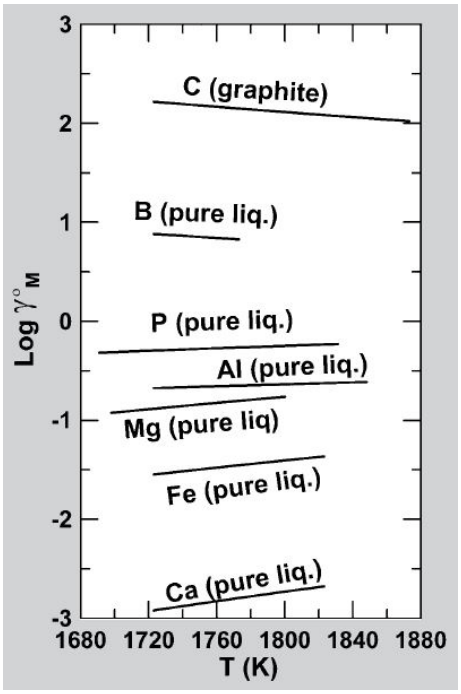

(a) Figure from Lynch(2009) [20] giving the Henrian activity coefficients for solutes in molten silicon.

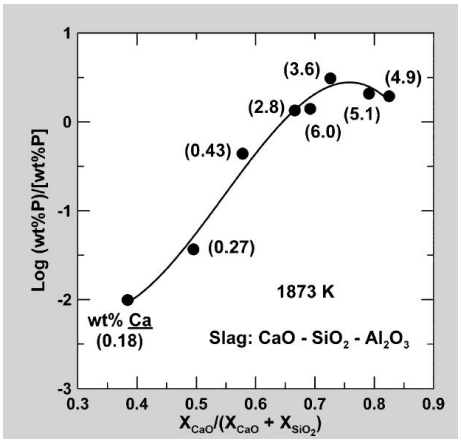

(b) Figure from Lynch(2009) [20] showing the effect of slag composition on the distribution of P between slag and molten Si. In addition the wt% of Ca in Si is given in parentheses.

Figure 2.23: Figures from Lynch(2009) [20].

Huang et al.(2013)

Huang et al.(2013) [43] studied de-phosphorisation of metallurgical grade silicon using slag refining and vacuum treatment. The slag utilized was $CaO-SiO_2-CaCl_2$. 600 g of metal and 600g of slag was used for equilibration. Metal and slag were held at a temperature of 1750 °C for 0.5 hrs under Ar-atmosphere. Graphite was the crucible material, and the furnace an intermediate frequency induction melting furnace. Slag was then mechanically separated from silicon and the silicon was melted further in vacuum. Figure 2.24 gives the effect of slag refining and acid leaching as a function of CaO : SiO_2 ratio. Results from their study showed that increasing the CaO : SiO_2 ratio decreased the removal efficiency of P after slag refining and vacuum treatment. This is contradicting results to the work of Johnston and Barati and Jung et al. Varying the $CaCl_2$ content did not have an apparent effect on the distribution of phosphorus. Wang et al.(2017) studied $CaO-SiO_2-CaCl_2$ slag with Raman Spectroscopy analysis and found that increasing $CaCl_2$ concentration of the slag decreases the slag viscosity because of decreasing polymerization of the slag due to $CaCl_2$.

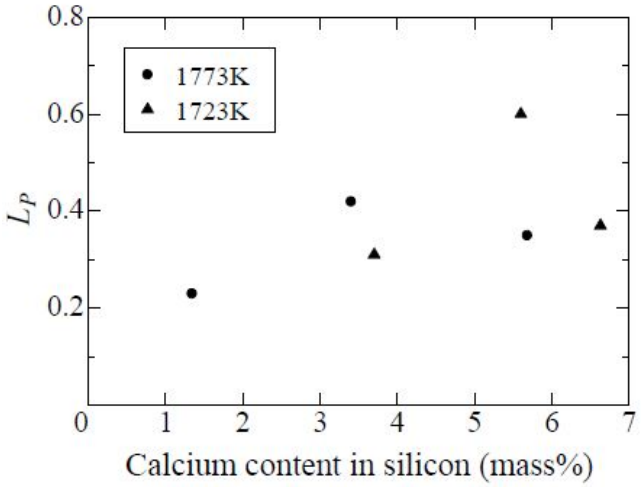

Figure 2.25: Figure from Kawamura et al. presenting the distribution coefficient as a function of Ca content in Si.

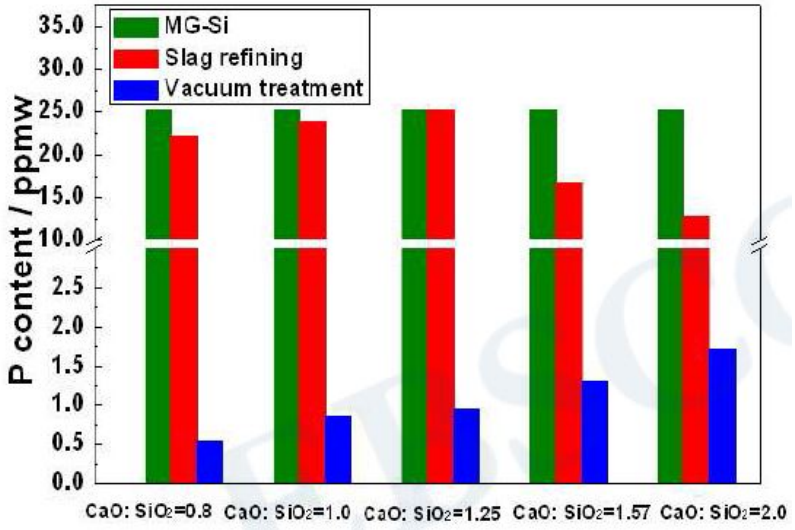

Figure 2.24: Figure from Huang et al. presenting the effect of slag refining and vacuum treatment with increasing CaO : SiO_2 ratio.

Kawamura et al.(2013)

Kawamura et al.(2013) studied the removal of phosphorus from silicon using a $CaO-CaF_2$ slag [24]. Acid leaching was also conducted in this work. 5 grams of MG-Si was equilibriated with 10 grams of slag in a graphite crucible at 1450 and 1500 °C. The furnace was a $MoSi_2$ furnace and argon gas was continuously fed to the furnace during the 3 hour holding time. After the slag was separated from Si, Si was leached with aqua regia at 90 °C. The maximum phosphorus distribution coefficient was 0.6.

Figure 2.25 presents the distribution coefficient as a function of calcium content in silicon. The main trend is that the distribution ratio increases with increasing Ca content in silicon.

Li et al.(2014)

Li et al.(2014) alloyed MG-Si with pure Cu and equilibriated the alloy with $CaO-SiO_2-Na_2O-Al_2O_3$ slag [26]. The alloy contained 30 wt% Si and 70 wt% Cu and was doped with 3000 ppm of P. Experiments were conducted in a resistance furnace with Ar-atmosphere. 10 grams of slag was first heated to 1500 °C in an alumina crucible . When the slag was molten, 1 gram of alloy was added to the crucible. The authors found that the equilibration time for phosphorus was close to 10 minutes. After the experiments slag and metal were separated, ground to powder and analyzed by ICP.

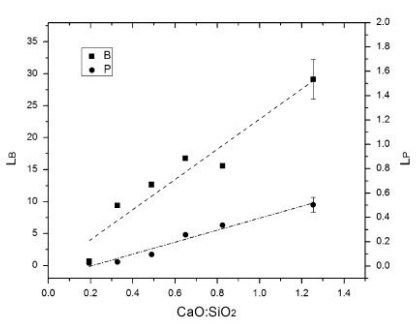

(a) Distribution coefficient as a function of $CaO:SiO_2$.

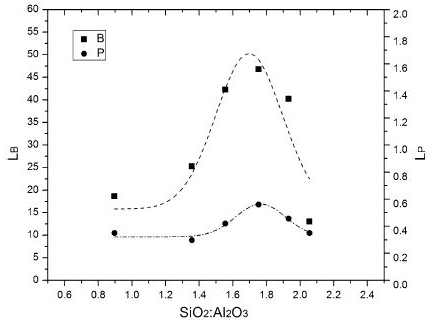

(b) Distribution coefficient as a function of $SiO_2 : Al_2O_3$.

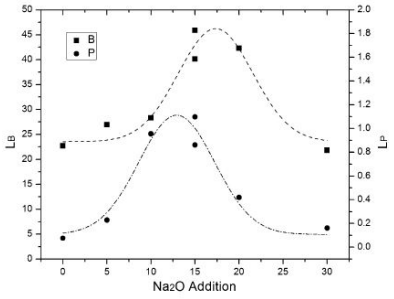

(c) Distribution coefficient as a function of Na_2O addition.

Figure 2.26: Results from experiments conducted by Li et al. with Si-Cu and $CaO-SiO_2-Na_2O-Al_2O_3$.

Figure 2.26 presents images collected from Li et al. Figure 2.26a gives the distribution coefficient of phosphorus as a function of $CaO:SiO_2$ content with 20 wt% of Na_2O and 24 wt% of Al_2O_3. As shown in the figure, the coefficient increases with increasing CaO content. However the highest value is still below 1,

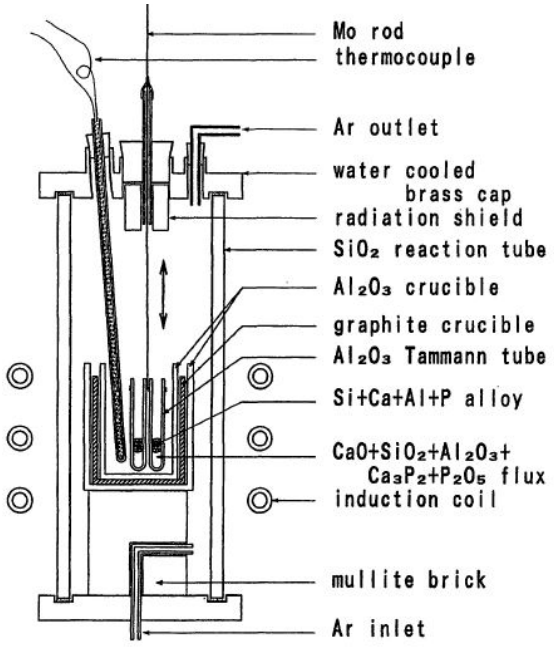

Figure 2.27: Image from Fujiwara presenting the experimental set up [25].

meaning a preference of P for the metal phase. Figure 2.26b gives the distribution coefficient as a function of SiO_2 : Al_2O_3 ratio. SiO_2 and Al_2O_3 are the species contributing to the oxygen potential, so the figure can bee seen as the distribution as a function of different oxygen potentials of slag. According to the figure, the maximum distribution is 0.55 at SiO_2 : Al_2O_3 equal 1.7. Figure 2.26c shows the distribution coefficient as a function of added Na_2O. There is a maximum Lp at 10-15 wt% Na_2O. For 15 wt% Na_2O addition, Lp is actually 1.1 which means a tendency of P going into the slag phase.

Fujiwara et al.(1996)

Fujiwara et al.(1996) studied the distribution of phosphorus between Si-Ca-Al-P alloy and $CaO-Al_2O_3-SiO_2-P_2O_5$ slag [25]. In their study they used an induction furnace with graphite heating elements. The experimental set up is shown in figure 2.27. As shown in the figure the alloy and slag is put in an alumina crucible which is then places in a graphite crucible with an outer protection alumina crucible. 4 to 6 grams of $CaO-SiO_2-Al_2O_3-P_2O_5$ flux and 2 to 3.5 grams of Si-Al-Ca alloy was moved to the zone where the furnace had a temperature of 1600 °C and was held for 5 hours in Ar-atmosphere.

Figure 2.28 shows how the distribution coefficient increases with increasing CaO content. The maximum distribution coefficient is 3. Fujiwara et al.(1996) claimed that increasing the basicity and decreasing the oxygen potential increased the

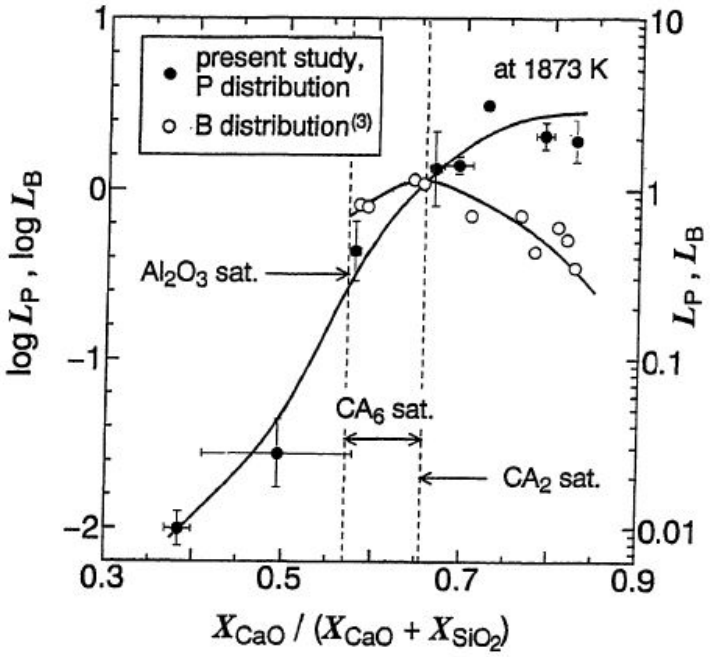

Figure 2.28: Figure from Fujiwara et al. [25] illustrating how the distribution coefficient increases with increasing CaO content.

distribution coefficient L_p. The authors also say that the transfer of phosphorus into slag is a reducing reaction as in equation 2.18 and that it is endothermic meaning a higher temperature will increase the distribution of phosphorus towards slag.

Yoshikawa and Morita [44] found that alloying Si with Al lowered the distribution coefficient of phosphors to 0.06 between Si-Al melt and solidified silicon compared to 0.35 between liquid and solid silicon. The solidification temperature was also greatly reduced.

Fujiwara et al. also reported the concentration of the slag and the phosphorus distribution coefficient as a function of SiO_2 : Al_2O_3 concentration has been calculated and is presented in figure 2.29. There is a decreasing trend in distribution coefficient with increasing SiO_2 : Al_2O_3 ratio. However, the CaO content was not held constant with varying Al_2O_3. The CaO content was equal for two measurements where slag compositions were $31.1\,CaO - 55.8\,Al_2O_3 - 12.6\,SiO_2$(wt%) and $31.1\,CaO - 59.6\,Al_2O_3 - 8.8\,SiO_2$ (wt%). This gave Lp values of 3.1 and 2.0 respectively.

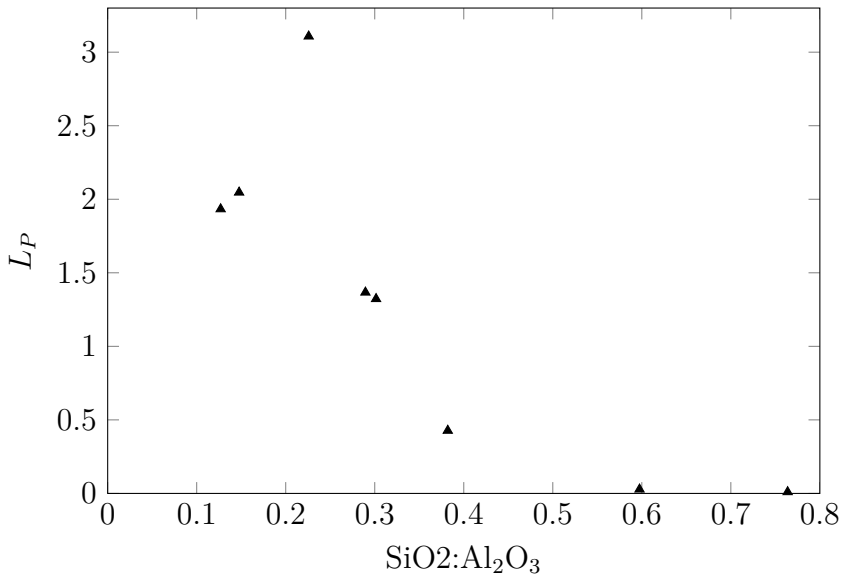

Figure 2.29: Phosphorus distribution coefficient as a function of SiO_2 : Al_2O_3 ratio calculated from data collected from Fujiwara et al. [25].

Thermodynamic calculations of dephosphorization of silicon using slag

Thermodynamic calculations for the dephosphorization reaction equilibria between molten CaO based slag and Si were conducted by Jung and Zhang(2012) [45] at a temperature of 1600 °C. Both oxidizing and reducing conditions were evaluated by the use of FactSage calculations.

Oxidative refining has shown effective for Fe, but according to calculations by Jung and Zhang under oxidizing conditions where phosphorus is present as phosphate, there is hardly any dephosphorization of Si happening.

Figure 2.30 gives the calculated distribution of phosphorus between liquid slag and molten metal as a function of mole fraction of SiO_2 under oxidizing conditions. As presented by the figure the distribution is quite low.

Figure 2.31 presents the Gibbs energy of dephosphorization of both Fe and Si. The Gibbs energy of dephosphorization of Si is significantly higher than for Fe. Actually the Gibbs energy is large and positive for the dephosphorization of Si. Dephosphorization with reducing conditions is found to be possible, but not an efficient method. The authors refer to the results by Jung et al.(2011) [27] where they found $Lp \approx 2.5$ and say that a slight dephosporization can be achieved using a reducing slag. Use of reducing conditions could cause Ca dissolving in Si according to reaction 2.35.

$$Si(l) + 2CaO(s, slag) = SiO_2(s, slag) + 2Ca(l, moltenSi) \tag{2.35}$$

Figure 2.32 collected from Jung and Zhang give the calculated activity of Ca

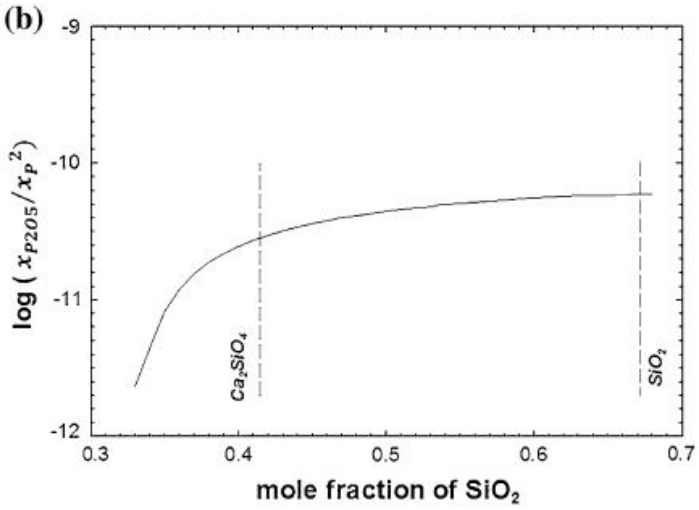

Figure 2.30: Figure from Jung and Zhang [45] presenting the distribution of P between Si and CaO – SiO_2 slag.

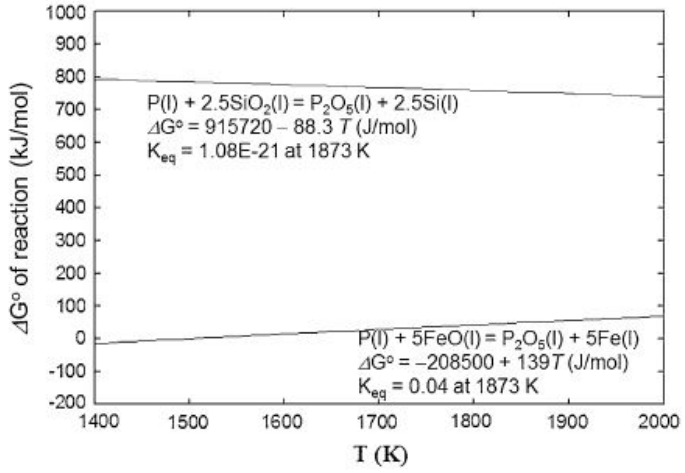

Figure 2.31: Image from Jung and Zhang(2012) [45] giving the Gibbs energy of dephosphorization of Fe and Si.

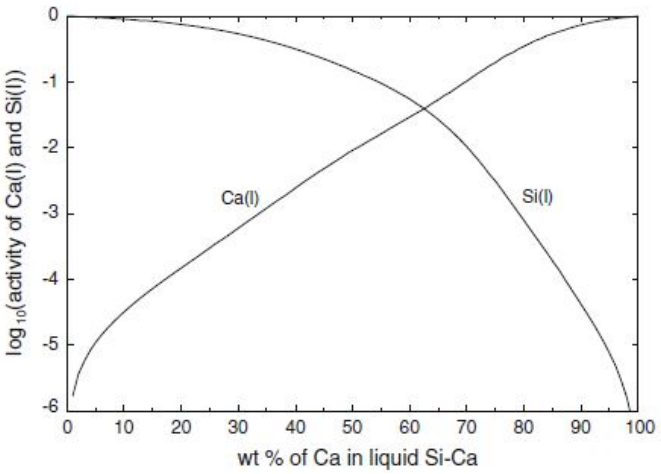

Figure 2.32: Image from Jung and Zhang presenting the activity of Ca in molten Si at 1500 °C calculated with FactSage.

in molten Si at 1500 °C. The calculations were conducted with the binary Si-Ca thermodynamic parameters in the database FTlite. The thermodynamic calculations show that there is a negative interaction between Ca and Si which is strong giving a small activity coefficient of Ca in Si, favouring Ca dissolution.

2.6.3 Distribution of P between slag and Fe

Extensive research has been conducted on the dephosphorization of steel. P can be transferred into slag in the form of phosphate (PO_4^{3-}) or phosphide (P^{3-}) depending on partial pressure of oxygen as explained previously in the section "P in slag". Oxidative refining of P as PO_4^{3-} in slag has been the traditional method of phosphorus removal from steel, but also reductive refining has been applied if steel contains components which will oxidize more readily than phosphorus. Two articles on the distribution of P between Fe and slag will be described in this section.

Between carbon saturated Fe and $CaO-CaF_2-SiO_2$ / $CaO-Na_2O-SiO_2$ slags

Tagaya et al. (1991) [30] investigated the distribution of phosphorus between carbon saturated iron and slags. The slags used were $CaO-CaF_2-SiO_2$ and $CaO-Na_2O-SiO_2$. The experiments were conducted by holding 2 g of slag and 2 g of Fe-P-C alloy in a graphite crucible for 18 hrs at temperature raging from 1200 to 1350 °C if $CaO-CaF_2-SiO_2$ slag was utilized. Holding time if $CaO-Na_2O-SiO_2$ slag was utilized was 1 or 2 hrs because of loss of Na_2O with time due to a reaction

with carbon. The furnace was a SiC electrical resistance furnace and a gas mixture of CO-Ar was continuously fed to the furnace.

$$L_p = \frac{(\%P)}{[\%P]} \tag{2.36}$$

$$L_p = \frac{(\%P)}{[\%P]^2} \tag{2.37}$$

Since the dominant species affects the distribution ratio of phosphorus between metal and slag, it is important to know which species is dominating at what phosphorus content. The distribution ratio could be equal to equation 2.36 or 2.37 depending on the specie. The relevant species are $PO_4{}^{3-}$ and $P_2O_7{}^{4-}$.

$$[P] + \frac{5}{4}O_2 + \frac{3}{2}O^{2-} = PO_4^{3-} \tag{2.38}$$

$$2[P] + \frac{5}{2}O_2 + 2O^{2-} = P_2O_7^{4-} \tag{2.39}$$

They found that the dominant species of phosphorus was $PO_4{}^{3-}$ up to 2 mass percent of phosphorus in the $CaO-CaF_2-SiO_2$ melt. The reaction equation is shown in equation 2.38. Therefore the distribution coefficient is equivalent to equation 2.36. This was when the melt was doubly saturated with CaO and $3CaO \cdot SiO_2$. At a mass percent larger than 2, $P_2O_7{}^{4-}$ is the dominant species and the distribution coefficient is equal to equation 2.37. The reaction equation is presented in equation 2.39. Figure 2.33a shows the distribution as a function of phosphorous content.

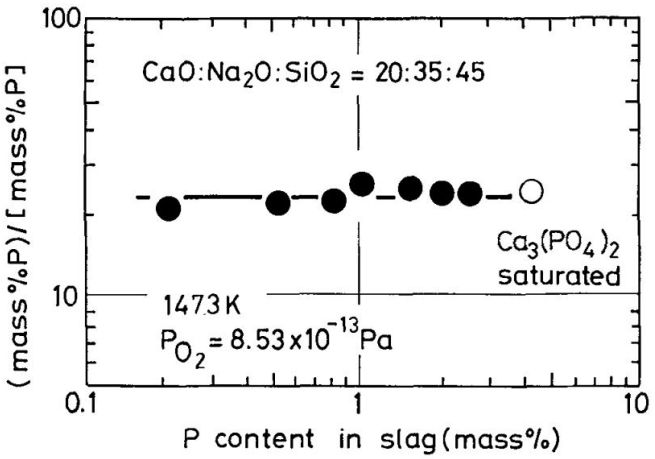

Figure 2.34: Results from experiments conducted by Tagaya et al. with $CaO-Na_2O-SiO_2$ slags.

Temperature affects the critical phosphorus content as shown in figure 2.33b.

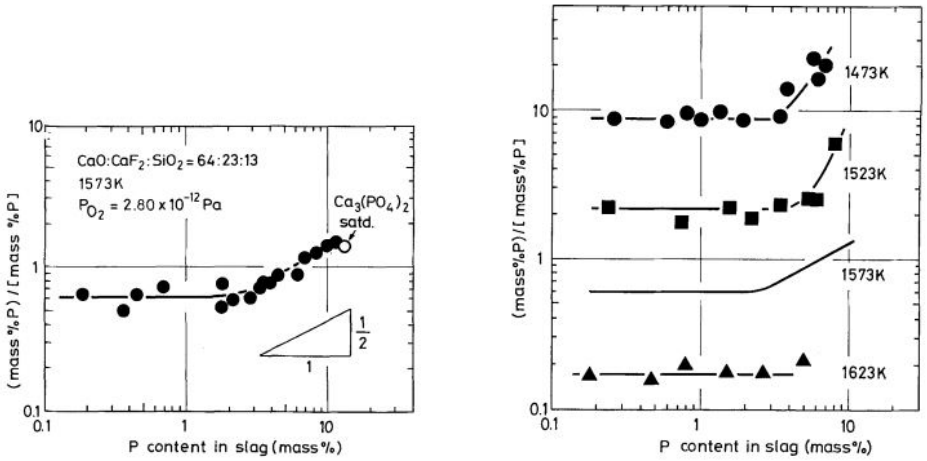

(a) Distribution coefficient as a function of P content in the melt.

(b) Distribution coefficient as a function of P content at different temperatures.

Figure 2.33: Results from experiments conducted by Tagaya et al. with $CaO-CaF_2-SiO_2$ slags.

The distribution coefficient decreases with increasing temperature. The value of the distribution coefficient is approximately 9 for 1473 K(1200 °C) and approximately 0.2 for 1623 K (1350 °C).

The second slag used was $CaO-Na_2O-SiO_2$. Here the distribution coefficient was determined at 1473K(1200 °C). As shown in figure 2.34 it was constant up to 4 mass percent of phosphorus when saturation with $Ca_3(PO_4)_2$ occurred.

Comparing the distribution coefficient of the two slags, they found that the slag containing sodium has a higher value and therefore assumed to be more basic than the slag containing fluorine. The dominant specie for the slag with sodium is $PO_4{}^{3-}$.

Between liquid steel and $CaO-SiO_2-P_2O_5-MgO$ slag with low FeO content

Basu et al.(2007) studied the partition of phosphorus between liquid steel and $CaO-SiO_2-P_2O_5-MgO$ slag with low FeO content [46]. The slag utilized in their study is a common slag in the basic oxygen steel-making process.

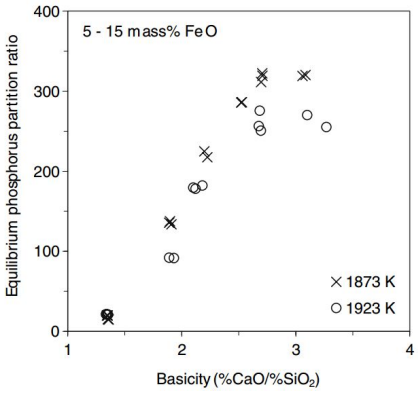

(a) Image from Basu et al.(2007) presenting the equilibrium P partition ratio as a function of basicity.

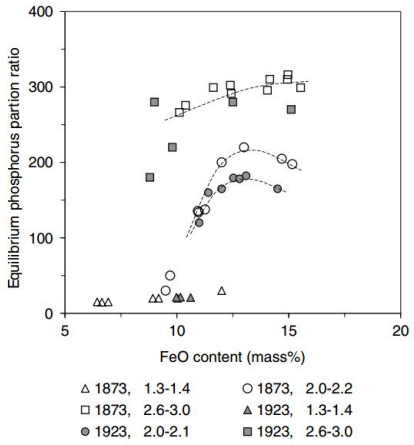

(b) Image from Basu et al.(2007) presenting the equilibrium P distribution as a function of %FeO.

Figure 2.35: Images collected from Basu et al.(2007)

Experiments were conducted in a horizontal tube furnace with $MoSi_2$ electrical heating. The crucible material was dense-sintered MgO. Ten grams of electrolytic iron was heated together with synthetic slag at temperatures 1600 and 1650 °C in Ar gas mixture. The authors found 8 hours to be the accurate equilibrium time according to preliminary experiments. After the experiment was held for 8 hours, the crucible was cooled rapidly. All experiments were conducted with a FeO content below 15 wt%.

The results found by the authors were that the distribution ratio increases up to a basicity of 2.5 as shown in figure 2.35a. At higher basicities, the partition ratio was stabilized. There seems to be a maximum partition ratio at a FeO content of 13 % as shown in figure 2.35b. MgO was dissolved in the molten slag and the amount of dissolved MgO decreased with inreasing basicity. This is believed to be because MgO is also a basic slag and when the basicity is increased the slag capacity to dissolve additional basic oxides is lost.

2.6.4 Distribution of P between slag and Fe-Si

Enebakk et al.(2010) with the company ELKEM patented a method for removing phosphorus from $CaO-SiO_2$ slag by treating it with a molten ferrosilicon alloy with a composition of up to 30 wt% of silicon [47]. This method was developed in order to use the slag with low phosphorus content to remove boron and phosphorus from metallurgical grade silicon.

Slag treatment with $CaO\text{-}SiO_2$ slags has shown efficient for removing boron from metallurgical grade silicon. However as claimed by the author, CaO used to

produce the slag initially has a high phosphorus concentration and the distribution coefficient of phosphorus between slag and silicon is very low, in the range of 0.1 and 0.3, which can increase the phosphorus content of silicon. Therefore the patent gives a method to reduce the phosphorus content of the slag before using it for slag treatment of boron.

The patent presents a procedure where a FeSi alloy with 85 wt% Fe and 15 wt% Si were put in an induction furnace. Then 120 g of SiO_2 and 130 g of CaO were added to the top of the FeSi alloy. The total initial P content of the slag was 20 ppmw. An inert or reducing gas was added to stir the ferrosilicon and slag. Finally the slag was tapped from the induction furnace. The table in figure 2.36 collected from Enebakk et al.(2010) presents the composition of the slag after being treated with the FeSi alloy and different gas compositions. As shown in the table the final phosphorus content of the slag was below the detection limit for ICP-analysis, which is 2.5 ppmw.

TABLE 1

		Chemical Analysis				
Test No.	Stirring gas	P* [ppmw]	B [ppmw]	CaO [wt %]	$Si0_2$ [wt %]	Fe_20_3 [wt %]
A	Ar—5%H_2	<2.5	8.1	53.44	46.48	0.12
B	Ar—25%CO	<2.5	8.4	53.36	46.55	<0.12
C	Ar	<2.5	8.1	53.01	47.60	0.12

*detection limit for P in slag: 2.5 ppmw (ICP)

Figure 2.36: Image collected from Enebakk et al.(2010) giving the slag composition after being treated with FeSi 85:15 and different gas compositions.

From the information given in Enebakk et al.(2010) [47], it is possible to calculate the distribution coefficient. However, 2.5 ppmw which is the measured content of phosphorus in slag is the detection limit for ICP. The authors calculated the real phosphorus content of the slags to be 0.1 ppmw based on mass balance calculations. The calculated distribution coefficients are given in table 2.2.

Table 2.2: Calculated values of phosphorus distribution coefficient from data collected from Enebakk et al.

$CaO : SiO_2$	P in slag [ppmw]	P in metal [ppmw]	Lp
1.1497	0.1	3	0.033
1.1463	0.1	4	0.025
1.114	0.1	4	0.025

2.7 Summary of main finding from literature

This section presents a summary of the main finding from the literature review. References have been given previously, and will not be repeated here.

The first part of the theory section dealt with the micro structure and thermodynamics of phosphorus in Si and FeSi. Jung et al.(2011) found that a Ca_3P_2 phase formed at the Si grain boundary after equilibration with $CaO-SiO-CaF_2$ slag. Møll(2014) studied the solidification of metallurgical grade silicon and saw that phosphorus existed in Al_2CaSi_2 inter-metallic phase in solid silicon. Meteleva Fischer found phosphorus to exist in $FeSi_2Ti$ phase when alloying MG-Si with Ca. Horn et al.(1998) studied the micro-structure of FeSi75 alloy and saw that phosphorus existed as phosphide inclusions including Ca_3P_2, AlP and Mg_3P_2. Shimpo et al.(2004) calculated the interaction parameter between Ca and P in Silicon to be, $\varepsilon^P_{CainSi} = -14.6(\pm 1.7)$. Ueda et al.(1997) determined that alloying of silicon with iron up to a mole fraction of 0.23 increases the activity coefficient in FeSi, thereby decreasing the amount of P in the alloy. At higher mole fractions than 0.23 the activity coefficient of P in FeSi decreases and therefore increases the amount of P in FeSi. Lynch(2009) claims that phosphorus is less volatile in FeSi alloys with iron contents above 65 wt% than in Si.

The next section dealt with phosphorus in slag. Literature has shown that phosphorus can exist as both phosphide and phosphate in slag. Table 2.1 presents an overview of the dominant phosphorus species in slag after equilibration with various alloys. The oxygen potential of the system arises from the equilibrium of SiO_2 and O_2. The general trend is that ${PO_4}^{3-}$ is dominating at higher oxygen potentials while P^{3-} dominates at lower oxygen partial pressures. It is believed that there exists a critical oxygen partial pressure where the dominant specie in the slag changes from phosphide to phosphate. Momokawa and Sano(1982) studied the effect of oxygen potential on phosphorus in the $CaO\text{-}Al_2O_3$ system and equilibrated the slag with Fe-P-Al alloy at 1500 °C in Ar-atmosphere. They found that the critical partial pressure of oxygen where the dominant specie of phosphorus in slag changed from phosphide to phosphate was 10^{-18} atm. The phosphorus specie is slag can be determined by dissolving slag in HCl with a flow of Ar gas. Phosphine will then evaporate and PH_3 can be captured by bromine water. Phosphate on the other hand dissolves in the HCl solution.

The equilibrium time for boron transfer between Si and a 50:50 (wt%) CaO : SiO_2 slag is found to be two hours by Krystad et al.(2012). Diffusivity affects the mass transfer and diffusivity of boron and phosphorus are found to be quite similar in liquid Si. The diffusivity can be expressed by Stoke-Einstein equation and as given in the equation, an increase in viscosity decreases the diffusivity. From the

Slag Atlas(1995) it is found that increasing the SiO_2 content of slag increases the viscosity of $CaO-SiO_2$ slags. Increasing the Si content of FeSi alloy up to 50 atomic percent will decrease the viscosity. However, it was found by Nishimoto et al.(2012) that the mass transfer of boron between Si and $CaO-SiO_2$ is controlled by the mass transfer in slags. It is believed that this is also the case for phosphorus.

The distribution of phosphorus between FeSi and Si was studied by Esfahani and Barati(2011) and Khajavi and Barati(2012). The authors did controlled cooling of FeSi alloys of composition 72Si-28Fe(wt%) and 80Si:20Fe (wt%) respectively. It was found that Si dendrites grew from the alloy melt when solidifying. Phosphorus distributed towards the FeSi phase. This was due to iron having high affinity for phosphorus. Khajavi and Barati(2012) also determined the interaction parameter between P and Fe in solid Si at various temperatures. At a temperature of 1310 °C, the interaction parameter, $\varepsilon^P_{insolidSi} = -6115$.

The distribution of phosphorus between Si and slag were found to be generally below 0.5 in the literature. However, Johnston and Barati found the highest phosphorus distribution coefficient reported of 8.8. The phosphorus distribution coefficient was found at a slag composition of $9\,\%Al_2O_3 - 24\,\%CaO - 33\,\%MgO - 34\,\%SiO_2$. Fujiwara alloyed Si with Ca and Al and equilibrated the alloy with $CaO-Al_2O_3-SiO_2-P_2O_5$ slag and found a maximum phosphorus distribution coefficient of 3. According to literature, the phosphorus distribution coefficient increases with increasing basicity of slag. Jung et al. (2011) found that phosphorus exists as Ca_3P_2 in both Si and slag after equilibration. Thermodynamic calculations on the dephosphorization of slag has been done by Jung and Zhang(2012) and they found that dephosphorization under oxidizing conditions merely happens while dephosphorization under reducing conditions is possible, but not efficient.

Distribution of P between slag and Fe has been studied extensively. This is however usually done under oxidizing conditions. Tagaya et al. found that the dominant phosphorus speices in $CaO-CaF_2-SiO_2$ melts were changing with the concentration of phosphorus in the melt. ${P_2O_7}^{4-}$ is dominant at mass percent of phosphorus above 2 and at lower phosphorus contents, $PO4^{3-}$ is dominating.

There is limited research on the phosphorus distribution between FeSi and slag. Enebakk et al.(2010) equilibrated FeSi alloy with up to 30 wt% Si with $CaO-SiO_2$ slag. They managed to remove phosphorus from $CaO-SiO_2$ slag since it transferred into FeSi.

Chapter 3

Experimental

The experimental process is given in figure 3.1. This chapter describes the experimental work of preparing slags and alloys in addition to the procedure for the equilibrium experiments both with quenching and one experiment with controlled cooling. Equilibrium experiments with quenching were done with the aim of determining the equilibrium distribution of phosphorus between FeSi/Si and $CaO-SiO_2$ slags at 1600 °C in argon atmosphere. The sample preparation method for inductively coupled mass spectrometry (ICP-MS) analysis after the experiments is also explained. Slow cooling was conducted in one experiment with FeSi 20:80 and a $SiO_2-CaO-P_2O_5$ slag with 5.4 wt% of P_2O_5. This was done to study the distribution of phosphorus between FeSi, Si and slag. According to solidification theory, Si should precipitate out with controlled cooling of a FeSi alloy with a Si content larger than 58.2 wt% of Si. The analysis method for this purpose was electron probe micro analyzer (EPMA).

Finally the approach of thermodynamic modeling in FactSage 7.1 is presented. FactSage calculations are conducted in order to compare with the experimental values.

Figure 3.1: Overview of experimental process

3.1 Materials

Purity of materials used in the preparation of slags and alloys in addition to in the equilibrium experiments is given in table 3.1.

Table 3.1: Materials and their purity

Material	Purity [%]	Producer
CaO powder	99.9	Sigma-Aldrich
SiO_2 powder	99	-
P_2O_5 powder	≥ 98	Sigma-Aldrich
B powder	≥ 99	Sigma-Aldrich
Fe powder	99	VWR
Si lumps	99.999999	-

3.2 Experimental work

Master slags and master alloys were prepared in induction furnaces. Slags and alloys were then used for equilibrium experiments in a resistance heating furnace. These experiments were conducted to investigate the equilibrium distribution of phosphorus between slag and metal. One experiment was also conducted with slow cooling in order to study the distribution of phosphorus between Si,FeSi and slag in the same sample.

3.2.1 Slag production

Three synthetic slags of different compositions, each of 500 grams, were made in an induction furnace named IF-75. The targeted slag compositions were 43%-57%, 50%-50% and 65%-35% SiO_2-CaO in weight percent as shown in table 3.2. Slags were made by mixing powders of CaO and SiO_2, both with purities above 99%. In addition 300 ppm of P was added by adding P_2O_5 powder. The mixture was then heated to 1600 °C and casted into a graphite container when molten. The crucible material was graphite. After cooling in room temperature, slags were crushed to smaller lumps in an agate mortar. Thereafter the slag lumps were crushed in a ring mill with tungsten carbide chamber. Finally, slags were remelted in the same induction furnace to ensure a homogeneous distribution.

The slag compositions were chosen to get a basic as possible and an acidic as possible slag in the liquid area at 1600 °C according to the phase diagram in figure

Table 3.2: Target composition of slags produced

nr.	SiO_2 [wt%]	CaO [wt%]	P [ppm]
1	43	57	300
2	50	50	300
3	65	35	300

Table 3.3: Actual composition of slags produced given as normalized values. Recovery before normalization is also presented

nr.	SiO_2 [wt%]	CaO [wt%]	P_2O_5 [wt%]	MgO [wt%]	Fe_2O_3 [wt%]	Recovery [%]
1	42.5	56.9	0.07	0.2	0.2	102.4
2	49.0	50.7	0.07	0.0	0.1	101.8
3	63.7	36.0	0.06	0.0	0.1	100.3

3.2. The red lines in the figure present the most acidic and most basic composition at 1600 °C.

XRF-analysis was conducted on the prepared slags. The composition from the analysis is presented in table 3.3. These values are normalized and represent an average of three parallels which were all run twice.

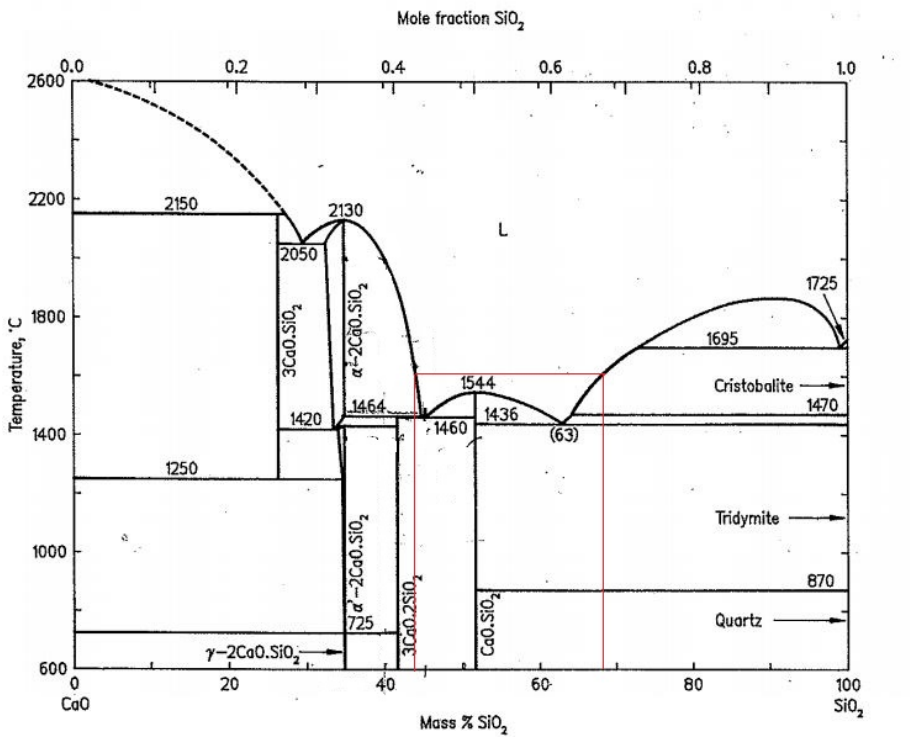

Figure 3.2: Phase diagram of CaO-SiO_2 presenting the most basic and most acidic composition of liquid slag at 1600 °C [35]

3.2.2 Ferrosilicon alloy production

Three different ferrosilicon alloys were made by mixing iron powder with silicon lumps to a total mass of 200 grams. The mixture was then heated until melted and then held for a couple of minutes before it was casted into a water cooled copper container. This was done in an induction furnace named the Blue Furnace and the crucible material was graphite. Argon gas was purged two times before starting the furnace. The target compositions of the different alloys are shown in table 3.4. The compositions were 20:80, 50:50 and 80:20 wt% Fe:Si. The alloys produced were then analyzed by inductively coupled mass spectroscopy (ICP-MS) and the results are presented in table 3.5. The standard deviation includes the relative standard deviation of each sub-sample from the ICP-MS analysis as given in equation A.5 in appendix A.

Table 3.4: Target composition of ferrosilicon alloys produced

alloy nr.	Fe [wt%]	Si [wt%]
1	20	80
2	50	50
3	80	20

Table 3.5: Composition of alloy from ICP-MS analysis given as an average of three replicate splits.

alloy nr.	Fe [wt%]	Si [wt%]	P [ppm]
1	16.1 ± 1.0	75.1 ± 6.9	28.8 ± 2
2	27.6 ± 9.1	46.4 ± 2.1	39.2 ± 2
3	69.0 ± 1.3	17.1 ± 0.8	129.7± 2

3.2.3 Equilibrium experiments

The plan for equilibrium experiments is given in table 3.6. Here the compositions of slags and alloys are given in weight percent. The number in the matrix represents the number of repetitions that will be done with equilibration of a given slag and metal. Experiments with Si and 65:35(wt%) SiO_2–CaO were not conducted in this thesis due to time limitations. The Fe:Si alloy of 80:20 which was previously prepared, was not used in experiments either for the same reason.

Table 3.6: Matrix of experimental plan, compositions of slags and metals are given in weight percentage

	SiO_2-CaO 43:57	SiO_2-CaO 50:50	SiO_2-CaO 65:35
Fe20:Si80	2 + 1 with slow cooling	2	2
Fe20:Si80	2	2	2
Si	2	2	2

Quenching

Equilibrium experiments were conducted to study the equilibrium distribution of phosphorus between $CaO-SiO_2$ slags and FeSi or Si. The experiments were conducted in a graphite tube furnace with resistance heating. The furnace is named TF2 and is designed at NTNU and shown in figure 3.3.

Pre-melting of metals was conducted to ensure that it was possible to separate slag and metal after the equilibrium experiments. Pre-melting was done by heating 10 grams of metal lumps in a graphite crucible at 1600 °C for 7 minutes. Si was held at 1600 °C for 10 minutes as it did not appear melted after 7 minutes.

The crucible material was graphite with a conical bottom to avoid cracking because of silicon expansion when cooling. The crucible dimensions used in experiments 1 through 6 as given in table 4.1 was Ø30mm/22·50mm. For experiments 7 through 15, the crucible dimensions were Ø30mm/22·45mm.

10 grams of slag was added as fine powder to the pre-melted metal in the graphite crucible. The furnace was first heated to 1600 °C and then the sample with metal and slag was placed in a sample holder and inserted into the hot furnace. The sample holder with crucible inside is given in figure 3.3b. Argon gas was continuously fed to the furnace during the experiments to ensure an inert atmosphere. The holding time at 1600 °C was three hours in order to reach equilibrium. Afterwards the sample was quenched by removing it from the hot zone into the cooled zone of the furnace. Quenching was done to ensure a concentration equal to the equilibrium concentration when solidifying. During the experiments the argon gas pressure was controlled manually to be in the range of 1.2 and 1.3 bar. This was done to avoid oxygen of getting in contact with the melt. Temperature was controlled using a C-type thermocouple and an additional B-type thermocouple was used as a backup.

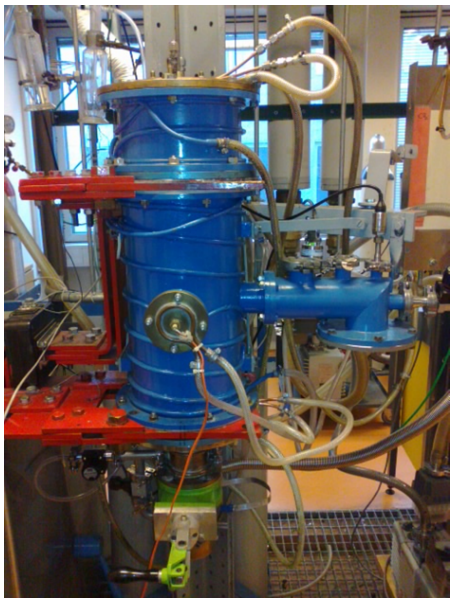

(a) TF2 graphite tube furnace

(b) Crucible holder with crucible inside

Figure 3.3: Pictures of furnace and crucible holder

Controlled cooling

One experiment was conducted with slow cooling to study the distribution of P between Si, FeSi and slag.

The experiment was done with slag of normalized composition 45.8wt%CaO, 47.6wt% SiO_2 and 5.4 wt% P_2O_5 and ferrosilicon with 80wt% Si and 20 wt% Fe. This slag was prepared by the author in earlier work. The slag also contained 0.9 wt% of MgO.

Metal was pre-melted at 1600 °C for 7 minutes and then quenched. Slag was added to the graphite crucible with the pre-melted metal and the mixture was inserted into the graphite tube furnace named TF2 at 1600 °C. The holding time at 1600 °C was 3 hours. Then the sample was cooled down at a rate of 1°C per minute down to 1354 °C. When the temperature reached 1354 °C, the furnace was turned off. The sample was mounted in epoxy and studied with electron probe micro analyzer (EPMA).

Temperature control

Previous temperature profiles for the TF2-furnace were made by Bjørnstad(2016) [48] at NTNU and are shown in figure 3.4. The temperature profile was also tested to ensure that the conditions were consistent with Bjørnstad's results. This was done to make sure that the sample was in a zone where the temperature was stable

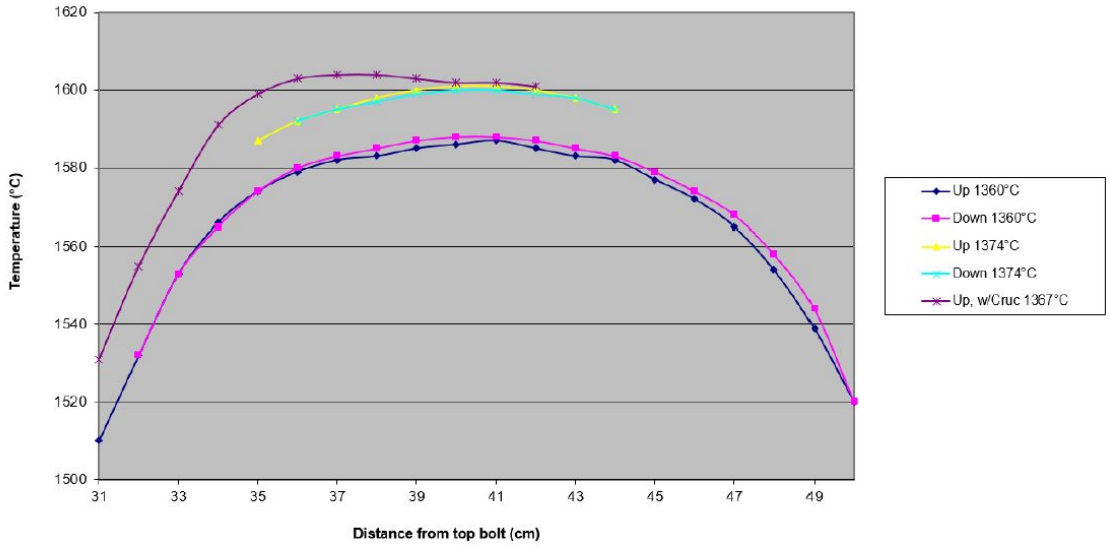

Figure 3.4: Temperature profile from Bjørnstad(2016) [48]

while running the experiments.

3.3 Preparation for sample analysis

The sample with controlled cooling was mounted in epoxy before analyzing with EPMA. Samples conducted with quenching was analyzed by ICP-MS analysis. This section presents the sample preparation method for ICP-MS.

(a) Crucible after experiment with slow cooling.

(b) Crucible after experiment with quenching.

Figure 3.5: Pictures of crucibles after experiments.

Figure 3.5 presents two images of crucibles after experiments have been con-

ducted. Figure 3.5a illustrates the crucible after the experiment with slow cooling. Figure 3.5b is an image of the crucible after experiment with Fe20:Si80(wt%) and 57:43(wt%) CaO-SiO_2 slag with quenching.

Preparations of samples were done to be able to analyze slag and metal separately. The graphite crucible was first removed by Ove Darell at SINTEF by lath turning. A thin layer of graphite remained which was later removed by a power tool. Figure 3.6 shows slag and metal when the graphite layer has been removed and before slag and metal have been separated. In order to separate slag and metal phase, pliers were used in addition to power tools. Pieces of metal inside the slag phase were removed and pieces of slag inside the metal phase were also taken out. Metal pieced in the slag were ground away. The separation of metal and slag was conducted inside a fume hood because of graphite dust formation and its hazard to health. The smallest pieces were rejected because of the difficulty of removing small contaminations. It was particularly difficult to remove silicon from slag because of its large expansion coefficient when solidifying. Slag pieces where it was not possible to remove the metal contamination were thrown away. This lead to only 10% of slag collected after separation from experiments with Si. However the separation was easier for experiments with ferrosilicon of different compositions. Here at least 40% of slag was collected after separation.

After slag and metal were separated, they were crushed to powder in a tungsten carbide chamber. The chamber was cleaned using ethanol and fused silica before crushing was initiated and in between the metal and the slag samples. In addition ethanol was used to clean the chamber in between each slag and each metal sample. Figures 3.7a and 3.7b shows crushed metal and slag respectively. Samples from experiments 1-6 given in table 4.1 were crushed in a steel chamber.

3.4 Sample analysis

Sample analysis was conducted using inductive coupled plasma mass spectroscopy (ICP-MS). Three sub-samples were taken from each metal and slag sample. These samples were dissolved in 1.5 mL 68% HNO_3 og 0.5 mL 40% HF. The sample sizes varied from 20 mg to 47.1 mg. Thereafter the samples were diluted with de-ionized water to a final mass of 217.4-224 mg.

In order to calibrate the ICP-MS machine, three blank samples and NIST 195 ferrosilicon standard were analyzed together with the sub-samples.

There were some issues dissolving a few of the samples. Table C.1 in appendix C presents an overview of how well the metal and slag samples were dissolved in the acid mix.

Figure 3.6: Picture of metal and slag before separation

(a) Metal after crushing in ring mill

(b) Slag after crushing in ring mill

Figure 3.7: Pictures of slag and metal after crushing in ring mill

3.5 Thermodynamic modeling

Equilibrium calculations using FactSage 7.1 thermochemical software were conducted in cooperation with postdoctoral researcher Elmira Moosavi-Khoonsari to study the theoretical equilibrium partition ratio of phosphorus between the SiO_2-CaO liquid slags and the FeSi and Si liquid metals.

The FactSage databases FToxide, FTlite and FactPS were used to describe thermochemical properties of the slags, metallic phases and pure substances including gas species, respectively.

According to the documentation in FactSage, the metal database including Si, Fe, P and Ca was reasonably optimized. The FactSage FToxide database incorporates phosphorus only in the form of phosphate which is the major phosphorous species in oxidizing conditions. However, under reducing environment, e.g. Ar atmosphere, phosphide could be dominant rather than phosphate.

Elmira Moosavi-Khoonsari made a mini database for the liquid slag including the species calcium phosphide Ca_3P_2, calcium phosphate $Ca_3(PO_4)_2$, SiO_2 and CaO. The slag liquid solution was treated using the Capacity model [49]. Gibbs energy of liquid Ca_3P_2 is equal to the expression in equation 3.1.

$$G^o_{Ca_3P_2(l)} = G^o_{Ca_3P_2(s)} + G^{add} \tag{3.1}$$

$G^o_{Ca_3P_2(s)}$ was taken from FactSage FactPS database, and G^{add} is the model parameter which was fixed in order to reproduce the phosphide solubility in the slag or phosphorus distribution between the liquid metal and the slag in this work.

Since the thermodynamic properties of the $CaO-P_2O_5$ system including partial Gibbs energies of the species CaO and P_2O_5 in the slag liquid solution, $G_{CaO(l)}$ and $G_{P_2O_5(l)}$, were previously well optimized [50], the Gibbs energy of liquid $Ca_3(PO_4)_2$ was described using the equation 3.2.

$$G^o_{Ca_3(PO_4)_2(l)} = 3G_{CaO(l)} + G_{P_2O_5(l)} \quad (1000K(727°C) - 3000K(2727°C)) \tag{3.2}$$

The activity coefficient of liquid $Ca_3(PO_4)_2$,$\gamma^o_{Ca_3(PO_4)_2(l)}$, was then optimized to reproduce the *Lp* trend versus the oxygen partial pressure varying by the slag composition (CaO/SiO_2 ratio). According to the model with optimized parameters, Ca_3P_2 is the major species in the liquid slag under the current experimental conditions, where very negligible amount of $Ca_3(PO_4)_2$, maximum 0.09 wt%, forms in the liquid state.

Chapter 4

Results

The aim of the experimental work conducted in this thesis was to determine the equilibrium distribution of P between FeSi and CaO-SiO_2 slag, and the equilibrium distribution of P between Si and CaO-SiO_2 slag. One experiment has also been conducted with controlled cooling in order to study the distribution of P between FeSi, Si and CaO$-SiO_2$ slag in the same sample. This section presents results from the equilibrium experiments with quenching and the experiment with slow cooling. Results from modeling in FactSage thermochemical software 7.1 are also included. Error bars in figures presented in this section represent the uncertainty calculated by t-distribution for small samples with a sample size of 2 and a 95% confidence interval. Appendix A presents the statistical analysis conducted in this work and sample calculations for the experiments with Fe50:Si50 (wt%) and $CaO : SiO_2$ 50:50(wt%). In general the error bars are quite large as a result of the small sample size. Standard deviations between sub-samples are given in given in figures C.1 through C.4 in appendix C.

4.1 Phosphorus distribution between FeSi and slag and Si and slag

Table 4.1 presents an overview of the composition of slag and metal before and after the equilibrium experiments with quenching. In the rest of this thesis slag and metal compositions will be referred to according to the targeted compositions as previously given in tables 3.4 and 3.2 due to the uncertainty in ICP-MS measures of main slag and metal constituents. All experiments except one were repeated in order to check the repeatability of the results. The experiment with Fe20:Si80 (wt%) and $SiO_2 : CaO$ 43:57(wt%) was only conducted once because of time issues. The general trend observed from the table, is that the phosphorus content in the

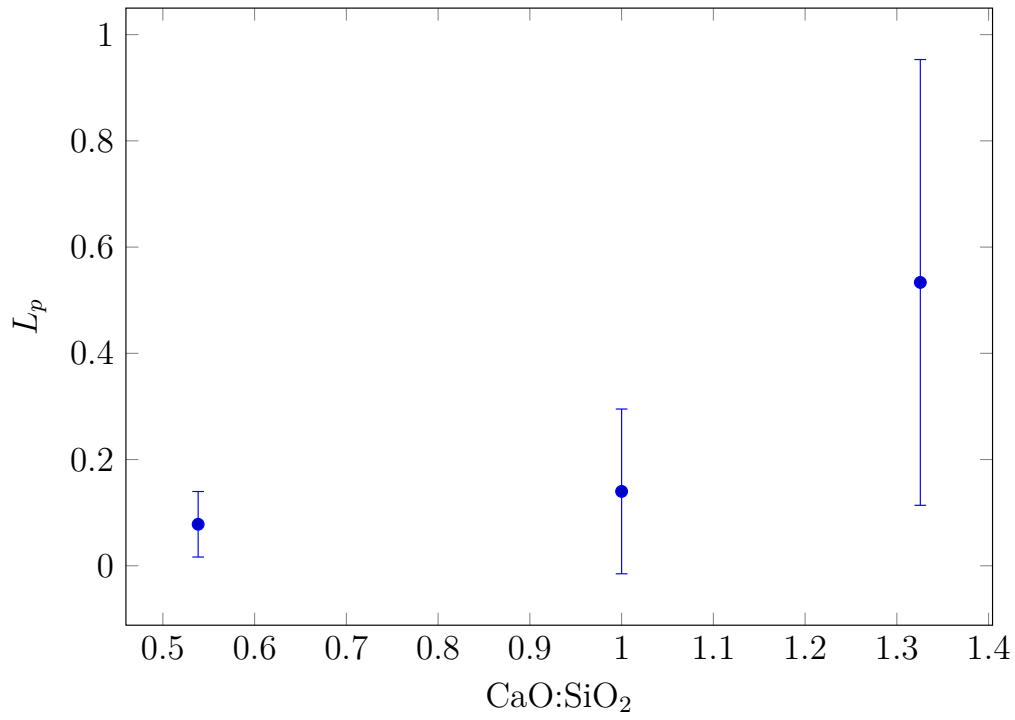

Figure 4.1: Phosphorus distribution coefficient between CaO – SiO_2 slags and Fe50:Si50 (wt%).

metal is higher than in the slag after the experiments. Since phosphorus was initially added to the slag, there has been a transfer of P from slag to metal during the experiments.

4.1.1 *Lp* as a function of slag content

This subsection presents the distribution coefficient of phosphorus between CaO – SiO_2 slag and metal as a function of slag content for the various metals utilized in the experiments. Concentration of P in slag and metal after the experiments were measured by ICP-analysis and the distribution coefficient, *Lp*, was calculated according to equation 2.30. In the end of the subsection there is a figure combining the distribution coefficient as a function of CaO : SiO_2 ratio of slag for all metals used in this work.

Figure 4.1 presents the phosphorus distribution coefficient between Fe50:Si50 (wt%) and the CaO – SiO_2 slags used in this thesis as a function of CaO : SiO_2 ratio. As shown in the figure, the distribution coefficient increases with increasing CaO : SiO_2 ratio. The increase is highest between 50 and 57 wt% of CaO. The maximum mean value of the distribution coefficient is 0.53.

Figure 4.2 depicts the distribution coefficient of phosphorus between Fe20:Si80 (wt%) and the CaO – SiO_2 slags as a function of CaO : SiO_2 ratio. According to the

Table 4.1: Summary of initial and final composition of slag and metal.

Experiment no.	Initial condition						Final condition					
	Metal (wt%)			Slag(wt%)			Metal(wt%)			Slag(wt%)		
	[Fe]	[Si]	[P](ppm)	(SiO2)	(CaO)	(P)(ppm)	[Fe]	[Si]	[P](ppm)	(SiO_2)	(CaO)	(P)(ppm)
1	50	50	39.2	49.0	50.7	218.3	38.3	48.4	139.3	44.4	19.4	24.7
2	50	50	39.2	49.0	50.7	218.3	33.9	47.8	133.5	45.8	17.0	13.7
3	50	50	39.2	42.5	56.9	197.5	31.3	43.6	127.3	41.5	21.1	83.2
4	50	50	39.2	42.5	56.9	197.5	31.4	49.0	169.3	40.1	18.4	70.0
5	50	50	39.2	63.7	36.0	182.2	27.5	45.6	96.1	59.2	11.5	10.3
6	50	50	39.2	63.7	36.0	182.2	28.6	45.8	84.1	63.1	12.7	4.1
7	20	80	28.8	49.0	50.7	218.3	15.5	72.2	109.5	49.8	20.0	11.4
8	20	80	28.8	49.0	50.7	218.3	16.0	73.7	110.6	48.6	21.4	17.3
9	20	80	28.8	42.5	56.9	197.5	16.0	75.5	106.7	42.7	23.6	51.9
10	20	80	28.8	42.5	56.9	197.5	16.5	73.5	122.7	45.5	25.4	67.3
11	20	80	28.8	63.7	36.0	182.2	16.0	74.6	61.6	59.5	20.3	10.0
12	20	80	28.8	63.7	36.0	182.2	16.7	77.2	53.6	64.5	19.4	6.6
13	0	100	0	49.0	50.7	218.3	0	94.3	162.0	50.8	30.3	18.8
14	0	100	0	49.0	50.7	218.3	0	94.8	141.8	46.4	26.1	18.0
15	0	100	0	42.5	56.9	197.5	0	90.4	112.4	46.9	41.9	45.1

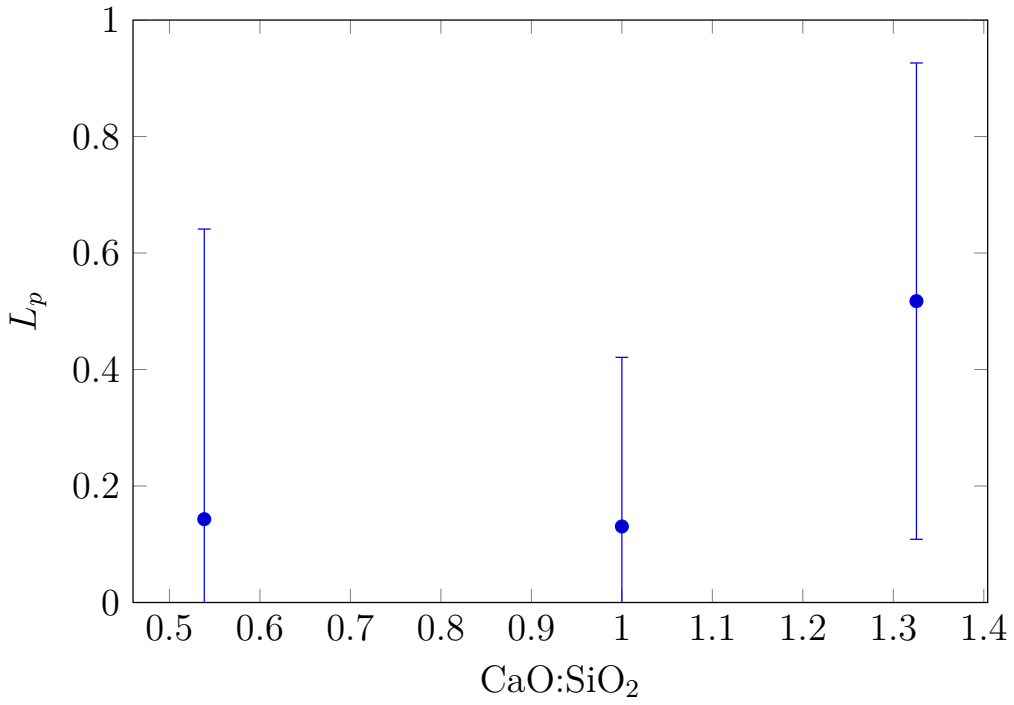

Figure 4.2: Phosphorus distribution coefficient between CaO – SiO_2 slags and Fe20:Si80 (wt%).

figure, the distribution coefficient first decreases with increasing CaO:SiO_2 ratio, then it increases. However the decrease seems to be below the error limit. The increase in the distribution coefficient is highest from 50:50(wt%) CaO:SiO_2 slag to 57:43(wt%) CaO:SiO_2. The maximum mean value of the distribution coefficient is 0.52.

Figure 4.3 illustrates the phosphorus distribution coefficient between Si and CaO – SiO_2 slags used in this work. As presented in the figure, there is an increase in the distribution coefficient with increasing CaO:SiO_2 ratio. Only one experiment was conducted with Si and 57:43(wt%) CaO – SiO_2. Therefore error bars are not added to this point. Because of time limit, experiments were not conducted with silicon and 65:35 (wt%) CaO – SiO_2 slag . The highest mean value of Lp for Si and CaO – SiO_2 slag is 0.4, but as explained previously this value is the result of only one experiment.

Figure 4.4, presents the phosphorus distribution coefficient as a function of CaO : SiO_2 ratio of slag for Si, Fe50:Si50 (wt%) and Fe20:Si80 (wt%). The overall trend is that the coefficient increases with increasing CaO : SiO_2 ratio. The increase is higher from 50 to 57 wt% of CaO than from 35 to 50 wt% of CaO. The deviation between the different metals does not seem significant. However since the experimental values lie inside the error bars of the other experiments it is difficult to conclude. The distribution coefficients all have values lower than 1,

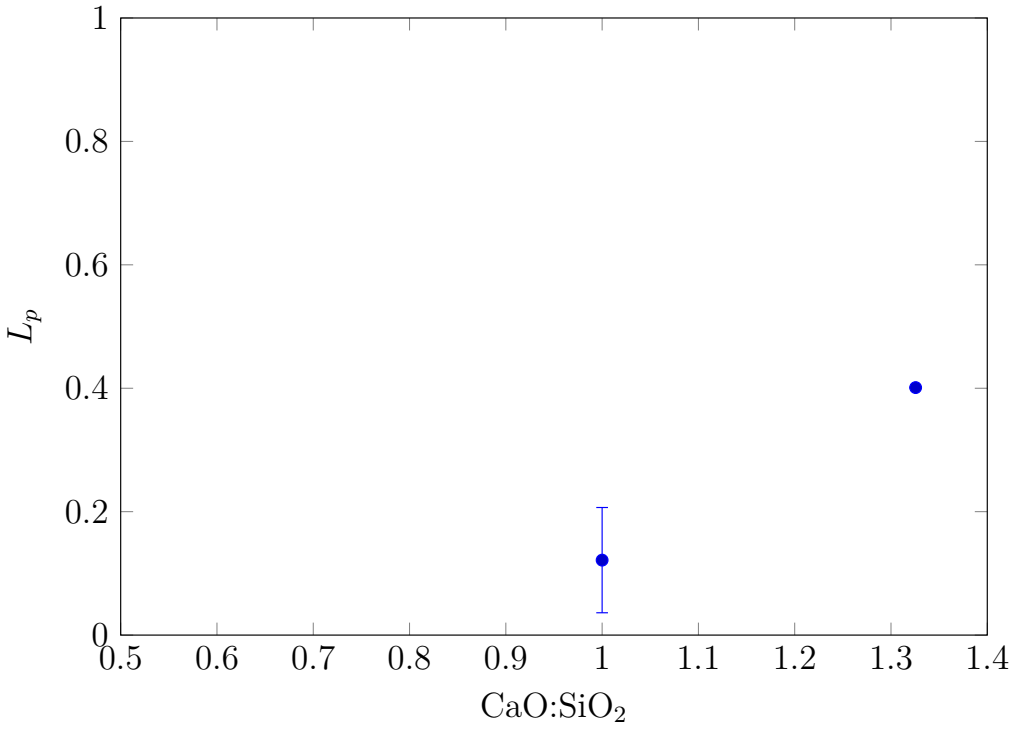

Figure 4.3: Phosphorus distribution coefficient between Si and CaO – SiO_2 slags.

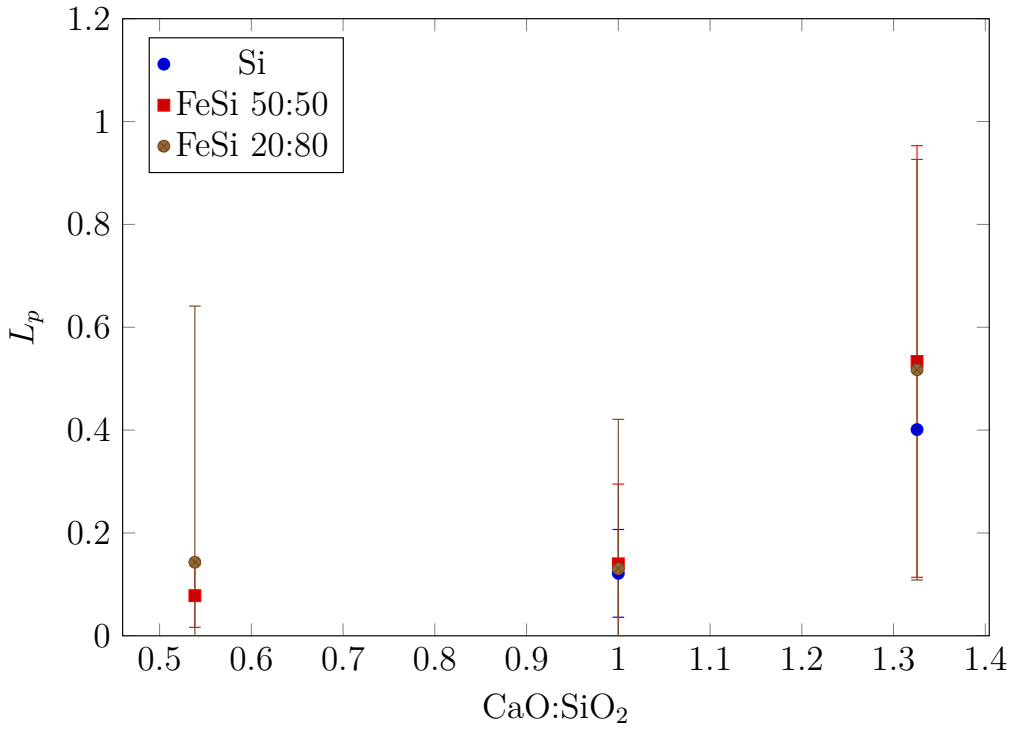

Figure 4.4: Phosphorus distribution coefficient of phosphorus between CaO – SiO_2 slags and various metals.

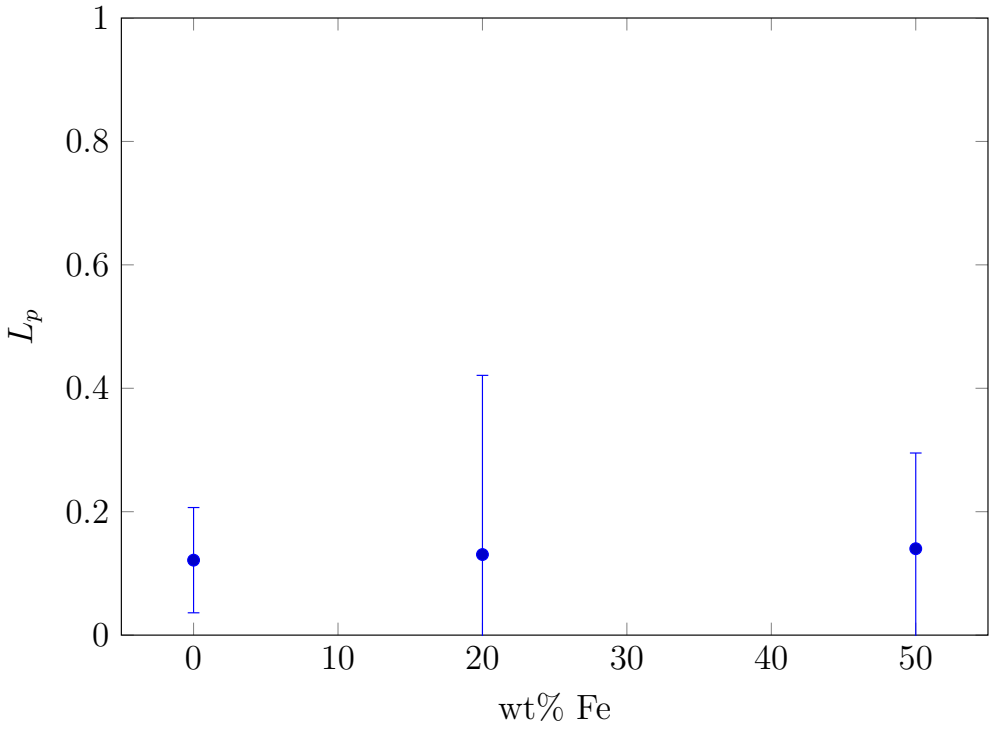

Figure 4.5: Phosphorus distribution coefficient between 50:50(wt%) CaO–SiO_2 slag and metal as a function of iron content of metal.

which means there is a tendency of P going into the metal phase.

4.1.2 *Lp* as a function of metal content

This sub-section presents the distribution coefficient of phosphorus between metal and SiO_2–CaO slags as a function of wt% Fe in the metal for each slag composition utilized in this work. In the end of the subsection there is a figure combining the phosphorus distribution for all slags.

Figure 4.5 presents the distribution coefficient of phosphorus between metal and 50:50(wt%) CaO : SiO_2 slag as a function of iron content of the metal. As seen in the figure, the distribution coefficient seems quite stable with increasing wt% Fe. The maximum mean value of L_p is 0.14.

Figure 4.6 gives the phosphorus distribution coefficient between metal and 43:57(wt%) SiO_2 : CaO slag as a function of iron content in the metal. According to the figure, the distribution coefficient increases only slightly and is almost constant with increasing iron content. The maximum mean value of L_p is 0.53.

Figure 4.7 gives the distribution coefficient between metal and 65:35(wt%) SiO_2 : CaO slag as a function of iron content in the metal. According to the figure the distribution coefficient decreases with increasing iron content. This is opposite to the trend for the other two slags used in this thesis. The maximum mean value

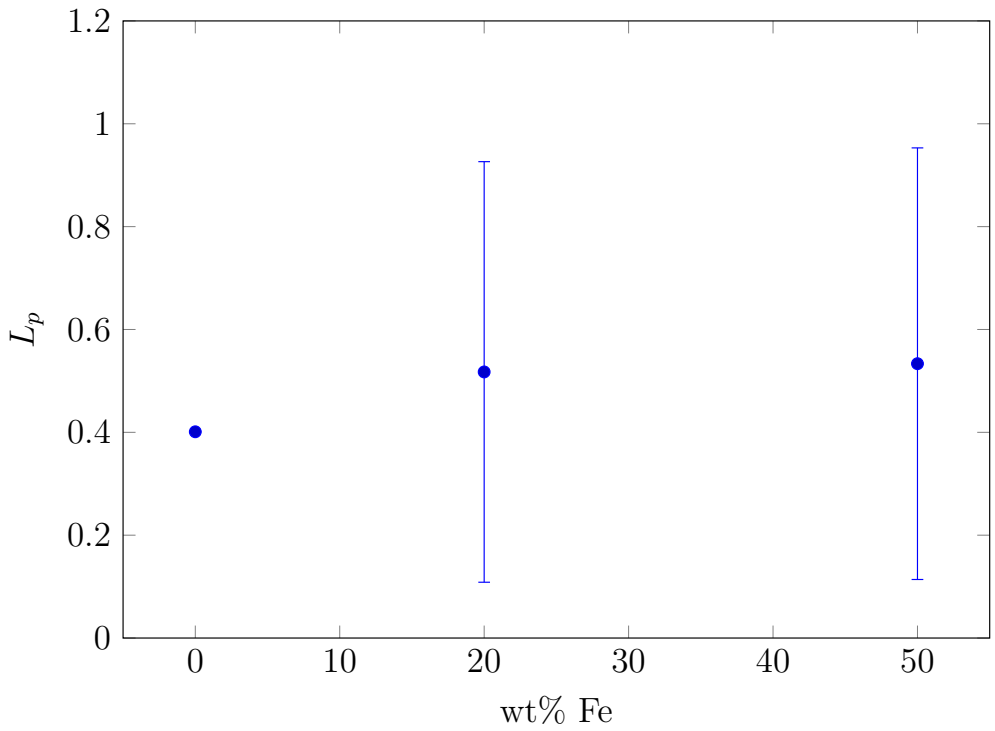

Figure 4.6: Distribution coefficient of phosphorus between slag and alloy as a function of iron content for 57:43 CaO : SiO_2.

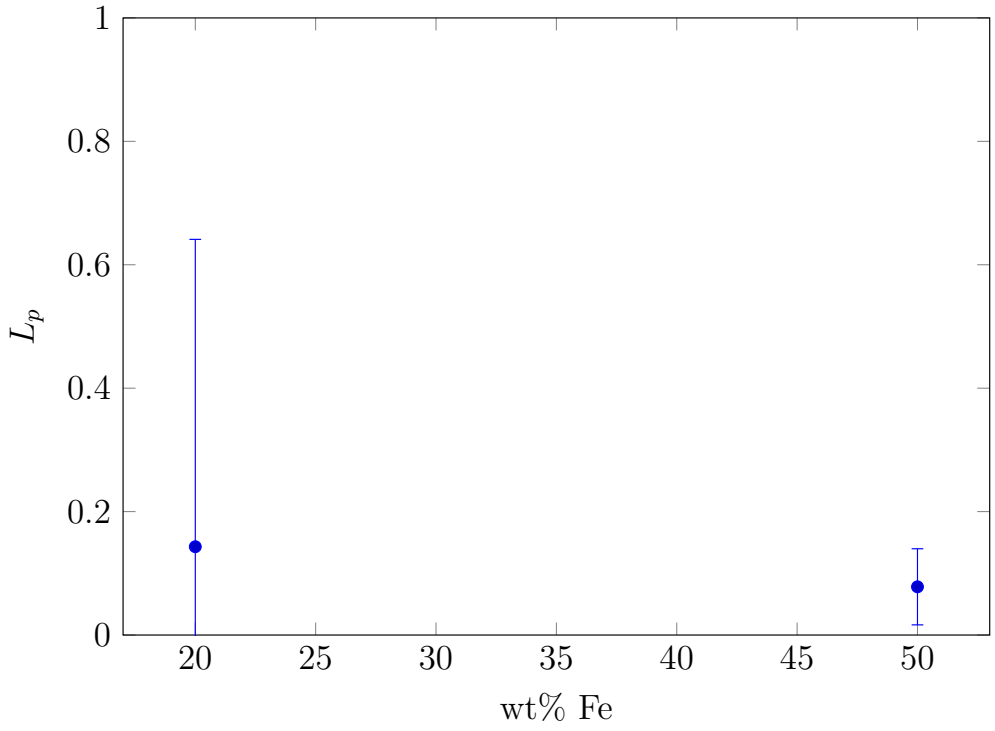

Figure 4.7: Distribution coefficient of phosphorus between slag and alloy as a function of iron content for 35:65 CaO–SiO_2.

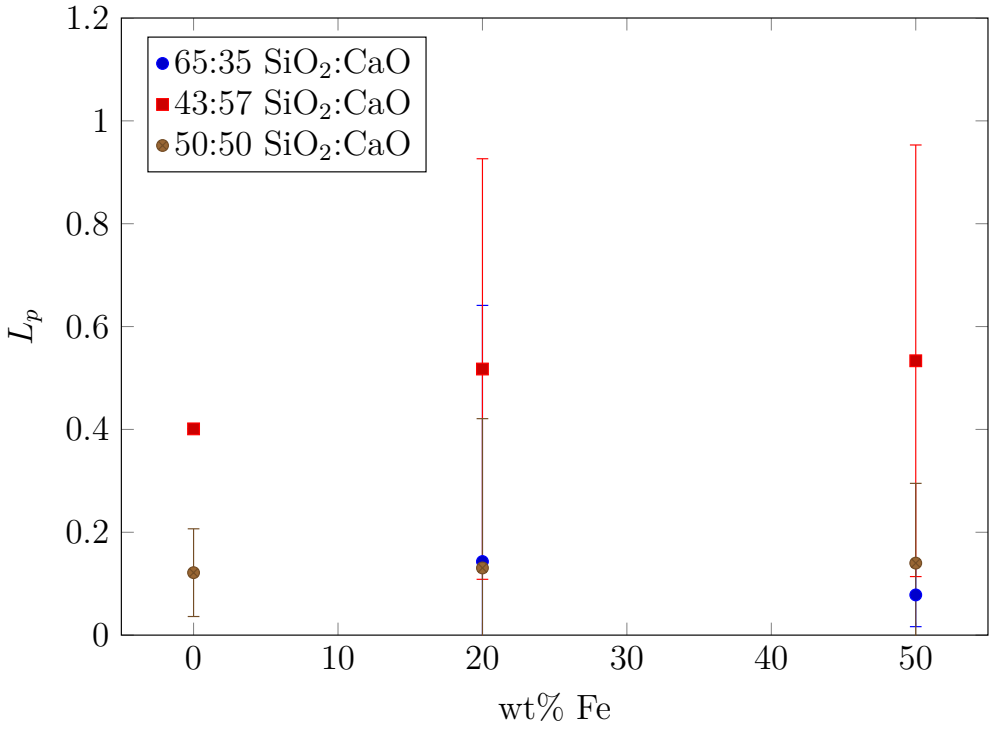

Figure 4.8: Distribution coefficient of phosphorus between slag and alloy as a function of wt % of iron.

of L_p is 0.14.

Figure 4.8 gives the distribution coefficient of phosphorus between metal and SiO_2-CaO slags as a function of Fe content in the metal for all slags utilized in this thesis. As seen in the figure there is a slight increase in the distribution coefficient as a function of iron content in the metal for all slags except for 65:35(wt%) SiO_2 : CaO. The distribution coefficient is highest for the slag with a composition of 43:57(wt%) SiO_2 : CaO which has the highest CaO content. The distribution coefficient is below 1 for all slags, which means a tendency of P going into the metal phase. However, as mentioned previously the experimental values lie inside the error bars of other experimental values, so it is difficult to conclude.

Ca dissolution in metal

Figure 4.9 presents the concentration of Ca in metal as a function of CaO:SiO_2 ratio in the slag. The Ca content in the metal increases with increasing CaO:SiO_2 ratio. In addition the Ca content increases with increasing Si content of the metal. The change with increasing Si content is quite significant at high CaO content of the slag.

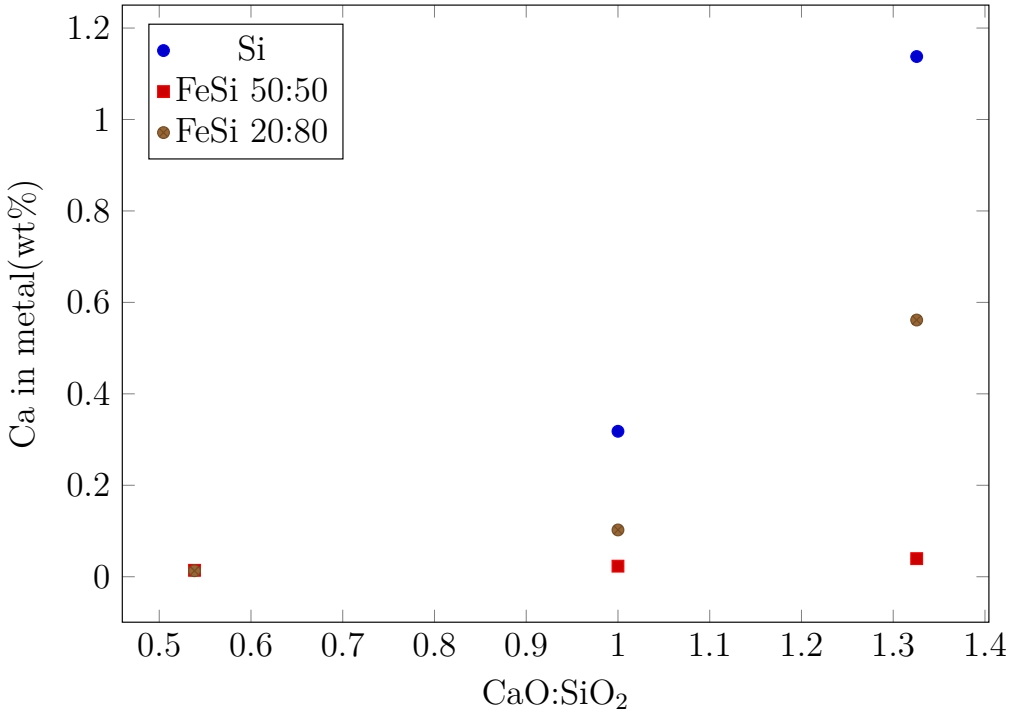

Figure 4.9: Ca pick up in metal as a function of CaO content of slag.

Table 4.2 gives the Ca content in Si for each slag and metal. The values are given as an average of two experiments which have been analyzed with three sub-samples.

Table 4.2: Concentration of Ca in Si and FeSi.

Fe [wt%]	Si [wt%]	SiO_2 [wt%]	CaO [wt%]	Ca [wt%]
50	50	50	50	0.02
50	50	43	57	0.04
50	50	65	35	0.01
20	80	50	50	0.10
20	80	43	57	0.56
20	80	65	35	0.01
0	100	50	50	0.32
0	100	43	57	1.14

4.1.3 Mass loss

Table 4.3 gives an overview of phosphorus content in metal and slag before and after the equilibrium experiments with quenching. The mass loss is calculated as the difference between initial and final values. Loss of phosphorus is in general

relatively high with an average loss of 95 ppm of P. The results indicate that there is lower mass loss for Fe50:Si50 (wt%) and Fe20:Si80 (wt%) equilibriated with 43:57(wt%) SiO_2-CaO slag. This slag type is the slag with the lowest content of SiO_2. The highest mass loss is after equilibration of Fe20:Si80 (wt%) with 65:35 (wt%) SiO_2 : CaO slag.

The phosphorus content in the metal is initially quite low, and goes up after the experiment. This indicates that there has been a transfer of phosphorus from slag to metal. Solar grade silicon is used for the experiments with Si, so the initial value of P in Si is set equal to zero.

The mass balance can be given as presented in equation 4.1. Here m_{slagg} is the mass of slag, m_{met} is the mass of metal, (wt%P) is the phosphorus concentration in slag and [wt%P] the concentration of phosphorus in metal. P_4 is what is lost of phosphorus to the gas phase.

$$m_{slagg} \cdot (wt\%P)_{initial} = m_{slagg} \cdot (wt\%P)_{final} + m_{met} \cdot [wt\%P]_{final} + P_4(g) \quad (4.1)$$

Table 4.3: Table presenting mass loss of P.

Slag Composition SiO_2:CaO (wt%)	Metal Composition Fe:Si (wt%)	P in slag initially (ppm)	P in metal initially (ppm)	Ptot initially (ppm)	P in slag final (ppm)	P in metal final (ppm)	Ptot final	Loss of P
50:50	50:50	218.3	39.2	257.5	24.7	139.3	164	93.5
50:50	50:50	218.3	39.2	257.5	13.7	133.5	147.2	110.3
43:57	50:50	197.5	39.2	236.7	83.2	127.3	210.5	26.2
43:57	50:50	197.5	39.2	236.7	70.0	169.3	239.3	-2.6
65:35	50:50	182.2	39.2	221.4	10.3	96.1	106.4	115
65:35	50:50	182.2	39.2	221.4	4.1	84.1	88.2	133.2
50:50	20:80	218.3	28.8	257.5	11.4	109.5	120.9	136.6
50:50	20:80	218.3	28.8	257.5	17.4	110.6	128	129.5
43:57	20:80	197.5	28.8	236.7	51.9	106.7	158.6	78.1
43:57	20:80	197.5	28.8	236.7	67.3	122.7	190	46.7
65:35	20:80	182.2	28.8	221.4	10.0	61.6	71.7	149.7
65:35	20:80	182.2	28.8	221.4	6.6	53.6	60.2	161.2
50:50	0:100	218.3	≈ 0	257.5	18.8	162.0	180.8	76.7
50:50	0:100	218.3	≈ 0	257.5	18.0	141.8	159.8	97.7
43:57	0:100	197.5	≈ 0	236.7	45.1	112.4	157.5	79.2

4.1.4 Reproducibility of results

NIST 195 FeSi, a standard reference material from National Institute of Standards and Technology [51], was analyzed together with metals from experiments in order to compare the phosphorus concentration measured by ICP-MS at NTNU with the certified value of 190 ppm.

Table 4.4: Analyzed and certified values of NIST 195 FeSi

Analyzed [ppm]	certified [ppm]	deviation [%]
162	190	-17.3

As shown in table 4.4, there is a deviation of 17.3 % between the analyzed value of phosphorus from ICP-MS at NTNU and the certified value from NIST.

4.2 Phosphorus distribution between FeSi, Si and slag

EPMA analysis was conducted on the sample from the experiment with Fe20:Si80 wt% and $CaO-SiO_2-P_2O_5$ (45.8-47.6-5.4 wt%) slag which was held for three hours at 1600 °C and cooled in a controlled manner of 1 °C per minute down to 1360 °C. Figure 4.10 gives an overview of the micro-structure of both slag and metal. The area marked with "1" is the FeSi matrix and the area marked with "2" is the Si dendrite structure. Slag is marked with "3" in the figure.

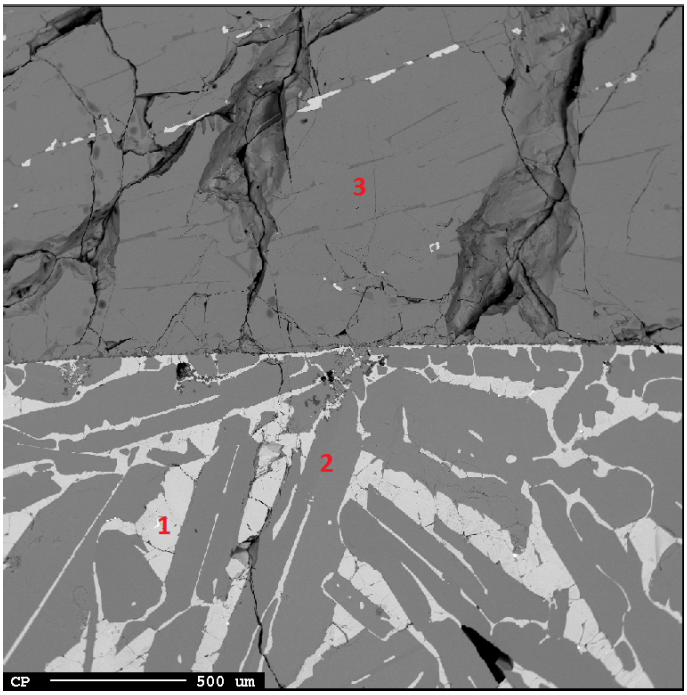

Figure 4.10: Overview of slag phase and metal phase after experiment. 1:FeSi, 2:Si,3:Slag.

The compositions of the metal phases are given in table 4.5. Three points were analyzed in each area. For instance the amount of Si in the area towards the slag phase is given in normalized weight percent as an average of three analyzed points. As shown in the table, silicon phase contains mainly silicon with an average value of 97.2 wt%. Both phosphorus content and iron content have an average value of 0.1 wt% in the Si-phase.

Ferrosilicon phase contains in average 55.4 wt% Si and 42.5 wt% Fe. The average phosphorus content is 0.1 wt%. Areas towards slag, in the middle of the metal and towards the crucible were all analyzed. As for silicon, the value for one area in FeSi matrix represents the average of three analyzed points. The metal composition before the experiment was FeSi with 80 wt% Si and 20 wt% Fe.

Carbon is also included in the table, but is not accurately determined by EPMA analysis.

Table 4.5: EPMA analysis of metal phases in experiment with slow cooling.

Phase	Si [norm.wt%]	Fe [norm.wt%]	P [norm.wt%]	C [norm.wt%]
Si towards slag	96.8	0.2	0.1	2.8
Si middle	97.7	0.1	0.1	2.1
Si towards crucible	97.2	0.1	0.1	2.5
avg. Si phase	97.2	0.1	0.1	2.5
FeSi towards slag	55.4	42.5	0.1	2.0
FeSi middle	55.5	42.5	0.1	1.9
FeSi towards crucible	55.2	42.5	0.1	2.2
avg. FeSi phase	55.4	42.5	0.1	2.1

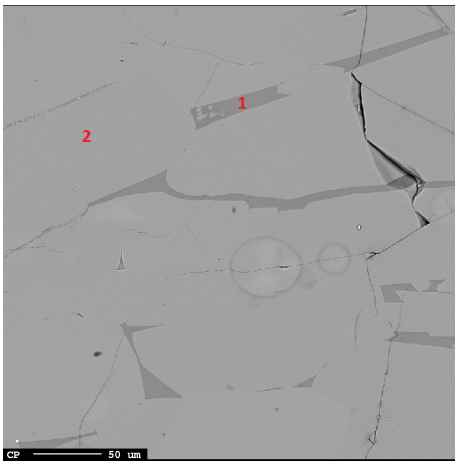

(a) Figure presenting main slag matrix (2) and darker areas (1).

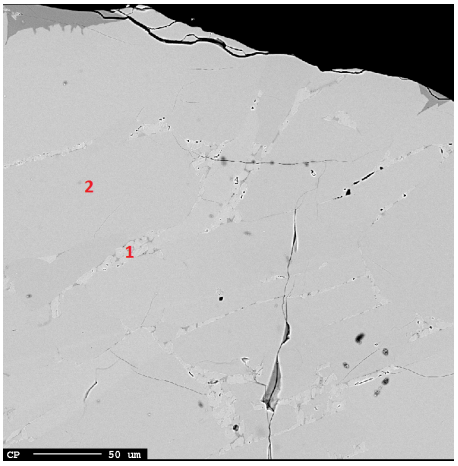

(b) Figure presenting main slag matrix (2) and lighter areas (1).

Figure 4.11: Figures of slag phases from experiment with slow cooling.

The compositions of slag phases are given in table 4.6. Three points were analyzed in each area for slag phases, similar as for metal phase. The areas studied were slag towards metal, middle of slag and slag towards top of crucible. In addition some darker spots were observed in the slag matrix as shown in figure 4.11a. The particles are given as "dark particles in slag" in the table. The average composition of the particles was 43.8 wt% SiO_2, 28.1 wt% CaO, 24.1 wt% MgO and 3.6 wt% Al_2O_3. Some areas which were lighter than the slag matrix were also observed towards the surface of the slag. In table 4.6 the lighter particles are given

as "light grey particles in slag". The particles contained in average 36.1 wt% SiO_2, 50.4 wt% CaO and 13.4 wt% MgO. Figure 4.11b shows the lighter areas in the main slag matrix. The total initial value of MgO in the slag was only 0.9 wt% according to XRF analysis.

Table 4.6: EPMA analysis of slag phases

comment	Phase	SiO_2 [norm.wt%]	CaO [norm.wt%]	P_2O_5 [norm.wt%]	MgO [norm.wt%]	Al_2O_3 [norm.wt%]
Main slag phase	Towards metal	51.9	48.0	0	0.1	0
	Middle	52.0	47.9	0	0.1	0
	Towards top	51.9	48.1	0	0.1	0
	avg slag main	51.9	48.0	0	0.1	0
Dark particles in slag	Towards metal	43.7	27.2	0.6	24.8	3.7
	Middle	43.3	28.9	0.4	24.1	3.2
	Towards top	44.3	28.3	0.3	23.3	3.8
	avg dark	43.8	28.1	0.4	24.1	3.6
Light grey particles in slag	Towards top	36.1	50.4	0	13.4	0.1

4.3 Thermodynamic modeling

Thermodynamic modeling of phosphorous distribution between liquid metal and slag solutions was conducted in cooperation with postdoc Elmira Moosavi-Khoonsari using FactSage 7.1 thermochemical software [15]. As explained in the experimental section, calculations were performed using a liquid slag mini-database newly optimized by Moosavi-Khoonsari. The mini-database incorporates phosphorus in the form of both phosphide and phosphate, the major phosphorous species in reducing and oxidizing conditions, respectively, thus allowing the phosphorous distribution calculations under various partial pressures of oxygen. The FactSage FToxide database [15] contains phosphorus only as phosphate.

The newly optimized database was used together with other databases in FactSage and the Gibbs energy minimization routine to calculate phosphorous distribution in slag/metal/gas equilibria. Thermodynamic calculations conducted with respect to experimental conditions already elaborated in section 3.2.3 of the thesis are depicted in Figures 4.12 through 4.26. The solid lines in the figures represent the phosphorous distribution coefficient, where the liquid phase is stable, and the dash dotted lines represent the predicted phosphorous distribution coefficient of the metastable liquid phase, where all solid phases were suppressed in the calculations. Figures of the phosphorus distribution coefficient is divided according to the different phase regions of the $CaO-SiO_2$ phase diagram at 1600 °C. For comparison, the phosphorous distribution calculations between the slags and Fe80:Si20(wt%) and pure Fe were also carried out.

4.3.1 Si/slag equilibration

Figure 4.12 presents the measured and calculated phosphorus distribution coefficients between Si and $CaO-SiO_2$ slags at 1600 °C in Ar-atmosphere. The red lines in the lower part of the figure represent the calculations from FactSage FToxide database including only phosphate species. The phosphorus distribution coefficient as presented in equation 2.30 is calculated from the equilibrium concentrations of phosphorus in slag and metal. The line towards the top of the figure is the calculated equilibrium phosphorus distribution from the optimized mini-database by Moosavi-Khoonsari. Experimental values from Krystad [42] are marked in the figure with circles and experimental values obtained in this study are marked with triangles. As shown in the figure, calculations using FToxide database give significantly lower values (about 12-14 orders of difference in logarithmic scale) for the phosphorus distribution coefficient than the experimental values and those from the optimized database. The overall trend is that with increasing the basicity

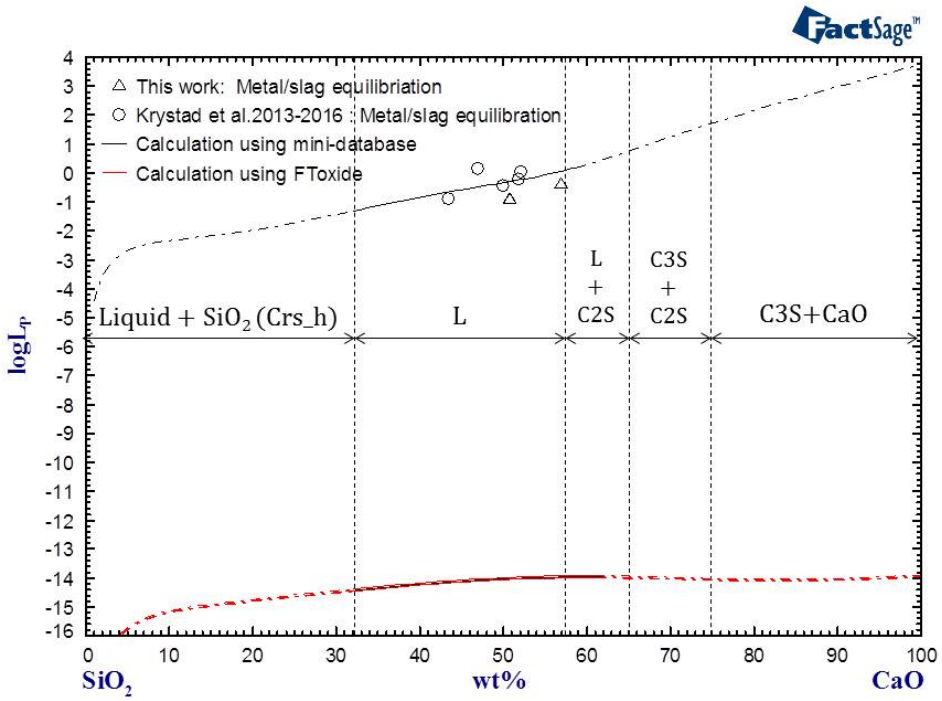

Figure 4.12: Calculated phosphorus distribution coefficient between Si and $CaO-SiO_2$ in comparison to experimental data (1600 °C, Ar atmosphere). L:liquid, C2S:Ca_2SiO_4, C3S:Ca_3SiO_5, Crs_h: high_temperature cristobalite.

(CaO/SiO_2), the phosphorus distribution coefficient increases.

Figure 4.13 presents the composition of the liquid metal calculated from our model with optimized parameters after Si/$CaO-SiO_2$ slag equilibration at 1600 °C. As seen in the figure the amount of Ca in the metal increases with increasing CaO content of the slag.

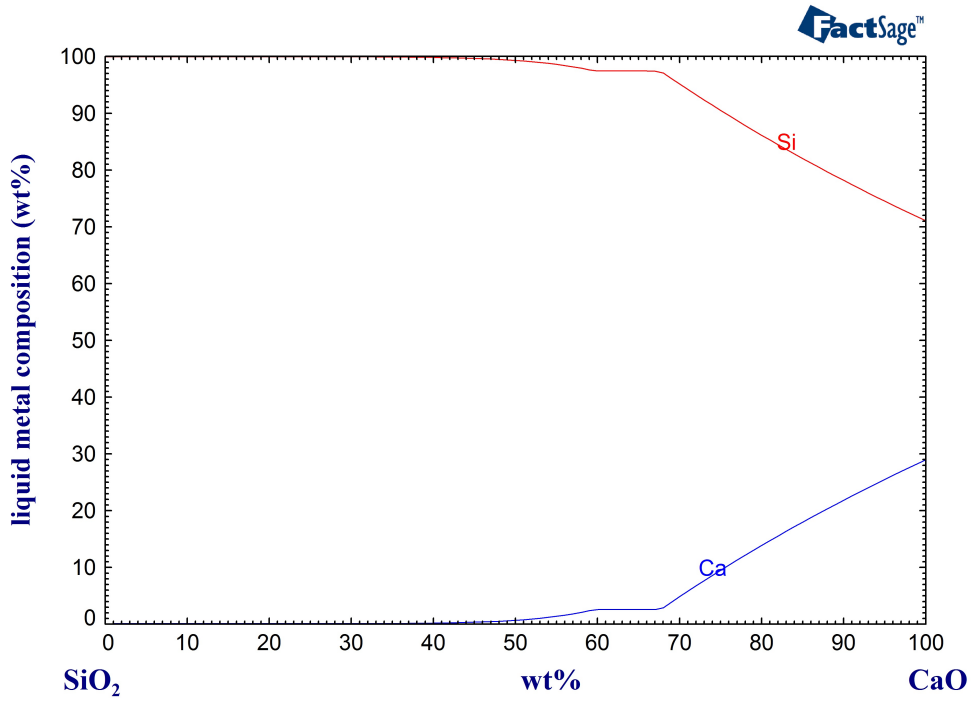

Figure 4.13: Calculated composition of liquid metal as a function of CaO weight percent after Si/$CaO-SiO_2$ slag equilibration (1600°C, Ar).

Figure 4.14 gives the Ca concentration of Fe20:Si80(wt%) metal after equilibration with $CaO-SiO_2$ slags in the slag composition range equivalent to the experimental values in this work. The experimental Ca concentration in Si seems to follow the same trend as the calculated values, but are a bit lower than the calculated ones.

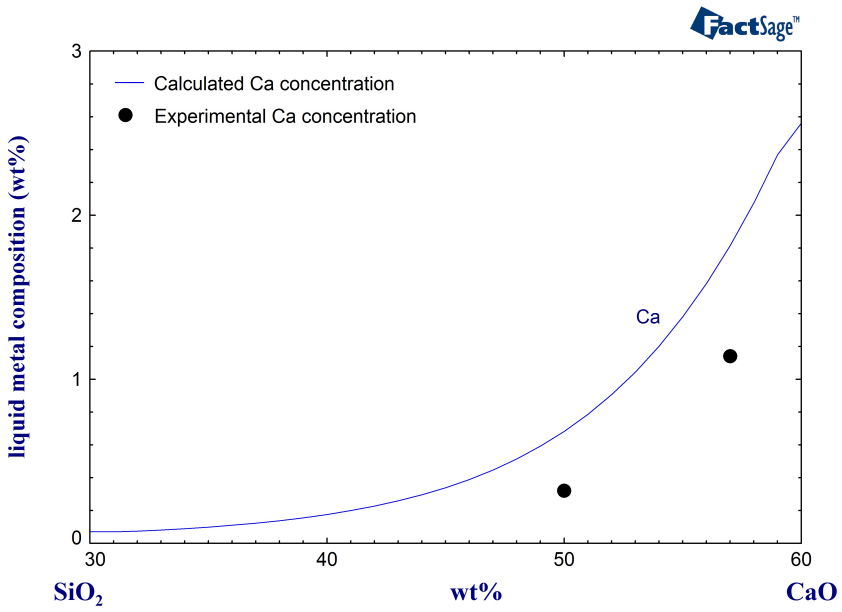

Figure 4.14: Ca concentration of metal in relevant slag composition area.

4.3.2 Fe20:Si80/ slag equilibration

Figure 4.15 depicts the measured and calculated phosphorus distribution coefficients between Fe20:Si80 (wt%) and CaO – SiO_2 slags at 1600 °C in Ar-atmosphere. As mentioned before, the red lines in the lower part of the diagram represent the phosphorus distribution calculated for slag from FactSage FToxide database comprising only phosphate species. The line in the upper part of the diagram represents the phosphorus distribution calculated by including the slag from the newly optimized mini-database by Moosavi-Khoonsari which contains both phosphide and phosphate. The experimental values obtained for the phosphorus distribution between Fe20:Si80 (wt%) and slags from this thesis are presented as circles in the figure. Deviation between the calculated values from FToxide database and the experimental values and those from the optimized database is in the order of 14 in logarithmic scale. According to calculations there is an increase in the phosphorus distribution coefficient with increasing CaO content in the liquid slag. The experimental data also show increasing trend within the experimental error range as seen in figure 4.2.

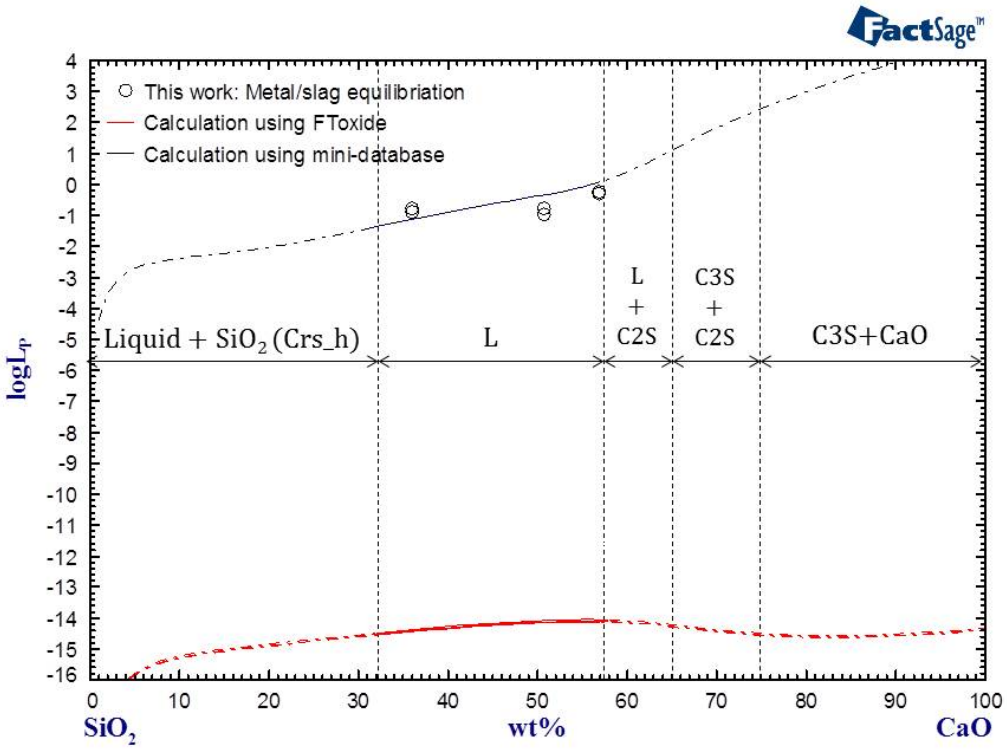

Figure 4.15: Calulated phosphorus distribution coefficient between Fe20:Si80 (wt%) and CaO–SiO_2 (1600 °C, Ar). For abbreviations see figure 4.12.

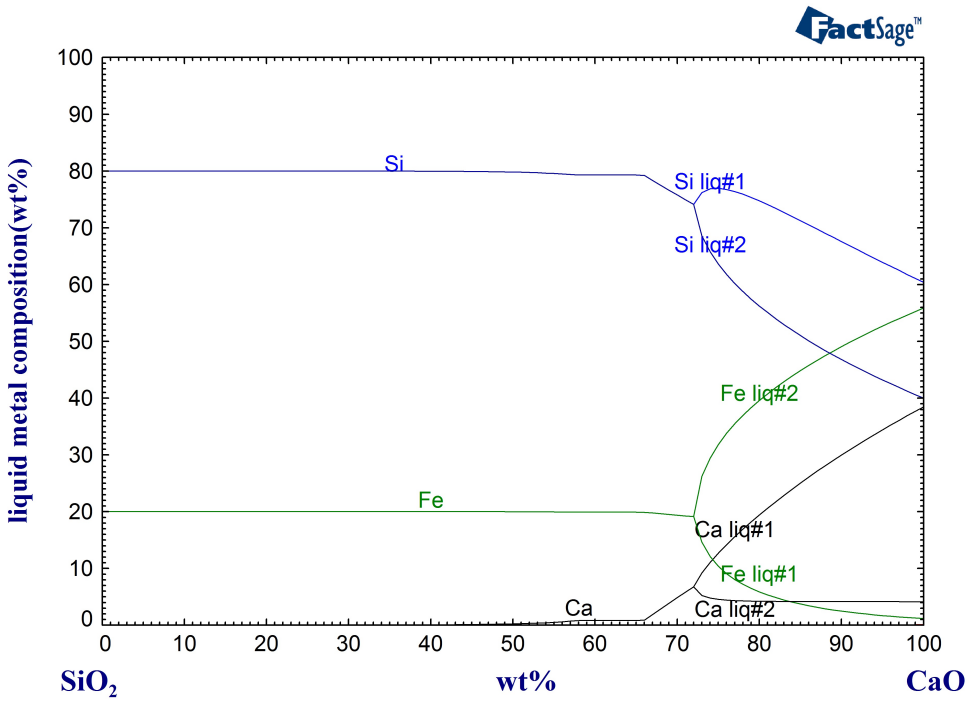

Figure 4.16: Calculated composition of liquid metal after Fe20:Si80 (wt%)/CaO–SiO_2 slag equilibration (1600°C, Ar).

Figure 4.16 presents the composition of the liquid metal calculated from our model with optimized parameters at 1600 °C after Fe20:Si80(wt%) equilibration with CaO–SiO_2 slags. As seen in the figure, the amount of Ca pick up in the liquid metal increases with increasing CaO content of slag. Below 50 wt% CaO, the Ca content of metal is almost zero. At higher contents of CaO than what is used in this work, two liquids form. The Fe-Si-Ca ternary phase diagram at 1600 °C was calculated using FactSage 7.1 FTlite database, and is given in figure 4.18. It is evident from the phase diagram that Fe and Ca are immiscible.

Figure 4.17 gives the calculated and measured values of Ca in Fe20:Si80 after equilibration with CaO–SiO_2 slags in the composition range of slag equivalent to the experimental conditions of this work. The experimental and calculated values of Ca in Si seems to follow the same trend, but the experimental values are a bit lower than the calculated ones.

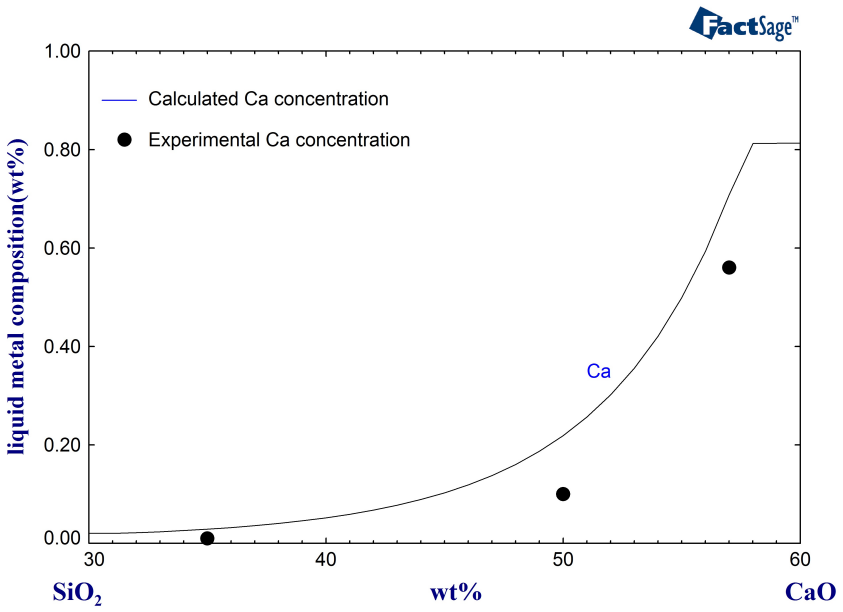

Figure 4.17: Calculated and measured values of Ca in Fe20:Si80(wt%) after equilibration with $CaO-SiO_2$ slags.

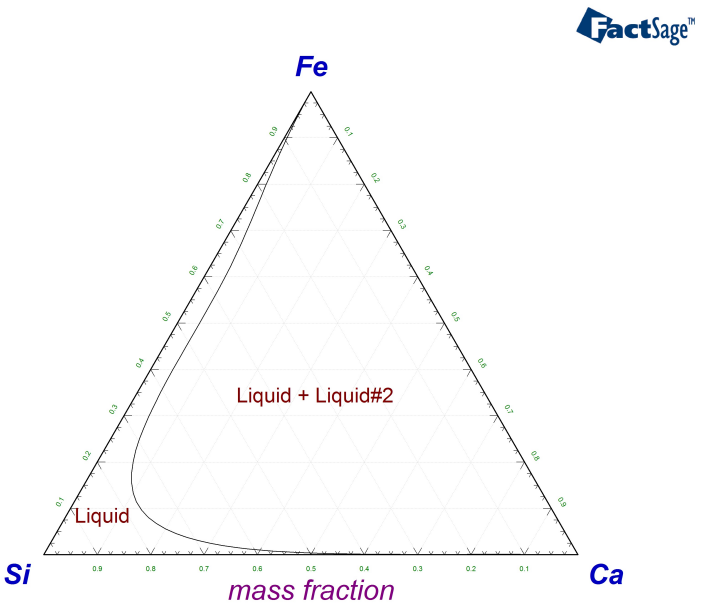

Figure 4.18: The Fe-Si-Ca ternary phase diagram at 1600 °C calculated using FactSage 7.1 FTlite database

4.3.3 Fe50:Si50/slag equilibration

Figure 4.19 presents the measured and calculated phosphorus distribution coefficients between Fe50:Si50 (wt%) and CaO – SiO_2 slags at 1600 °C in Ar-atmosphere. The red lines in the lower part of the figure represent the phosphorus distribution calculated for slag from FactSage FToxide database incuding phosphate species. The line in the upper part of the figure represents the phosphorus distribution calculated for slag from the newly optimized mini-database by Moosavi-Khoonsari. The experimental phosphorus distribution coefficients between Fe50:Si50(wt%) and slag obtained in this work are presented as circles in the figure. According to the calculations, the phosphorus distribution coefficient increases with increasing the slag basicity (CaO/SiO_2). The experimental data also show increasing trend within the experimental error range.

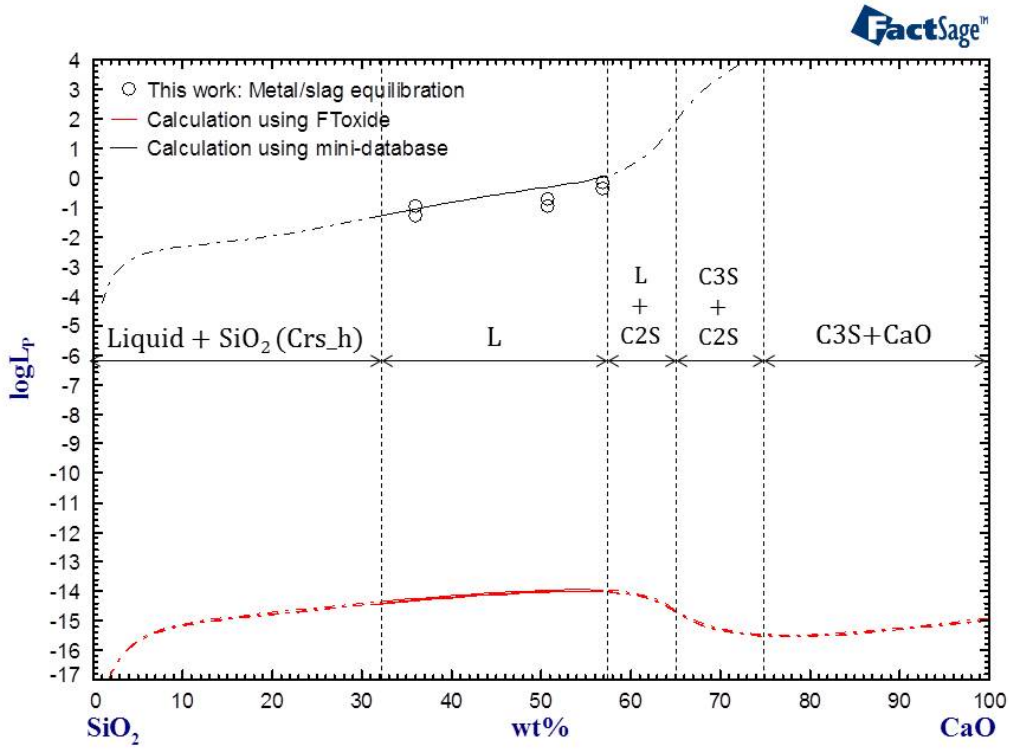

Figure 4.19: Calculated phosphorus distribution coefficient between Fe50:Si50(wt%) and CaO – SiO_2 slags.

Figure 4.20 depicts the liquid metal composition calculated from our model with optimized parameters at 1600 °C in Ar-atmosphere. As for Si and Fe20:Si80(wt%), the amount of Ca in liquid metal increases with CaO content of slag. At higher CaO concentrations than 70 wt%, two liquids form. As shown in the figure, the

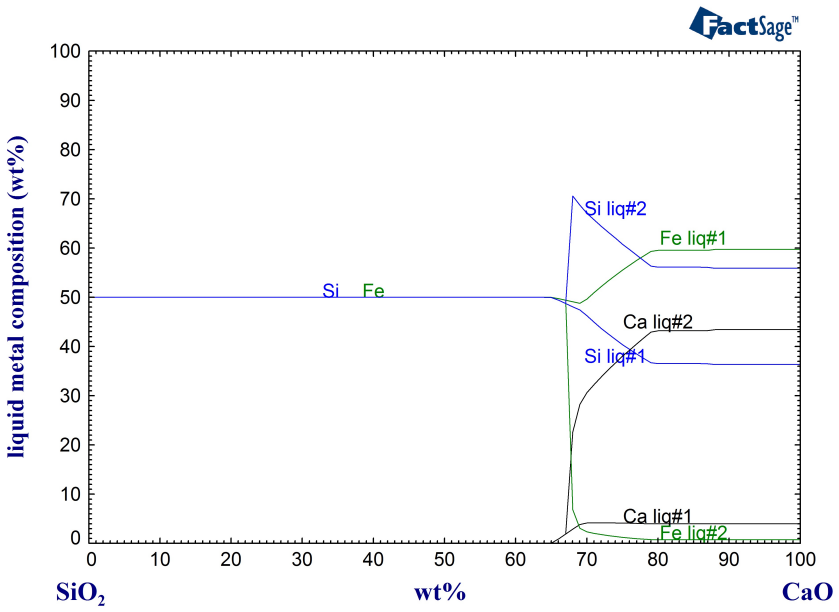

Figure 4.20: Calculated composition of liquid metal after Fe50:Si50 (wt%)/CaO–SiO_2 slag equilibration (1600°C, Ar).

amount of Ca in liquid 2 is larger than that in liquid 1. Liquid 2 contains the most Si.

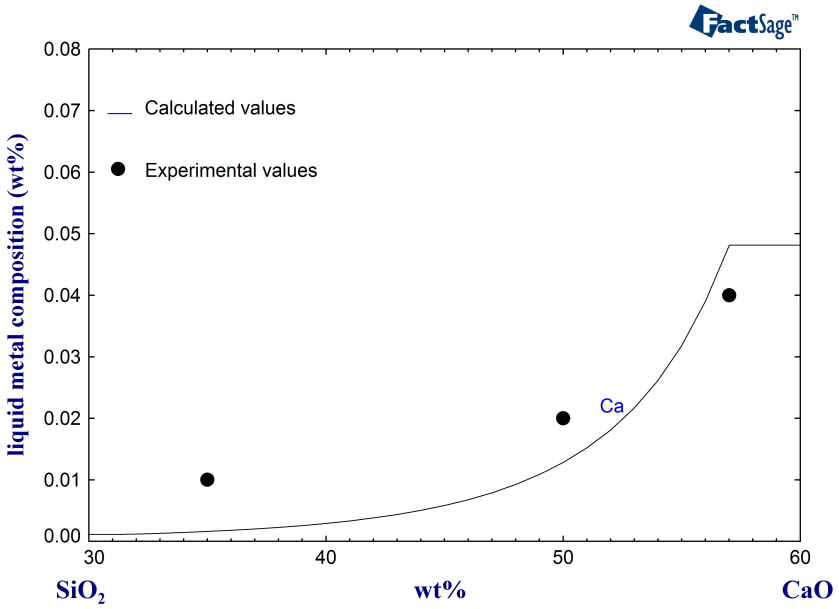

Figure 4.21: Figure presenting Ca concentration in Fe20:Si80 after equilibration with CaO–SiO_2 slag. Both calculated values and experimental values are included.

Figure 4.21 gives the calculated and measured values of Ca in Fe50:Si50 after equilibration with $CaO-SiO_2$ slag in the composition range equivalent to the experimental conditions. The calculated and measured concentrations seems to follow the same trend. However, the measured values are a bit higher than the calculated ones at 35 and 50 wt% CaO.

4.3.4 Fe and Fe80:Si20/ slag equilibration

Figure 4.22 presents the calculated phosphorus distribution coefficients between Fe80:Si20 (wt%) and $CaO-SiO_2$ slags at 1600 °C in Ar-atmosphere. The red lines represent the phosphorus distribution coefficient calculated for slag from FactSage 7.1 FToxide database including only phosphate species. According to the calculations, the phosphorus distribution coefficient increases with increasing CaO content in the liquid region represented by the solid lines. Experiments were not conducted for the alloy composition Fe80:Si20(wt%). This is included to get an idea of how the phosphorus distribution changes with iron content of the alloy.

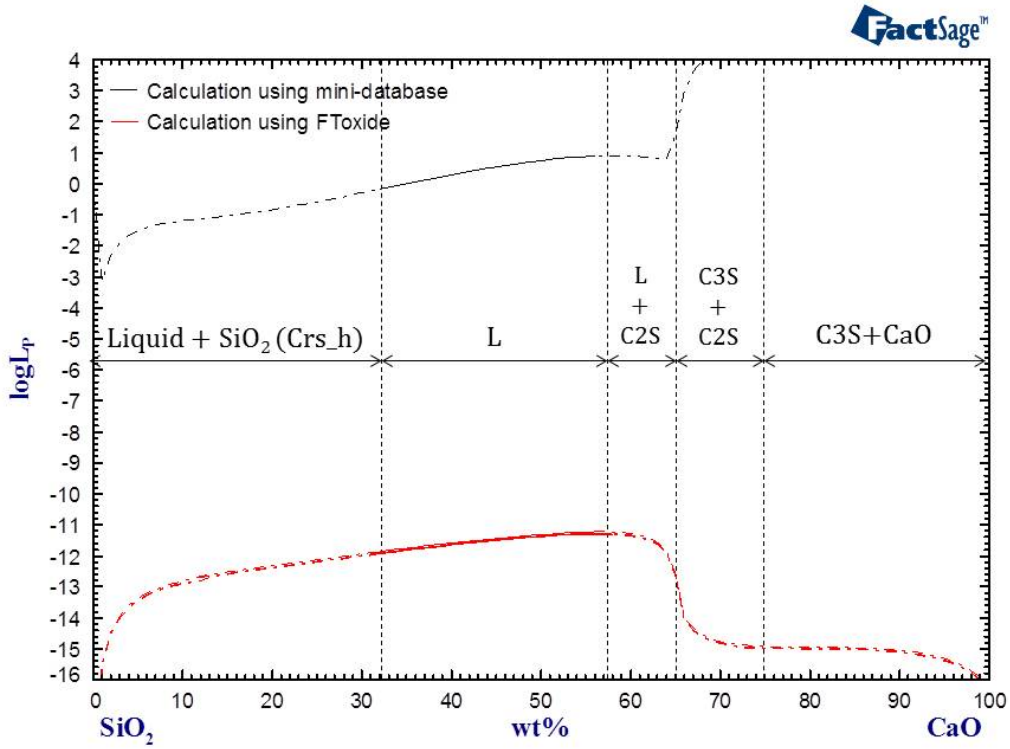

Figure 4.22: Calculated phosphorus distribution coefficient between Fe80:Si20 (wt%) and $CaO-SiO_2$ slags (1600 °C, Ar).

Figure 4.23 shows the calculated phosphorus distribution coefficients between

Fe and $CaO-SiO_2$ slags at 1600 °C in Ar-atmosphere. The phosphorus distribution coefficient increases with increasing the slag CaO content. Comparing with the previous FeSi alloys, the logarithmic values of Lp are significantly higher for Fe. The phosphorus distribution coefficients , calculated from FactSage FToxide database, are in the order of 10^{-8} to 10^{-5} compared to 10^{-14} to 10^{-12} for silicon containing alloys.

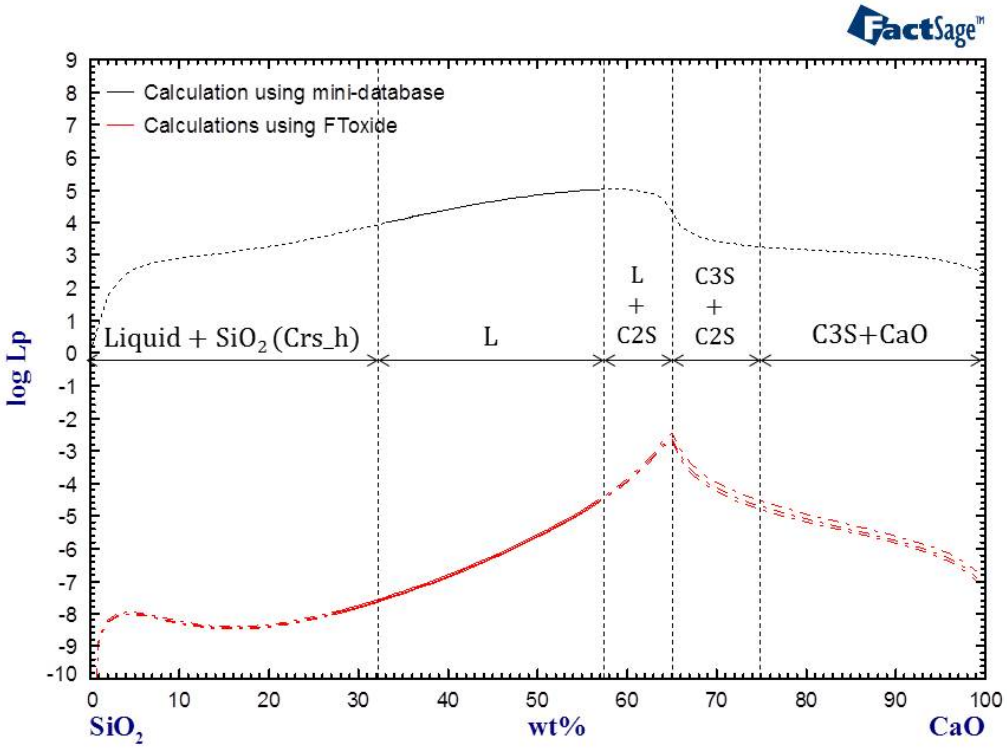

Figure 4.23: Calculated phosphorus distribution coefficients between Fe and $CaO-SiO_2$ slags (1600 °C, Ar).

4.3.5 Stable phases

The following subsection presents calculated values from the newly optimized slag database for Moosavi-Khoonsari.

Figure 4.24 illustrates the calculated stable phase of phosphorus in slag as Ca_3P_2 or $Ca_3(PO_4)_2$ for Si, Fe and various compositions of FeSi alloys. The $Ca_3(PO_4)_2$ phase is marked with a blue color and as illustrated in the figure, the amount of $Ca_3(PO_4)_2$ increases with increasing iron content of the alloy. The Ca_3P_2 phase is marked with a purple color and as presented in the figure, the amount of Ca_3P_2 increases with increasing silicon content of the FeSi alloy. There

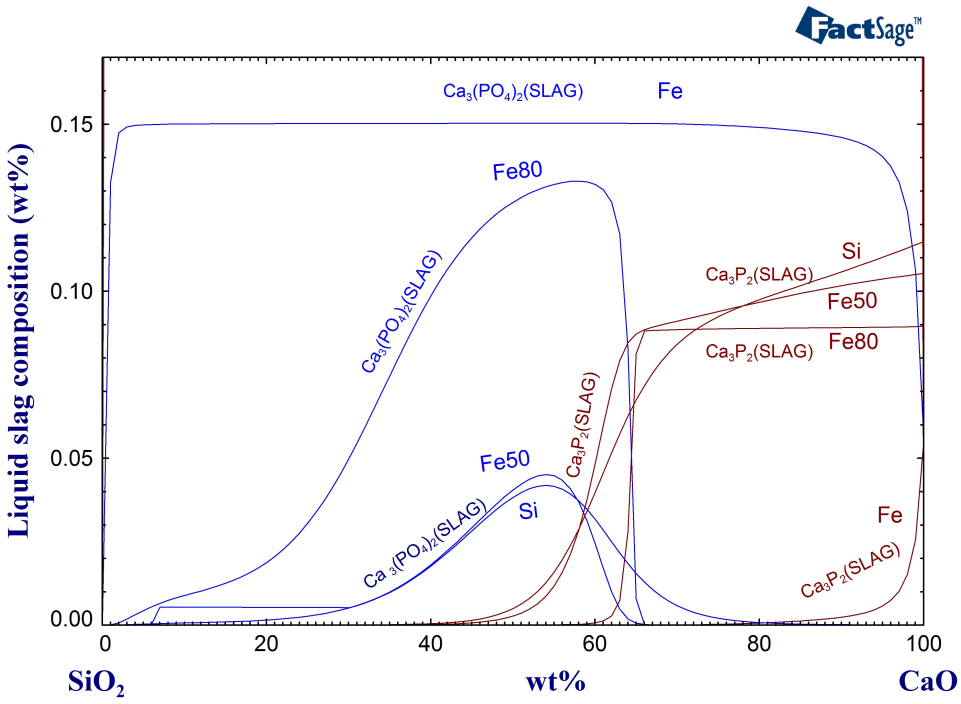

Figure 4.24: Calculated stable phosphorus species in slag after equilibration with metals at 1600 °C

is a shift from $Ca_3(PO_4)_2$ to Ca_3P_2 with increasing CaO content of the slag. Calcia-silica slag with a CaO concentration of 35 wt% CaO has only $Ca_3(PO_4)_2$ present in slag after equilibration with metals. At 50 wt% CaO there are small amounts of Ca_3P_2 forming in slag after equilibration with Fe20:Si80 and Si. At 57 wt% CaO, the concentration of Ca_3P_2 is higher than the concentration of $Ca_3(PO_4)_2$ for both Fe20:Si80 and Si. $Ca_3(PO_4)_2$ is still the dominating phosphorus slag species at high CaO concentrations for alloys with high iron contents.

The activity coefficient of P in FeSi as a function of iron content is calculated using FactSage and presented in figure 4.25. As shown in the figure, the activity coefficient is decreasing with increasing iron content. This is calculated by the activity and mole fraction from FactSage calculations. Here it is assumed that Henry's law is applicable due to phosphorus being a dilute specie.

Figure 4.26 presents how the oxygen potential in the system changes when equilibrating $CaO-SiO_2$ slags with various metals. Increasing the iron content appears to increase the oxygen partial pressure.

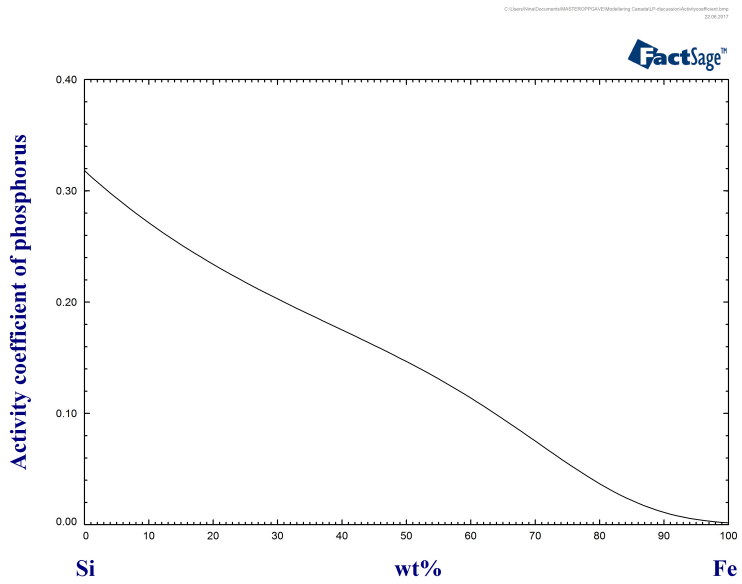

Figure 4.25: Activity coefficient of P in FeSi as a function Fe content of the alloy at 1600 °C.

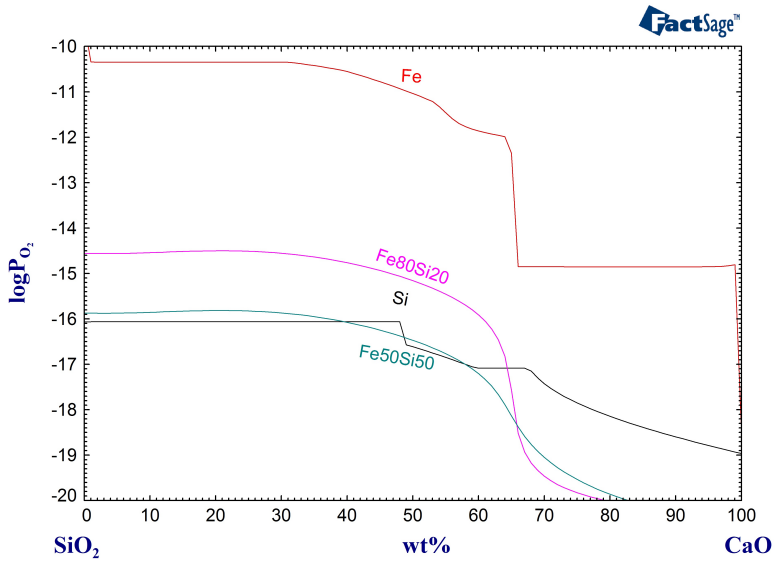

Figure 4.26: Calculated oxygen partial pressure of system with equilibration of $CaO-SiO_2$ slags with various alloys.

Chapter 5

Discussion

In this section experimental data of the phosphorus distribution coefficient between $CaO-SiO_2$ slags and FeSi/Si will be compared with data from the literature and with data from thermodynamic modeling conducted in FactSage 7.1. The experimental setup, industrial application and the reproducibility of the results will be evaluated. A discussion on the validity of thermodynamic modeling for the system is also included.

5.1 Phosphorus distribution between FeSi and slag and Si and slag

Figure 5.1 gives the phosphorus distribution coefficient between slag and metal as a function of $CaO : SiO_2$ ratio of slag. Plot I through V are collected from the literature and plot VI through VIII are experimental values from experiments conducted in this study.

Due to limited available literature on phosphorus distribution between FeSi and slag, this section includes a joint discussion on the distribution of phosphorus between FeSi and slag and between Si and slag.

The only available literature on the phosphorus distribution between FeSi and $CaO-SiO_2$ slag, according to this authors knowledge, is the patent from Enebakk et al.(2010) [47] where ferrosilicon with a silicon content below 30 wt% was used to remove phosphorus from the slag. Their intention was then to use the slag further in slag refining of boron from metallurgical grade silicon. The total initial value of phosphorus in the slag was 20 ppmw and the value of phosphorus in the slag after the reaction with ferrosilicon was less than 2.5 ppmw. The real final value of phosphorus in slag was calculated to be 0.1 ppmw according to mass balance. Phosphorus content of silicon after equilibration with the slag was 4 ppmw. The

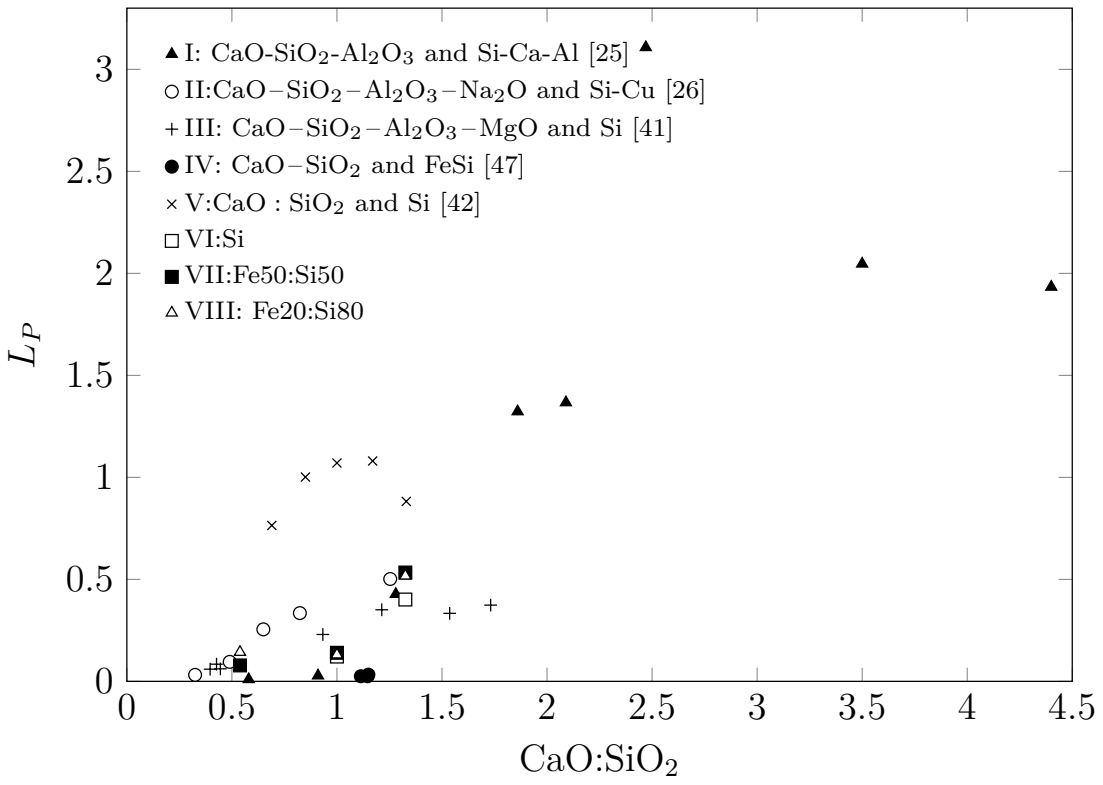

Figure 5.1: Distribution coefficient from various articles

calculated phosphorus distribution coefficients from values of Enebakk et al.(2010) are given in figure 5.1 and labeled with IV. Compared to the experimental values of phosphorus distribution between Fe20:Si80 and CaO : SiO_2 slags and between Fe50:Si50 and CaO : SiO_2 slags given as VII and VIII in the figure, the values from Enebakk et al. are lower. Experiments conducted with ferrosilicon in this thesis had a silicon content of 50 and 80 wt%, which is higher than the silicon content of the ferrosilicon used in Enebakk et al.(2010).

Lynch(2009) [20] made a representation of the activity coefficient of phosphorus in ferrosilicon as a function of wt% of iron in the alloy as shown in figure 5.2. Phosphorus in silicon is an ideal solution since the activity coefficient is equal to one. The activity coefficient is lower than unity at an iron content above 65 wt% of Fe. Iron contents from zero and up to 65 wt% show a positive deviation from ideality. An activity coefficient lower than unity means that phosphorus is stable in the alloy because of the ternary interaction in the system. According to the figure from Lynch, phosphorus should be more stable in Fe20:Si80(wt%) than in Fe:Si 50:50(wt%) because of a lower activity coefficient ,fp, in Fe20:Si80(wt%) than Fe50:Si50(wt%). As a consequence the phosphorus distribution coefficient between slag and metal should be lower for Fe20:Si80(wt%). The experimental values of phosphorus distribution between Fe20:Si80 (wt%) and CaO−SiO_2 slags

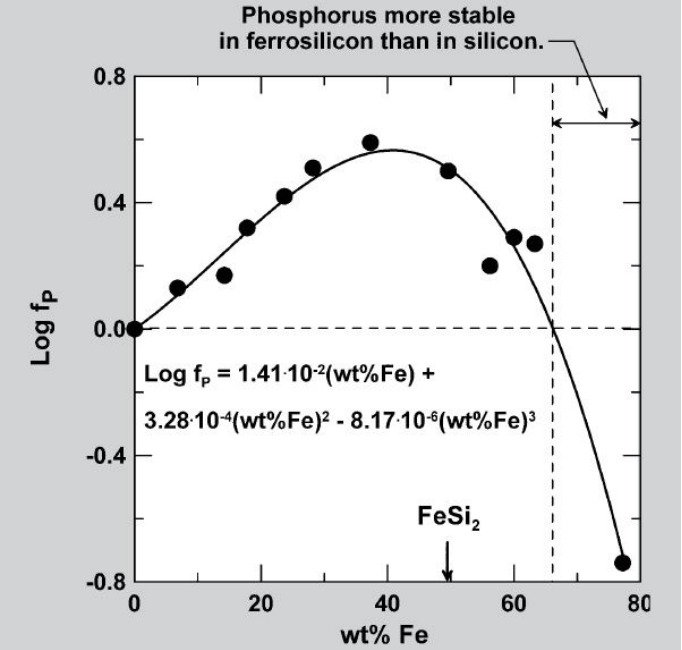

Figure 5.2: Activity coefficient of phosphorus in ferrosilicon from Lynch(2009)

and Fe50:Si50 and $CaO-SiO_2$ slags are quite similar as illustrated in figure 5.1. The trend for both FeSi alloys is that the distribution coefficient increases with increasing basicity ($CaO : SiO_2$ ratio). This fits well with the results from Johnston and Barati(2010,2011), Lynch(2009) and Li et al.(2014) and Fujiwara(1996). Huang et al.(2013) found that the removal efficiency actually decreased with increasing $CaO : SiO_2$ ratio when equilibrating with a $CaO-SiO_2-CaF_2$ slag. The holding time for Huang et al.(2013) was only 0.5 hours, so it might be that equilibrium was not attained. Wang et al.(2017) found that $CaCl_2$ in $CaO-SiO_2-CaCl_2$ slag decreases the viscosity of the slag, which might increase the mass transfer. However, Huang et al. found that $CaCl_2$ did not affect the distribution after slag refining, so no obvious reason for the decrease in phosphorus distribution with increasing $CaO-SiO_2$ ratio is found.

Figure 5.3 presents the phosphorus distribution coefficient as a function of weight percent of iron in the metal for all metals and slags used in experiments of this study. As shown in the figure there is a slight increase in Lp with increasing iron content for slags with compositions of SiO_2-CaO 43:57 and 50:50(wt%). The distribution seems to decrease with increasing iron content for 65:35 SiO_2-CaO slag. However, it is difficult to observe the trend for the various FeSi alloys since one set of experiments lies inside the error rage of other sets. As explained by Lynch(2009), there will be an increased dissolution of Ca in the metal with increasing CaO content of slag. This was also found from experimental results as shown in figure 4.9 and from thermodynamic modeling in FactSage as presented

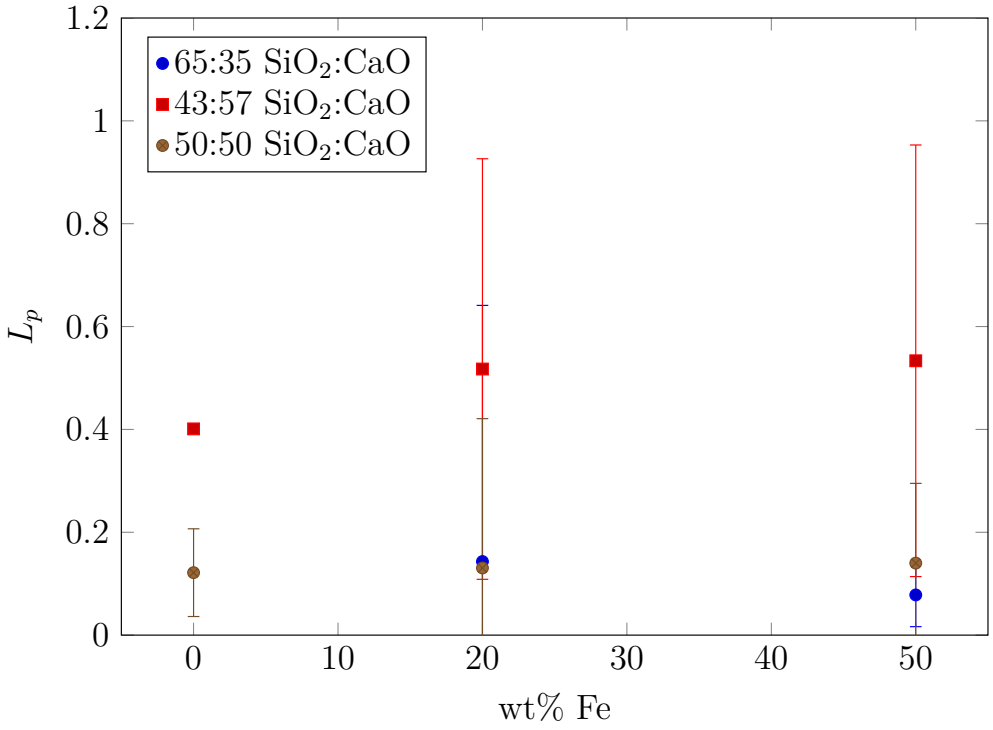

Figure 5.3: Distribution coefficient of phosphorus between slag and alloy as a function of wt % of iron.

in figures 4.13, 4.16 and 4.20. Horn et al.(1998) [18] previously found that Ca and P form a stable Ca_3P_2 phase in Fe25:Si75 and Jung et al.(2011) [27] studied silicon micro-structure after slag refining and found that Ca_3P_2 formed at the grain boundary in silicon. Therefore it might be that a stable compound of Ca and P is formed in the metal after slag refining with the highest CaO content. However, the highest slag basicity gives the highest phosphorus distribution towards slag phase. Kawamura et al.(2013) [24] found that the phosphorus distribution coefficient increased with increasing Ca pick up in Si as presented in figure 2.25. The dissolution of Ca was also increased with increasing silicon content of the alloy. The reason for this is believed to be because of the immiscibility of Fe and Ca as presented in the Fe-Si-Ca phase diagram at 1600 °C calculated by FactSage 7.1 and given in figure 4.18. According to the composition of liquid phase from FactSage calculations for Fe50:Si50(wt%) given in figure 4.20, Ca should not dissolve in metal phase in the CaO range of slag equivalent to this study. So in terms of Ca and P interactions in silicon, it might be that if iron concentration goes up, Ca dissolution decreases and less P will go into metal thereby increasing the distribution coefficient. However no obvious explanation was found on why the phosphorus distribution coefficient decreases with increasing iron content for the slag with composition 65:35 SiO_2 : CaO.

Reductive deposphorization has shown to produce Ca_3P_2 compound in slag at low oxygen potentials and with increasing basicity [25], [24]. According to FactSage calculations the oxygen potential is low for the experimental conditions used in the experiments in this thesis as given in figure 4.26. Therefore it might be that Ca_3P_2 compound formed in slag with increasing basicity and thereby increasing the distribution coefficient. This was as previously shown the trend in the experimental results. Since the oxygen potential is determined by the equilibrium of Si and SiO_2, the oxygen potential will decrease when increasing the CaO concentration in slag.

Figure 5.1 gives as previously mentioned an overview of the phosphorus distribution coefficient collected from articles where it was possible find data of *Lp* as a function of the $CaO : SiO_2$ ratio. It is evident from the figure that Fujiwara et al.(1996) [25] reported high values for the phosphorus distribution coefficient with a maximum value of 3 at a ratio of $CaO : SiO_2$ of 0.75. However metal phase was not pure silicon, but silicon alloyed with Ca and Al. The slag was composed of $CaO-SiO_2-Al_2O_3$. As shown in table 2.1 Jung et al.(2011) also reported a high maximum *Lp* of 2.5 at a oxygen potential of $1.5 \cdot 10^{-21}$ when equilibrating with silicon. The slag constituents utilized in Jung et al.(2011) were $CaO-SiO_2-CaF$. The largest value of the phosphorus distribution coefficient is however reported by Johnston and Barati(2010) with a value of 8.8 at a slag composition of $9\,\%Al_2O_3 - 24\,\%\,CaO - 33\,\%MgO - 34\,\%SiO_2$.

One reason for the high distribution coefficient of Fujiwara might be because of alloying with Ca and Al. Alloying leads to a lower segregation coefficient of P in the alloy then for pure Si. The eutectic of Si-Al is at 13 wt% Si and solidifies at 577 °C. The problem with alloying is that the alloying elements are impurities in silicon as well. Ca and Al are usually removed by oxidative refining of silicon.

Johnston and Barati also used a slag containing alumina in their refining of Si. Figure 5.4 is collected from Johnston and Barati(2010) and illustrates that increasing the amount of SiO_2 relative to Al_2O_3 increases the distribution coefficient. As presented in the figure, *Lp* has a value of 8.8 at a $SiO_2 : Al_2O_3$ ratio of 3.8. This leads to the belief that some Al_2O_3 is positive for the distribution as long as it is at low concentrations. Fujiwara which also reported high *Lp* values used concentrations of Al_2O_3 in slag varying from 45.3 to 59.6%. The highest *Lp* was at a slag composition of $31.1\,\%CaO - 55.8\,\%Al_2O_3 - 12.6\,\%SiO_2$. Figure 2.29 presents phosphorus distribution as a function of $SiO_2 : Al_2O_3$ ratio from data in the article by Fujiwara. Phosphorus distribution coefficient seems to decrease with increasing $SiO_2 : Al_2O_3$ ratio. However, the CaO content was also varied, so it is difficult to make a conclusion on how alumina affected *Lp*. Two experiments from Fujiwara were performed at the same CaO concentration, and the highest

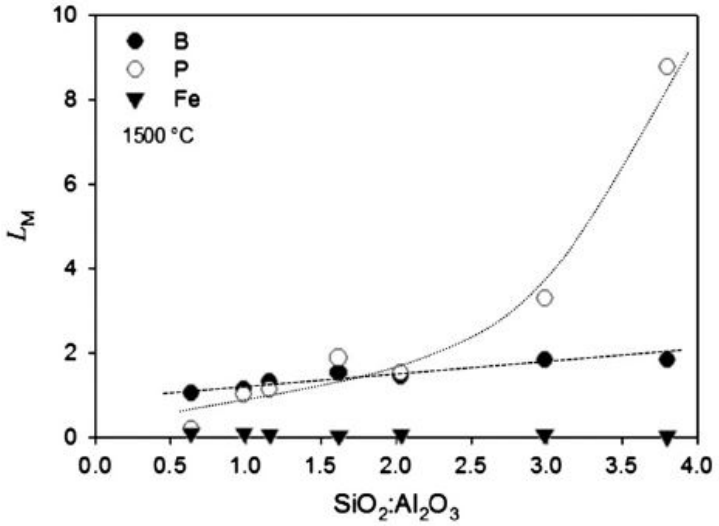

Figure 5.4: Image from Johnston and Barati(2010) [23] presenting *Lp* as a function of $SiO_2 : Al_2O_3$

$SiO_2 : Al_2O_3$ ratio gave the highest *Lp*, which was equivalent with results from Johnston and Barati(2010).

As explained in Johnston et al.(2012) [31], alumina might work as an acidic oxide, forming network with the SiO_4^{4-} chain. To achieve electrical neutrality, it is charge balanced with Ca^{2+}. Since the available amount of CaO decreases, the $CaO : SiO_2$ ratio which gives the highest *Lp* increases. Therefore it might be that the ratio of CaO/SiO_2 which gives the highest distribution coefficient is not reached where alumina is a slag constituent.

Jung et al.(2011) equilibriated $CaO-SiO_2-CaF_2$ slag with silicon. The authors report the distribution coefficient as a function of oxygen potential instead of basicity. Since Ar-H_2 gas was utilized and SiO_2 is the only oxide in the slag contributing to the oxygen potential, the oxygen potential is a measure of how much SiO_2 is present in the slag. Figure 5.5 is taken from Jung et al. and presents the phosphorus distribution coefficient as a function of oxygen potential. As shown in the figure *Lp* is highest at lower oxygen potentials or lower SiO_2 content which is equivalent to results from other literature sources. CaF_2 has shown previously to decrease the viscosity of $CaO-SiO_2-CaF_2$ slag [28], which might increase the mass transfer of phosphorus relative to a $CaO-SiO_2$ slag. The use of hydrogen in the gas mixture lead to phosphorus evaporating from the silicon melt. They also found that increasing the basicity lead to a decrease in evaporation believed to be because of formation of a stable Ca_3P_2 compound in the slag.

The holding time for experiments conducted in this study was 3 hours. Equilibrium time is dependent on the diffusivity of phosphorus. Krystad et al.(2012)

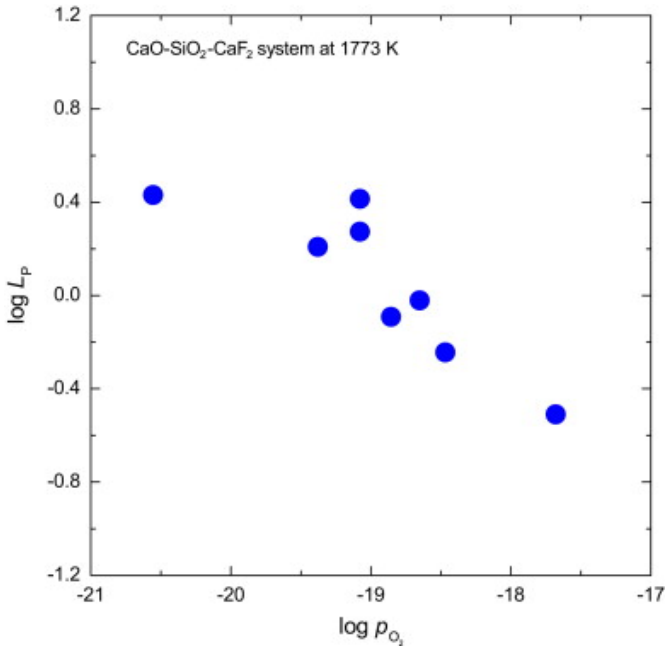

Figure 5.5: Phosphorus distribution coefficient as a function of oxygen potential collected from Jung et al. [27]

found that the boron equilibrium time for 15g of silicon and 15 g of slag with composition 50% CaO and 50% SiO_2 was approximately equal to two hours [34]. The diffusion coefficients of phosphorus and boron in silicon are similar as presented in figure 2.12 as a function of temperature. This indicates that a equilibrium time of three hours is long enough for 50:50 wt% SiO_2-CaO and Si. Figure 2.14 retrieved from Slag Atlas(2005) showed that increasing the SiO_2 content of the $CaO-SiO_2$ slag increased the viscosity. Therefore it is expected that the most acidic slag used in this thesis with a composition of 65 wt% SiO_2 and 35 wt% of CaO would have the slowest mass transfer rate of phosphorus. It is uncertain whether or not 3 hours equilibrium time is enough in order to reach equilibrium for this slag. Longer holding times should be investigated in order to see if equilibrium was in fact reached.

According to Stoke-Einstein equation given in equation 2.25, the diffusivity decreases with increasing viscosity. Bel'tyukov et al.(2014) presented the viscosity of ferrosilicon as a function of silicon content in the alloy up to 50 atomic percent. The viscosity decreases with increasing silicon content. Therefore if one assume that this is the case also at higher silicon contents, the diffusivity of phosphorus in silicon will be higher than the diffusivity of phosphorus in Fe20:Si80 which again will be higher than the diffusivity of Fe50:Si50. However, as found by Nishimoto et al.(2012) the mass transfer of boron between between Si and slag was controlled by the mass transfer of slag. Then if we assume as previously that phosphorus

behaves like boron, the viscosity of Fe:Si will not affect the mass transfer notably.

Table 2.1 gives the equilibrium time used in the various articles for determining the phosphorus distribution. The equilibration time is varying from 10 minutes to 12 hours. Li et al. used the shortest equilibrium time when equilibrating $CaO-Na_2O-Al_2O_3-SiO_2$ with Si-Cu alloy. Even though alloying has shown to decrease the segregation coefficient, it is not likely that alloying Si with Cu would reduce the equilibrium time with more than four hours compared to Fujiwara where the equilibrium time for Si-Ca-Al alloy with $CaO-Al_2O_3-SiO_2$ was 5 hours. Increasing temperature has shown to increase the viscosity and thereby increasing the mass transfer. However Fujiwara et al. did experiments at higher temperatures than Li et al.

5.2 Phosphorus distribution between FeSi, Si and slag

Equilibrium experiments were conducted by heating
45.8 wt% $CaO-47.6$ wt% $SiO_2-5.4$ wt% P_2O_5 with Fe20:Si80 (wt%) for three hours at 1600 °C and thereafter cooling it down with a rate of 1 °C per minutes to 1360 °C. This experiment was conducted in order to investigate the equilibrium phosphorus distribution between FeSi, Si and slag. Cooling a ferrosilicon alloy with silicon content above 58.2 wt% in a controlled manner will according to solidification theory precipitate out silicon.

The results from EPMA-analysis conducted in this thesis showed that the phosphorus content was equal in both FeSi and Si phase with an average value of 0.1wt%. This is contradicting to previous results by Esfahani and Barati (2011) [52] and Khajavi and Barati (2012) [39] where they found that phosphorus distributed towards FeSi. They calculated the distribution coefficient of P between FeSi and Si according to equation 5.1 and found that the value was lower than 0.35 at temperatures above 1285 °C. This means that the phosphorus concentration is higher in FeSi melt than in the solid Si. The experimental procedure that the mentioned authors utilized was somewhat different than the procedure in this thesis. They kept the sample of Fe and Si for 4 hours at 1600 °C, cooled it down to 1300 °C and held it for one hour at this temperature before quenching it in water. It might be that the authors were able to precipitate out more Si when solidifying to a lower temperature than what was done in the work of this thesis. Neither Esfahani and Barati nor Khajavai and Barati used slag in their experiments. Slag might effect the distribution of P between FeSi and Si since diffusion of species in slag phase is controlling the mass transfer as discussed previously.

$$Kp = \frac{C_{PinsolidSi}}{C_{PinFe:Simelt}} < 0.35 \tag{5.1}$$

As shown by Ueda et al.(1997) [19], the activity coefficient of phosphorus in ferrosilicon increases with increasing iron content up to a mole fraction of 0.23 which is equivalent to a weight fraction of Fe of approximately 50. This will lead to less phosphorus dissolving into FeSi even though Khajavi and Barati found that phosphorus had a great affinity for iron in silicon. This might be one reason for the low content of phosphorus observed in ferrosilicon and silicon.

Phosphorus was not detected in the main slag phase, but an average concentration of 0.4 wt% of P_2O_5 which corresponds to 0.2 wt% of P was found in darker areas of the slag matrix which contained in average 24.1 wt% MgO and 3.6 wt% Al_2O_3 in addition to CaO and SiO_2. The initial value of MgO in the slag matrix was only 0.9 wt%, so the dark areas should not account for a large part of the final slag matrix. Since phosphorus concentration is higher in areas of slag also containing MgO it might be that phosphorus has an affinity of Mg. According to Johnston and Barati(2011) phosphorus associates with magnesium forming $Mg_3(PO_4)_2$ compound in slag. This might be one reason for the high content of phosphorus in areas of slag containing MgO compared to the slag matrix. However, Johnston and Barati also found that phosphorus is more stable in Ca compounds in slag compared to Mg compounds.

5.3 Thermodynamic modeling

According to the literature, phosphorus can exist both as phosphide and phosphate in slag depending on the temperature and oxygen potential of the system. The FactSage FToxide database [15] for slags contains phosphorus only in the form of phosphate. Therefore, postdoc Elmira Moosavi-Khoonsari recently made a mini-database for liquid slag comprising phosphorus in the form of both phosphide and phosphate, elaborated in the experimental section 3.5.

The formation Gibbs energy of P_2O_5 when slag is in equilibrium with silicon is positive as given in equation 5.2 [45]. However, Fujiwara et al. [25] and Johnston and Barati [23] found phosphorus distribution coefficients larger than 1.0, showing a preference of phosphorus going into the slag phase. This means that phosphorus will most likely not exist only as P_2O_5 in the slag. This indicates that the formation Gibbs energy of phosphide, Ca_3P_2, as presented in equation 5.3 is negative.

$$[P] + (SiO_2) = (P_2O_5) + [Si] \quad \Delta G^o = 915720 - 88.3T \tag{5.2}$$

$$3(CaO) + 2[P] = (Ca_3P_2) + [O] \tag{5.3}$$

Momokawa and Sano [22] measured the phosphorus solubility in slag in the form of both phosphide and phosphate as a function of oxygen potential, shown in figure 5.6. They equilibriated CaO-Al_2O_3 melts with Fe-P-Al alloy in Ar at 1550 °C. According to Monokawa and Sano, there is a critical oxygen partial pressure where the the dominant phosphorus species changes from phosphide to phosphate with increasing oxygen potential. At oxygen potentials lower than $2.2 \cdot 10^{-18}$ atm, phosphide is the dominant species and at oxygen potentials higher than $2.2 \cdot 10^{-18}$ atm, phosphate is the main species. According to the FactSage calculations, the oxygen potential for the current experimental conditions is in the order of 10^{-17} atm. This is in the region where phosphate is dominating. However, since the metal and slag compositions in this thesis deviates from those of Momokawa and Sano, the critical oxygen potential might also deviate.

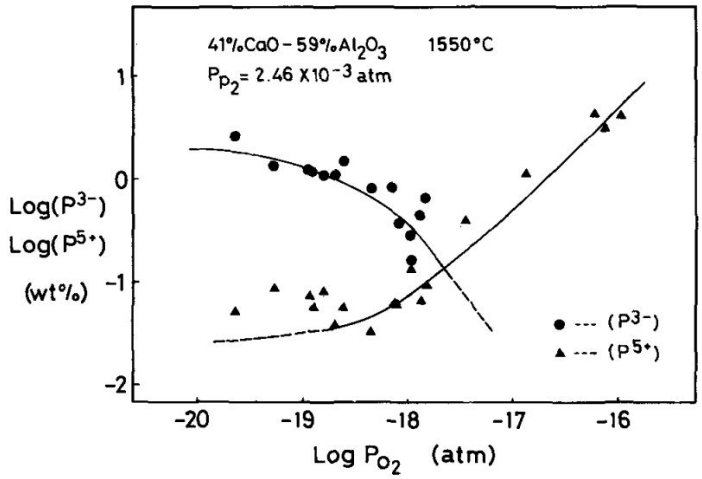

Figure 5.6: Concentrations of phosphide and phosphate in the CaO-Al_2O_3 melt(after Momokawa and Sano [21]).

As depicted in figures 4.12, 4.15 and 4.19, the calculated phosphorus distribution coefficients from FToxide are significantly lower than the experimental values. This is believed to be due to phosphate being the only form of phosphorus included in the FToxide database. The trend in the liquid area marked with solid lines is however the same. Increasing CaO/SiO_2 ratio increases the phosphorus distribution coefficients. Therefore, a new database for liquid slag including both phosphide and phosphate species was developed to reproduce the experimental phosphorous distribution ratio.

The dotted parts of the calculated lines in figures 4.12 through 4.23 present where solid phases are in equilibrium with the liquid phase. However, the cal-

culations were carried out including only the liquid slag solution over the entire composition range. Generally, the phosphorous distribution coefficient reveals an incremental trend with the basicity (CaO/SiO_2 ratio) of slag. However, for both Fe20:Si80 (wt%) and Fe50:Si50(wt%), it is evident that the phosphorous distribution coefficient decreases for slags with CaO content higher than 60 wt%, which might be related to a decrease in slag/metal mass ratio. At this composition, slag consists of liquid and the solid phase Ca_2SiO_4 which means less liquid slag present for interaction with metal phase. With further increasing the CaO content of slag above 80 wt%, the phosphorous distribution coefficient shows an increasing trend which could be due to the change in the metal chemistry. That is, more Ca dissolves into the metal and the concentrations of Si and Fe decrease. For Fe20:Si80(wt%) the metal chemistry is presented in figure 4.16. At approximately 75 wt% CaO, the Ca content exceeds the Fe content in liquid #1. The metal chemistry for Fe50:Si50(wt%) is given in figure 4.20. At 80 wt% CaO, the concentrations of Ca, Si and Fe become constant.

The calculated phase diagram of the Fe-Si-Ca ternary system at 1600 °C is illustrated in figure 5.7. As shown in the phase diagram, Ca and Fe are immiscible, leading to the formation of a two liquid region, Si-Ca and Fe-Si.

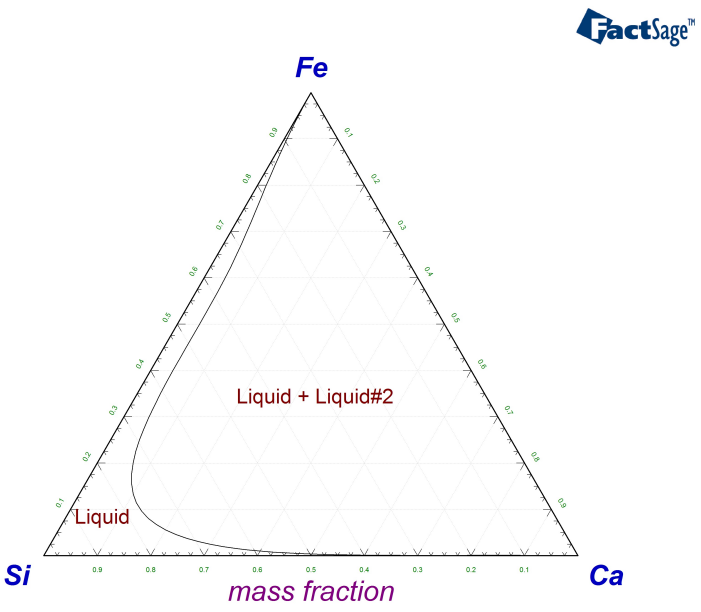

Figure 5.7: Calculated Fe-Si-Ca phase diagram at 1600 °C

As shown in the results section, the calculated phosphorus distribution coefficient increases with increasing the metal iron content. However, as illustrated in

figure 5.2, the activity coefficient of phosphorus in metal decreases with increasing iron content above approximately 50 wt%. A lower activity coefficient of phosphorus in FeSi than Si could result in higher phosphorous distribution coefficient for Si in comparison to FeSi.

The reason for the increase in phosphorus distribution coefficient, Lp, with increasing iron content is most likely because there is an increase in the oxygen partial pressure with increase in iron concentration which will lead to more $PO4^{3-}$ formation. Since $PO4^{3-}$ is the only element included in the FToxide database, it is reasonable that modeling shows an increase in phosphorus distribution coefficient with increasing amount of iron. On the other hand this is also the case for the newly optimized database by Moosavi-Khoonsari. The activity coefficient of P in FeSi as a function of iron concentration was calculated in FactSage from activities and molar fractions assuming Henry's law is applicable for phosphorus. As shown in figure 4.25, the activity coefficient decreases with increasing iron content. This should lead an decrease in the phosphorus distribution coefficient with increasing iron contents. However, as mentioned previously, the opposite was observed in the calculations. It is illustrated in figure 4.26 that oxygen potential also changes with iron content which likely contributes to formation of more $Ca_3(PO_4)_2$ in slag as given in figure 4.24. Therefore it is believed that there is a competition between oxygen potential and activity coefficient of phosphorus in FeSi.

Modeling is however only a simplified picture. In addition the input values are assumptions, and the real input might vary from the input values in the modeling.

5.4 Evaluation of experimental set up

Experiments were conducted in a vertical graphite tube furnace named TF2 with resistance heating. One advantage of the furnace is that it is build with a molybdenum rod connected to a crucible holder. This set-up makes it possible to insert the sample into the furnace when the temperature has reached 1600 °C, which is the target temperature. It is then possible to have a quite precise holding time of 3 hours. What was observed when inserting the sample was that the pressure and temperature in the furnace decreased,so that the effective time at 1600 °C was some minutes shorter than 3 hours. The TF2 furnace also allows a quick heat up to the targeted temperature.

After experiments with silicon and $CaO-SiO_2$ slag, a small amount of powder was observed on top of the melted slag. This might indicate that the temperature was actually deviating from 1600 °C.

In some of the experiments the power was uneven or oscillating, giving a sudden

increase in power and a following decrease. The temperature did not seem to deviate much due to this.

There were difficulties evacuating the furnace well enough in some cases, however all experiments were run with a over-pressure of argon of 1.2-1.3 bar, so that the oxygen pressure should still be low.

The separation method of slag and metal was tedious and resulted in large portions of slag being discarded because of silicon expansion when solidifying. The author is however not familiar with any other method of separating slag and metal in solid state. When separating slag and metal, only 10% of the total initial amount of slag(10g) was kept after equilibration with Si while 40% of slag was kept after equilibration with FeSi. If it was uncertain whether or not slag contained metal, the slag sample was discarded. If phosphorus is not evenly distributed in the slag phase, it might be that the concentration was higher in the slag which was discarded and therefore giving a lower phosphorus content than reality. Metal however stayed in one piece after the experiment and almost all metal was kept after separation. Metal and slag were crushed after separation in order to homogenize them before taking samples for ICP-analysis.

ICP-MS analysis is a good method for measuring trace elements like phosphorus. However it is not a good method for measuring the matrix elements like Si,Fe and Ca. Therefore the values given in table 4.1 can not be trusted except for the phosphorus concentration. EPMA analysis is only used for analysis of the surface, so if slag and metal was not homogenized this would result in deviation from real slag and metal concentrations. XRF analysis instrument was calibrated for main slag elements. The disadvantage of this method is that it does not measure oxides in trace concentrations.

5.5 Reproducibility of results

Two equilibrium experiments with equal composition of slag and metal have been conducted for each series in this study except for Si and SiO_2-CaO 43:57(wt%). In addition three sub-samples samples were taken for ICP-MS analysis. ICP-analysis of the initial metal and slag compositions were all run during the same day. Analysis of slag and metal samples after the experiments were also run during the same day. This removes the uncertainty due to deviation in apparatus from a day to day basis.

XRF-analysis was conducted for the initial composition of slags. As shown in table 3.3, the slag compositions were quite similar to the target compositions given in table 3.2. Three sub-samples were run for each slag. Each sub-sample was also

run twice.

EPMA analysis was done by analyzing three areas of each phase in addition to analyzing three points in each area. As shown in tables 4.5 and 4.6 in the results section, the values of the different areas seem quite uniform. This indicates good homogenization of slag and metal.

Equilibrium time has not been investigated, but assumed to be three hours. If equilibrium concentration was not reached, the concentration would deviate from the equilibrium concentration. As previously discussed an equilibrium time of three hours should be accurate for the slags with compositions of SiO_2 : CaO 43:57 and 50:50. However the most acidic slag might need a longer holding time in order to reach equilibrium.

As mentioned in section 3.4 slag and samples were dissolved in a mixture of 1.5 mL 68% NHO_3 and 0.5 mL 40 % HF. Precipitates were however observed in metal solution and slag solutions were opalescent. The author has not found any optimal acid solution which dissolves $CaO-SiO_2$ slag and FeSi alloys. In the PhD thesis by Jakobsson [32] the acid solution of slag was also heated to 240 °C in an autoclave with 100 bars pressure and held for 10 minutes. This procedure showed successful for dissolving the slag. However this method is currently not used at NTNU. One drawback of this method is that phosphorus might evaporate as phosphine if the temperature is high enough.

NIST 195 FeSi 75% Si was analyzed together with samples taken from metals after all experiments. As presented in table 4.4, there was a deviation of 17.3% between the phosphorus content from the ICP-MS analysis at NTNU and the certified value from NIST. It might therefore be that the analysis is a bit off. However it is the ratio of the concentration of phosphorus in metal and slag which is calculated, so if both analysis are off, the ratio should still be valid. Contaminations in the acid mixture was accounted for by also analyzing a blank sample and deducting it from the results of slag and metal.

The uncertainty calculated by t-distribution was quite high. By increasing the repetition of experiments from two to three, there will be a significant reduction in the uncertainty due to the t-value at a 95% confidence interval decreasing from 12.7 to 4.3.

5.6 Mass loss

The crucible material is graphite, so due to carbothermic reduction it is likely that some phosphorus goes off as gas. This might be one of the reasons why there is a mass loss of phosphorus before and after the experiments. It is likely that

phosphide is then the dominant species in slag, otherwise phosphorus would not exist in the gas phase.

Samples 1-6 were crushed in a steel chamber which might have contaminated the samples. Table 4.1 gives the values of phosphorus in slag and metal before and after the experiments. The total phosphorus concentration in slag and metal for the second experiment with 50:50 (wt%) Fe:Si and 43:57 (wt%) of CaO : SiO_2 is actually higher after the equilibration with slag. This might be because of contamination from the steel chamber. It seems like the SiO_2-CaO slag with composition of 43:57(wt%) gives the lowest mass loss for all metals. This is the slag which gives the lowest oxygen potential in the system. The highest mass loss is found after equilibration of Fe20:Si80(wt%) and 63:35 (wt%) SiO_2 : CaO slag.

As previously discussed in section 3.4 and given in table C.1 in appendix C some of the samples did not dissolve fully in the HNO_3 and HF acid mixture. All metal samples with Fe50:Si50 (wt%) had visible precipitates afterwards. If the precipitates are carbides of phosphorus, the real phosphorus concentration of the metal would be higher then what is detected by ICP-MS analysis. Dissolution of all slags gave a opalescent solution. As for metal, if there is undissolved slag which contains phosphorus, the real phosphorus concentration in slag will be higher than what is detected by the analysis.

5.7 Industrial application

Since the distribution coefficients in all experiments conducted in this thesis are lower than 1.0, it means that there is a preference for phosphorus to go into the metal phase. Therefore, it does not seem promising to use slag refining as a method of phosphorus removal from Si using $CaO-SiO_2$ slags containing from 35 to 57 wt% CaO. However, higher Lp values up to 8.8 have been reported for different slag compositions [23, 25, 27]. According to Johnston et al. [31], Lp value equal to 8.8, low enough for solar grade silicon specifications, was obtained for slag /metal mass ratio of 3.0. As given in table 4.3, the final phosphorus concentrations in metal after equilibration with $CaO-SiO_2$ slags are all significantly higher than the specification of phosphorus for solar grade silicon which is 0.1 ppmw.

It is shown in the results section (section 4) that the slag with the highest basicity has the highest phosphorus distribution coefficient. On the other hand, using the slag with the highest amount of CaO results in the highest amount of Ca pick up in the metal as given in table 4.2. Calcium is also an impurity in silicon and needs to be removed in a separate refining step. This is usually achieved by oxidation since Ca is less noble than Si.

As previously discussed, phosphorus can be stable as Ca_3P_2 in slag at low oxygen potentials. If the slag containing Ca_3P_2 reacts with moist atmosphere, there is a possibility of producing very toxic phosphine gas.

Chapter 6

Conclusion

In this work, phosphorus equilibrium distributions between silicon or ferrosilicon and CaO-SiO_2 slags doped with 300 ppm of phosphorus were studied at 1600 °C in Ar-atmosphere. Experiments were conducted by inserting slag and metal in graphite crucibles into a graphite tube furnace with resistance heating and holding them for 3 hours at 1600 °C. Various compositions of $CaO-SiO_2$ slags and FeSi metal were prepared and used in the experiments. One experiment was also conducted with Fe20:Si80(wt%) together with 45.8CaO-47.6SiO_2-5.4P_2O_5(wt%) slag in the same furnace with a 3 hours holding time at 1600 °C. Thereafter the sample was cooled down at a rate of 1 °C per minute to 1360 °C (solidification temperature of Fe20:Si80) and subsequently quenched. The purpose of this experiment was to study the distribution of phosphorus between FeSi, Si and $CaO-SiO_2$ slag in the same sample. Thermodynamic modeling was conducted in FactSage 7.1 with equivalent experimental conditions as in this work.

The main conclusion is that there is not a significant increase of phosphorus distribution coefficient with alloy composition. Slag composition on the other hand has a large impact on the distribution coefficient of phosphorus as it increases with increasing basicity(CaO/SiO2 ratio) of slag. Calcium pick up in the metal increased with increasing slag basicity and increasing silicon content of the alloy. These conclusions are consistent with previously published data. Thermodynamic modeling of the system should be conducted by including phosphorus both as phosphate and phosphide. The average loss of phosphorus after the experiment was 100 ppm. Using graphite crucibles there will be loss of phosphorus as P_4 gas because of carbothermic reduction.

The values of Lp have been determined as:

- 50Fe:50Si & 65:35 SiO_2-CaO : $Lp = 0.08 \pm 0.06$
- 50Fe:50Si & 50:50 SiO_2-CaO : $Lp = 0.14 \pm 0.15$

- 50Fe:50Si & 43:57 SiO_2–CaO : Lp= 0.53 ± 0.42
- 20Fe:80Si & 65:35 SiO_2–CaO : Lp= 0.14 ± 0.5
- 20Fe:Si80 & 50:50 SiO_2–CaO : Lp= 0.13 ± 0.3
- 20Fe:80Si & 43:57 SiO_2–CaO : Lp= 0.52 ± 0.41
- Si & 50:50 SiO_2–CaO : Lp= 0.12 ± 0.09
- Si & 43:57 SiO_2–CaO : Lp= 0.4

The deviations are calculated using t-distribution which is created for evaluating uncertainty in small sample sizes. The relatively large deviations are believed to be due to experimental inconsistency, inconsistencies in the analysis and due to a small sample size.

The experiment with controlled cooling showed equal concentration of phosphorus in Si and FeSi. Phosphorus was not detected in the slag matrix. Some smaller particles in slag which contained MgO and Al_2O_3 in addition to CaO and SiO_2, had a phosphorus concentration double of that in FeSi and Si. MgO did however only account for 0.8 wt% of the initial slag concentration.

6.1 Further work

The series of experiments with silicon and slag should be finished. Therefore one more experiment with SiO_2 : CaO 43:57(wt%) and Si in addition to two experiments with SiO_2 : CaO 65:35(wt%) and Si should be conducted. One experiment should also be performed with the most acidic slag (SiO_2 : CaO 65:35(wt%)) and Fe50:Si50 (wt%) with a holding time of four hours in order to test if 3 hours was enough to reach equilibrium. This experiment is believed to be the experiment with the slowest mass transfer of P because of the increase in viscosity with increasing SiO_2 content of slag.

The repeatability of the experiment with controlled cooling should be checked by conducting another experiment of this kind.

According to literature, slag systems containing Al_2O_3 and MgO have been effective for removing phosphorus for Si. It would be interesting for future work to also study the phosphorus distribution coefficient between FeSi/Si and slag using alumina and magnesia containing systems.

Bibliography

[1] Adrian Whiteman, Tobias Rinke, Javier Esparrago, and Samah Elsayed. Renewable energy highlights. Technical report, International Renewable Energy Agency, 2016.

[2] Bruno Burger, Klaus Kiefer, and Christoph Kost. Photovoltaics report. Technical report, Fraunhofer Institute for Solar Energy Systems, 2016.

[3] Takahiro Miki, Kazuki Morita, and Nobuo Sano. Thermodynamics of phosphorus in molten silicon. *Metallurgical and Materials Transactions B*, 27(6):937–941, 1996.

[4] E.H.Myrhaug and H.Tveit, editors. *Material Balances of Trace Elements in the Ferrosilicon and Silicon Processes*, volume 58. Electric Furnace Conference Proceedings, 2000.

[5] Dachuan Jiang, Shiqiang Ren, Shuang Shi, Wei Dong, Jieshan Qiu, Yi Tan, and Jiayan Li. Phosphorus removal from silicon by vacuum refining and directional solidification. *Journal of Electronic Materials*, 43(2):314–319, 2014.

[6] Tim Niewelt, Juliane Broisch, Jonas Schön, Jonas Haunschild, Stefan Rein, Wilhelm Warta, and Martin C. Schubert. Light-induced degradation and regeneration in n-type silicon. *Energy Procedia*, 77:626 – 632, 2015.

[7] B. R. Bathey and M. C. Cretella. Solar-grade silicon. *Journal of Materials Science*, 17(11):3077–3096, 1982.

[8] Meteleva-Fischer et al. Microstructure of metallurgical grade silicon and its acid leaching behaviour by alloying with calcium. *Mineral Processing and Extractive Metallurgy IMM Transactions section C*, 122:229–237, 2013.

[9] Cahn Robert W. Flemings Merton C. Ilschner Bernhard Kramer Edward J. Mahajan Subhash Buschow, K.H. Jürgen. *Silicon Steels*. Elsevier, 2001.

[10] WorldSteelAssociation. Steel recovery strengthens, but geopolitical uncertainty clouds outlook. *Worldsteel.org*, Apr 2017.

[11] Somnath Basu. *Studies on dephosphorization during steelmaking*. PhD thesis, Kungliga Tekniska Högskolan, 2007.

[12] B. Mintz, A. Cowley, C. Talian, D. N. Crowther, and R. Abushosha. Influence of P on hot ductility of high C, Al, and Nb containing steels. *Materials Science and Technology*, 19(2):184–188, 2003.

[13] Na Li, Zhen-yu Liu, Guo-ping Zhou, Xiang-hua Liu, and Guo-dong Wang. Effect of phosphorus on the microstructure and mechanical properties of strip cast carbon steel. *International Journal of Minerals, Metallurgy, and Materials*, 17(4):417–422, 2010.

[14] Sano N. and Katayama H. Dephosphorization of stainless steels. *Proceedings of the 1st International Chromium, Steel and Alloys Congress, Cape Town*, 2:25–35, 1992.

[15] Factsage 7.1. www.factsage.com.

[16] Maria Førde Møll. *Solidification of Silicon*. PhD thesis, Norwegian University of Science and Technology, 2014.

[17] Tomohito Shimpo, Takeshi Yoshikawa, and Kazuki Morita. Thermodynamic study of the effect of calcium on removal of phosphorus from silicon by acid leaching treatment. *Metallurgical and Materials Transactions B*, 35(2):277–284, 2004.

[18] Q. C. Horn, R. W. Heckel, and C. L. Nassaralla. Reactive phosphide inclusions in commercial ferrosilicon. *Metallurgical and Materials Transactions B*, 29(2):325–329, 1998.

[19] Shigeru Ueda, Kazuki Morita, and Nobuo Sano. Thermodynamics of phosphorus in molten Si – Fe and Si – Mn alloys. *Metallurgical and Materials Transactions B*, 28(6):1151–1155, 1997.

[20] David Lynch. Winning the global race for solar silicon. *JOM*, 61(11):41–48, 2009.

[21] H. Momokawa and N. Sano. The effect of oxygen potential on phosphorus in the $CaO - Al_2O_3$ system. *Metallurgical Transactions B*, 13(4):643–644, 1982.

[22] S. Tabuchi and N. Sano. Thermodynamics of phosphate and phosphide in $CaO - CaF_2$ melts. *Metallurgical Transactions B*, 15(2):351–356, 1984.

[23] M.D. Johnston and M. Barati. Distribution of impurity elements in slag–silicon equilibria for oxidative refining of metallurgical silicon for solar cell applications. *Solar Energy Materials and Solar Cells*, 94(12):2085 – 2090, 2010.

[24] Yanaba Y. Yoshikawa T. Kawamura, H. and K. Morita. Reductive removal of phosphorus in silicon using cao-caf2 slag. *EPD Congress 2013*, 2013.

[25] H Fujiwara, JY Liang, K Takeuchi, and E Ichise. Reducing removal of phosphorous from calcium containing silicon alloys. *Materials Transactions*, 37(4):923–926, APR 1996. International Symposia on Advanced Material and Technology for the 21st-Century - JIM 95 Fall Annual Meeting, HI, 1995.

[26] Mark Li, Torstein Utigard, and Mansoor Barati. Removal of boron and phosphorus from silicon using CaO-SiO2-Na2O-Al2O3 flux. *Metallurgical and Materials Transactions B*, 45(1):221–228, 2014.

[27] Eun Jin Jung, Byung Moon Moon, and Dong Joon Min. Quantitative evaluation for effective removal of phosphorus for sog-si. *Solar Energy Materials and Solar Cells*, 95(7):1779 – 1784, 2011.

[28] Joo Hyun Park, Dong Joon Min, and Hyo Seok Song. The effect of CaF2 on the viscosities and structures of CaO-SiO2(-MgO)-CaF2 slags. *Metallurgical and Materials Transactions B*, 33(5):723–729, 2002.

[29] Motohiro Sakamoto, Yutaka Yanaba, and Kazuki Morita. Local structure around phosphorus and silicon in the cao–sio2–po2.5 system. *Journal of Non-Crystalline Solids*, 358(3):615 – 619, 2012.

[30] Atsuko Tagaya, Hiroyuki Chiba, Fumitaka Tsukihashi, and Nobuo Sano. Thermodynamic behavior of phosphorus in $CaO-CaF_2-SiO_2$ and $CaO-Na_2O-SiO_2$ systems. *Metallurgical Transactions B*, 22(4):499–502, 1991.

[31] Murray D. Johnston, Leili Tafaghodi Khajavi, Mark Li, Samira Sokhanvaran, and Mansoor Barati. High-temperature refining of metallurgical-grade silicon: A review. *JOM*, 64(8):935–945, 2012.

[32] Lars Klemet Jakobsson. *Distribution of boron between silicon and CaO-SiO2, MgO-SiO2, CaO-MgO-SiO2 and CaO-Al2O3-SiO2 slags at 1600C*. PhD thesis, Norwegian University of Science and Technology, 2013.

[33] Cahn Robert W. Flemings Merton C. Ilschner Bernhard Kramer Edward J. Mahajan Subhash Buschow, K.H. Jürgen. *Silicon: Diffusion*. Elsevier, 2001.

[34] Egil Krystad, Kai Tang, and Gabriella Tranell. The kinetics of boron transfer in slag refining of silicon. *JOM*, 64(8):968–972, 2012.

[35] Verein Deutscher Eisenhuttenleute. *Slag Atlas*. Verlag Stahleisen mbH, Germany, 1995.

[36] A.L. Bel'tyukov, V.I. Lad'yanov, A.I. Shishmarin, and S.G. Menshikova. Viscosity of liquid amorphizing alloys of iron with boron and silicon. *Journal of Non-Crystalline Solids*, 401:245 – 249, 2014. Structure of non-crystalline materials 12 Proceedings of the 12th International Conference on the Structure of Non-Crystalline Materials (NCM 12).

[37] H.Nishimoto, Y.Kang, T.Yoshikawa, and K.Morita. The rate of boron remoal from molten silicon by cao-sio2 slag and cl2 treatment. *High Temperature Materials and Processes*, 31, 2012.

[38] Shaghayegh Esfahani and Mansoor Barati. *A Novel Purification Method for Production of Solar Grade Silicon*, pages 193–205. John Wiley & Sons, Inc., 2010.

[39] Leili Tafaghodi Khajavi and Mansoor Barati. *Thermodynamics of Phosphorous Distribution between Si and Fe–Si in Solvent Refining of Silicon*, pages 513–520. John Wiley & Sons, Inc., 2012.

[40] M Tangstad. *Handbook of Ferroalloys*. Elsevier Inc. Chapters, 2013.

[41] M.D. Johnston and M. Barati. Effect of slag basicity and oxygen potential on the distribution of boron and phosphorus between slag and silicon. *Journal of Non-Crystalline Solids*, 357(3):970 – 975, 2011.

[42] Egil Krystad. N/a. Private Communication, 2017.

[43] Liu qing Huang, Hui xian lai, et al. Effects of slag refining and vacuum treatment on de-phosphorus from mg-si using cao-sio2-cacl2 slag. *Advanced Materials Research*, 815:773–777, 2013.

[44] Takeshi Yoshikawa and Kazuki Morita. Removal of phosphorus by the solidification refining with si–al melts. *Science and Technology of Advanced Materials*, 4(6):531 – 537, 2003.

[45] In-Ho Jung and Yumin Zhang. Thermodynamic calculations for the dephosphorization of silicon using molten slag. *JOM*, 64(8):973–981, 2012.

[46] Somnath Basu, Ashok Kumar Lahiri, and Seshadri Seetharaman. Phosphorus partition between liquid steel and cao-sio2-p2o5-mgo slag containing low feo. *Metallurgical and Materials Transactions B*, 38(3):357–366, 2007.

[47] E. Enebakk, G.M. Tranell, and R. Tronstad. Calcium-silicate based slag for treatment of molten silicon, December 21 2010. US Patent 7,854,784.

[48] Erlend Lunnan Bjornstad. Mass transfer coefficients and bubble sizes in oxidative ladle refining of silicon. Master's thesis, Norwegian University of Science and Technology, 06 2016.

[49] A.D. Pelton, G. Eriksson, and A. Remero-Serrano. Calculation of sulfide capacities of multicomponent slags. *Metall. Trans.B*, 24B:817–25, 1993.

[50] P. Hudon and In-Ho Jung. Critical evaluation and thermodynamic optimization of the cao-p2o5 system. *Metall. Mater. Trans. B*, 46:494–522, 2014.

[51] NIST. Standard reference material 195, 2009.

[52] Shaghayegh Esfahani and Mansoor Barati. Purification of metallurgical silicon using iron as an impurity getter part i: Growth and separation of si. *Metals and Materials International*, 17(5):823–829, 2011.

[53] E.S. Lee and R.N. Forthofer. *Analyzing Complex Survey Data*. Analyzing Complex Survey Data. SAGE Publications, 2006.

Appendix A

Statistical analysis

Two experiments were conducted with equal slag and metal compositions and similar experimental conditions.

To this authors knowledge, the relationship between phosphorus concentration in slag and metal in one sample/experiment is biased, however it is assumed that the relationship of slag and metal in one sample and the relationship of slag and metal in another sample are independent variables.

The distribution coefficient is a fraction of two functions as shown in equation A.1. According to Lee and Forthofer(2006) [53], the variance of a function A/B can be calculated as presented in equation A.2. Here A represents concentration of P in slag and B represents concentration of P in metal.

$$Lp = \frac{(wt\%P)_{\text{ in slag}}}{[wt\%P]_{\text{ in metal}}} = f = \frac{A}{B} \tag{A.1}$$

$$\sigma^2 \approx f^2[(\frac{\sigma_A}{A})^2 + (\frac{\sigma_B}{B})^2 - 2\frac{\sigma_{AB}}{AB}] \tag{A.2}$$

Since the population parameters are not know, the sample parameters are used instead as shown in equations A.3 through A.5:

$$f \approx \frac{\overline{X}_A}{\overline{X}_B} = \frac{N_B \sum_{i=1}^{N_A} X_{A,i}}{N_A \sum_{i=1}^{N_B} X_{B,i}} \tag{A.3}$$

$$\sigma_{AB} = \approx \frac{1}{N-1}\sum_{i=1}^{N}(X_{A,i} - \overline{X}_A)(X_{B,i} - \overline{X}_B), \quad N_A = N_B \tag{A.4}$$

$$\sigma_A^2 = S_A^2 = \left[\frac{n(\sum_{i=1}^{n} x_i^2) - (\sum_{i=1}^{n} x_i)^2}{n(n-1)} + \frac{\sum_{j=1}^{n}(\frac{x_j RSD_j}{100})^2}{n(n-1)}\right] \tag{A.5}$$

While the set X1, X2, ..., Xi is expected to have a standard distribution the t distribution must be used instead with N- 1 degrees of freedom since we have a

small number of samples. Lp can therefore be represented as shown in equation A.6.

$$Lp = \overline{X} \pm t_{n-1,\frac{\alpha}{2}} \cdot \frac{S}{\sqrt{n}} Lp = \overline{X} \pm 12.706 \cdot \frac{S}{\sqrt{2}} \tag{A.6}$$

Here $\overline{X}$ represents the average of the ratios of the mean phosphorus concentration in slag and metal for sample 1 and 2 as shown in equation A.3 .

The average standard distribution is calculated according to equation A.9 which is found from equations A.7 and A.8.

$$\overline{\sigma}^2 = \frac{\sum_{i=1}^{N} \sigma_i^2}{N^2} \tag{A.7}$$

$$\overline{S}^2 = \frac{N}{N-1}\overline{\sigma}^2 = \frac{N}{N-1}\frac{\sum_{i=1}^{N} \sigma_i^2}{N^2} = \frac{N}{N-1}\frac{\sum_{i=1}^{N} (\frac{ni-1}{ni})}{N^2} \tag{A.8}$$

$$\overline{S}^2 = \frac{n-1}{N(N-1)n} \sum_{i=1}^{N} S_i^2, \quad ni = n \forall i \in \mathbb{Z}^+ \tag{A.9}$$

A.1 Example calculation of *Lp* with uncertainty

This section include one example calculation for experiment 1 and 2 which both were equilibrium experiments with 50:50 Fe:Si and 50:50 CaO : SiO_2.

Table A.1 gives the input for metal and table A.2 gives the input for slag for calculation of Lp. The standard deviations $\sigma_{B,1}$, $\sigma_{B,2}$, $\sigma_{A,1}$ and $\sigma_{A,2}$ are calculated from equation A.5.

Table A.1: Input for metal for calculation of Lp

Sub-sample	$X_{B,1}$	RSD	$\overline{X_{B,1}}$	$\sigma_{B,1}$	$X_{B,2}$	RSD	$\overline{X_{B,2}}$	$\sigma_{B,2}$
1	140.1	3.7	139.3	7.6	134.9	1.5	133.5	2.9
2	131.9	2.0			133.2	1.9		
3	145.8	2.9			132.3	4.2		

Table A.2: Input for slag for calculation of Lp

Sub-sample	$X_{A,1}$	RSD	$\overline{X_{A,1}}$	$\sigma_{A,1}$	$X_{A,2}$	RSD	$\overline{X_{A,2}}$	$\sigma_{A,2}$
1	26.2	8.9	24.7	2.9	13.0	8.4	13.7	1.1
2	26.3	5.2			14.6	8.7		
3	21.6	4.7			13.5	2.4		

Table A.2 presents the calculated values of Lp, co-variance and S_n^2 as calculated by equations A.3 for sub-samples, A.4 and A.2 respectively.

Table A.3: Calculations for samples 1 &2

sample(n)	Lp	cov	S_n^2
1	0.18	-15.4	0.0008
2	0.1	-0.5	7.6E-05

Table A.4 gives the Lp as calculated from samples 1&2 by equation A.3 and S^2 calculated from equation A.9. $t_{(2-1),0.05/2}$ is found from the t-distribution table at a 95% confidence interval. The value decreases from 12.7 to 4.3 with an additional sample.

Table A.4: Calculations for t-distribution

Lp	S^2	S	$t_{(2-1),0.05/2}$
0.14	0.0003	0.017	12.706

Inserting the values from table A.4 into equation A.6 gives equation A.10. This will be calculated for experiments and used in the results section.

$$Lp = 0.14 \pm 0.16 \tag{A.10}$$

Appendix B

XRF-analysis

XRF-analysis was conducted by Torill Sørløkk at Department of Geology and Mineral Resources Engineering at NTNU.

The instrument used is named S8 Tiger and uses a 4 kW X-ray spectrometer.

Table B.1: XRF-analysis of $CaO-SiO_2-P_2O_5$ slag

Compound	Amount Parallel 1 [%]	Amount Parallel 2 [%]
Fe_2O_3	0.14	0.15
TiO_2	0.01	0.02
CaO	40	40.12
K_2O	0	0
P_2O_5	0.05	0.05
SiO_2	50.73	50.76
Al_2O_3	0.15	0.05
MgO	9.94	9.93
Na_2O	0	0
MnO	0.01	0.01
LOI 100 degrees	0.18	0.18
SUM	101.22	101.27

The slag shown in table B.1 was contaminated with MgO. New slags were produced and the compositions are shown in table B.2.

Table B.2: XRF-analysis of $CaO-SiO_2-P_2O_5$ slags of different compositions as an average of three parallels which all were run twice

Compound	Amount Slag 1 [%]	Amount Slag 2 [%]	Amount Slag 3 [%]
Fe_2O_3	0.21	0.1	0.09
TiO_2	0	0	0
CaO	58.3	51.6	36.1
K_2O	0	0	0
P_2O_5	0.07	0.07	0.06
SiO_2	43.6	49.9	63.9
Al_2O_3	0	0	0
MgO	0.2	0.02	0.01
Na_2O	0	0	0
MnO	0.01	0	0
LOI 100 degrees	0.06	0.06	0.05
SUM	102.4	101.76	100.27

Appendix C

ICP-MS analysis

ICP-MS analysis was conducted by Syverin Lierhagen at Department of Chemistry at NTNU. Slag and metal were dissolved in 1.5 ml HCl and 0.5 ml HNO_3.

Table C.1 gives an overview of how well slag and metal were dissolved in the acid mix of 1.5 mL 68% HNO_3 and 0.5 mL 40% HF after the equilibrium experiments. Experiment numbers are equivalent to the experiments shown in table 4.1 in the results section.

Table C.1: Table showing the dissolution of slag and metal after equilibrium experiments.

Exp.nr.	metal Fe:Si	comment	slag SiO_2 : CaO	comment
1	50:50	precipitates	50:50	opalescent
2	50:50	precipitates	50:50	opalescent
3	50:50	precipitates	43:57	opalescent
4	50:50	precipitates	43:57	opalescent
5	50:50	precipitates	65:35	opalescent
6	50:50	precipitates	65:35	opalescent
7	20:80	dissolved	50:50	opalescent
8	20:80	dissolved	50:50	opalescent
9	20:80	dissolved	43:57	opalescent
10	20:80	dissolved	43:57	opalescent
11	20:80	dissolved	65:35	opalescent
12	20:80	some precipitates in sub-sample 1	65:35	opalescent
13	0:100	dissolved	50:50	some precipitates
14	0:100	dissolved	50:50	some precipitates
15	0:100	dissolved	43:57	opalescent

Slag nr	Subsample	P [ppm]	RSD [%]	Std dev.
1	1	203,53	3,1	9,87
	2	191,37	1,4	
2	1	221,94	1,4	6,36
	2	214,67	2	
3	1	178,63	1,6	6,44
	2	185,81	2,6	

Figure C.1: Initial phosphorus concentration of slag. Two sub-samples were taken from each slag. Slag numbers are corresponding to the numbers in table 3.3. Standard deviations are calculated from equation A.5.

Figures C.1 and C.2 present the initial phosphorus concentration of slag and metal produced in this work. Two sub-samples were taken from slag while three sub-samples were taken from the FeSi alloys.

Figures C.3 and C.4 give the values from ICP-analysis of metal and slag from experiments 1-15. The experiments are equivalent to the ones shown in table 4.1 in the results section.

Alloy	Sub-sample	P [ppm]	RSD [%]	Std.dev
1	1	29,2	5,8	1,64
	2	29,6	5,7	
	3	27,6	6,9	
2	1	38,2	4,5	1,58
	2	40,5	2,6	
	3	38,8	4	
3	1	133,3	2,4	4,95
	2	130,4	4,2	
	3	125,5	2,9	

Figure C.2: Initial phosphorus concentration of alloys. Three sub-samples were taken from each alloy. Alloy numbers are corresponding to the numbers in table 3.4. Standard deviations are calculated from equation A.5.

Experiment	Sub-sample	Slag [ppm]	RSD [%]	Std.dev	Metal [ppm]	RSD [%]	Std.dev
1	1	26,24	8,9	2,93	140,13	3,7	7,58
1	2	26,27	5,2		131,88	2	
1	3	21,59	4,7		145,80	2,9	
2	1	13,04	8,4	1,07	134,92	1,5	2,94
2	2	14,63	7,4		133,22	1,9	
2	3	13,46	2,4		132,32	4,2	
3	1	88,20	0,3	4,93	124,82	1,8	5,37
3	2	79,03	4,4		123,92	0,8	
3	3	82,23	2,3		133,05	2,9	
4	1	79,34	4,3	8,51	169,89	5,1	13,81
4	2	66,89	5,5		155,82	1,8	
4	3	63,81	2,9		182,13	2,5	
5	1	10,29	12,8	0,84	99,48	6,5	4,66
5	2	10,89	3,7		95,85	4,6	
5	3	9,76	6,1		92,82	1,7	
6	1	4,81	14,6	0,70	86,05	0,8	2,14
6	2	3,59	7,9		83,46	3,7	
6	3	3,94	3,8		82,87	0,6	
7	1	14,36	7,4	5,55	118,71	3,4	10,69
7	2	14,89	3,3		98,53	6,7	
7	3	5,05	3		111,36	0,5	

Figure C.3: Results from ICP-MS analysis of metal and slag from experiments 1-7. RSD: Relative standard deviation from the analysis. Standard deviations are calculated from equation A.5.

Experiment	Sub-sample	Slag [ppm]	RSD [%]	Std.dev	Metal [ppm]	RSD [%]	Std.dev
8	1	17,94	8,1	1,77	107,46	2,2	4,21
8	2	18,38	10,3		114,19	2,6	
8	3	15,72	5,9		110,28	4,4	
9	1	54,08	4,7	4,85	104,65	5,5	3,46
9	2	55,08	3,4		108,21	0,1	
9	3	46,64	4		107,17	4	
10	1	74,53	2,1	6,49	121,20	2,5	6,03
10	2	62,73	2,8		118,56	5,4	
10	3	64,50	3		128,40	2,7	
11	1	6,12	11,9	5,61	62,37	3,7	2,33
11	2	7,53	7,3		62,64	2,3	
11	3	16,41	6		59,67	5	
12	1	6,39	6,7	0,40	54,35	5	2,53
12	2	6,83	7		51,26	2,2	
12	3	6,64	7,3		55,27	3,2	
13	1	19,23	2,2	0,96	162,61	5,3	5,86
13	2	18,96	8,8		165,65	3,5	
13	3	18,06	3,1		157,87	1,5	
14	1	15,76	4,3	2,79	137,30	3,3	6,22
14	2	20,91	8,7		148,04	1,2	
14	3	17,46	7,6		140,16	3,4	
15	1	40,58	5,8	7,05	108,59	2,2	4,29
15	2	41,68	3,3		116,11	2,9	
15	3	53,01	4,9		112,61	2,6	

Figure C.4: Results from ICP-MS analysis of metal and slag from experiments 8-15. Standard deviations are calculated from equation refeq:std.

Appendix D

EPMA-analysis

Figure D.1 presents the metal analysis from EPMA.

Figure D.2 presents the slag analysis from EPMA.

Si	Si avg	P	P avg	C	C avg	Fe	Fe avg	Total	Comment
97,36	96,85	0,12	0,11	2,28	2,79	0,24	0,24	100	Si towards slag
96,19		0,09		3,59		0,13		100	
97,00		0,13		2,51		0,36		100	
55,71	55,41	0,06	0,08	1,92	2,03	42,32	42,48	100	FeSi towards slag
55,46		0,12		2,03		42,38		100	
55,06		0,07		2,13		42,74		100	
97,48	97,65	0,07	0,11	2,16	2,13	0,29	0,11	100	Si middle
97,79		0,12		2,08		0,01		100	
97,69		0,14		2,15		0,02		100	
55,47	55,50	0,10	0,09	2,21	1,90	42,23	42,52	100	FeSi middle
55,60		0,07		1,78		42,56		100	
55,42		0,09		1,71		42,78		100	
97,55	97,25	0,09	0,11	2,26	2,52	0,11	0,13	100	Si towards crucible
97,18		0,13		2,49		0,20		100	
97,02		0,10		2,80		0,08		100	
55,23	55,16	0,11	0,14	2,54	2,19	42,12	42,51	100	FeSi towards crucible
55,39		0,07		1,71		42,83		100	
54,86		0,24		2,32		42,58		100	

Figure D.1: EPMA analysis of metal

SiO2	avg. SiO2	MgO	avg MgO	P2O5	avg. P2O5	Al2O3	avg. Al2O3	CaO	avg CaO	Total	Comment
51,93	51,92	0,07	0,07	0,00	0,02	0,00	0,01	48,00	47,98	100	Slag matrix
52,00		0,10		0,03		0,02		47,86		100	towards metal
51,84		0,06		0,01		0,01		48,09		100	
43,09	43,68	25,75	24,83	0,77	0,62	3,88	3,66	26,50	27,21	100	Dark particles
43,40		24,25		0,59		3,51		28,26		100	towards metal
44,55		24,48		0,50		3,60		26,88		100	
51,84	52,05	0,07	0,07	0,00	0,00	0,00	0,02	48,09	47,86	100	Slag matrix
52,05		0,05		0,00		0,04		47,86		100	middle
52,26		0,08		0,00		0,02		47,64		100	
42,78	43,35	24,48	24,14	0,45	0,41	3,39	3,22	28,91	28,88	100	Dark particles
43,71		23,35		0,46		3,07		29,42		100	middle
43,55		24,60		0,32		3,22		28,32		100	
51,65	51,86	0,05	0,06	0,01	0,01	0,01	0,00	48,30	48,07	100	Slag matrix
52,27		0,06		0,00		0,01		47,66		100	top
51,65		0,06		0,03		0,00		48,26		100	
44,07	44,30	24,31	23,30	0,34	0,34	3,88	3,77	27,41	28,30	100	Dark particles
43,89		24,34		0,28		3,69		27,80		100	top
44,94		21,24		0,39		3,75		29,68		100	
36,29	36,13	13,50	13,42	0,00	0,03	0,07	0,07	50,14	50,35	100	Light grey
36,57		13,29		0,05		0,03		50,07		100	particles
36,32		13,28		0,06		0,10		50,24		100	
35,36		13,60		0,02		0,05		50,97		100	

Figure D.2: EPMA analysis of slag